UNIVERSITÄTSKLINIKUM HAMBURG-EPPENDORF

Institute of Neuropathology

Prof. Dr. Markus Glatzel

The Role of Specific Mutations in Presenilin 1 on Mitochondrial Morphology and Function

Dissertation

to obtain the doctoral degree Doctor of Philosophy (Ph.D.)
at the Medical Faculty of the University of Hamburg.

Presented by:

Liliana Rojas-Charry

From Bogotá D.C., Colombia

Hamburg 2019

Angenommen von der Medizinischen Fakultät am: 23.09.2019

Veröffentlicht mit Genehmigung der medizinischen Fakultät der Universität Hamburg

Prüfungsausschuss, der/die Vorsitzende: Prof. Dr. Markus Glatzel

Prüfungsausschuss, 2. Gutachter/in: Prof. Dr. Hans-Jürgen Kreienkamp

Table of Contents

1. Introduction

1.1 Alzheimer´s Disease

Alzheimer's disease (AD) is a progressive neurodegenerative disorder, characterized by memory decline and impairment of other cognitive functions, that leads to death. Dementia affects approximately fifty million people around the world, and as the elderly population is growing, some authors have predicted that in about 30 years, around 152 million people will have this illness, making it a very serious health problem (Patterson 2018). AD is a complex pathology whose molecular mechanisms are not completely understood. Its diagnosis is also challenging because only postmortem analysis of the brain can conclusively determine the presence of senile plaques and neurofibrillary tangles, which are the pathological hallmarks of a brain affected by this disease.

About thirty years ago, the main component of the plaques, the β-amyloid peptide (Aβ), was sequenced (Kang et al. 1987), and mutations in genes involved in the production of Aβ provided scientific evidence for the so-called "amyloid hypothesis" (Goate et al. 1991; Sherrington et al. 1995). This paradigm postulates that the aggregation and accumulation of the Aβ peptide are toxic and eventually leads to AD (Hardy and Higgins 1992).

Aβ is produced after the successive cleavage performed by β- and γ-secretases on the amyloid precursor protein (APP). Although the exact biological role of APP is not known, this roughly 100kDa protein located in the extracellular membrane is abundant in the brain and concentrates at the synapses of neurons. APP cleavage by α- and γ-secretases generates the p3 peptide which is not considered amyloidogenic (Figure 1). Meanwhile, its cleavage by β- and γ-secretases generates Aβ peptides of various lengths (Chow et al. 2010).

γ-Secretase is a large complex formed by four proteins: presenilins (PSs), nicastrin, anterior pharynx-defective-1 (APH-1), and presenilin enhancer 2 (PEN2) (Figure 2). The characterization of this complex has not been easy; the three-dimensional

structure of human γ-secretase was only determined with cryo-electron microscopy in 2014, together with the crystal structure of nicastrin (Lu et al. 2014; Xie et al. 2014).

The role of γ-secretase is not just restricted to the production of Aβ. It participates in Notch signaling, releasing the Notch receptor intracellular domain. Notch signaling regulates diverse and key biological functions, including cell differentiation at different cellular stages, cell-to-cell communication, proliferation, and survival. (Maillard, Fang, and Pear 2005). γ-secretase also cleaves E-cadherin, ErbB4, CD44, TREM-1, Alcadein, and tyrosinase, all of which are type I transmembrane proteins (Beel and Sanders 2008). At least 89 substrates have been postulated as targets for γ-secretase, including proteins that perform very different roles inside the cell (Haapasalo and Kovacs 2011). Additionally, each of its components its thought to work independently of this proteolytic function, intervening in different cellular processes, such as calcium (Ca^{2+}) regulation, apoptosis, and autophagy, among others (Zhang et al. 2014).

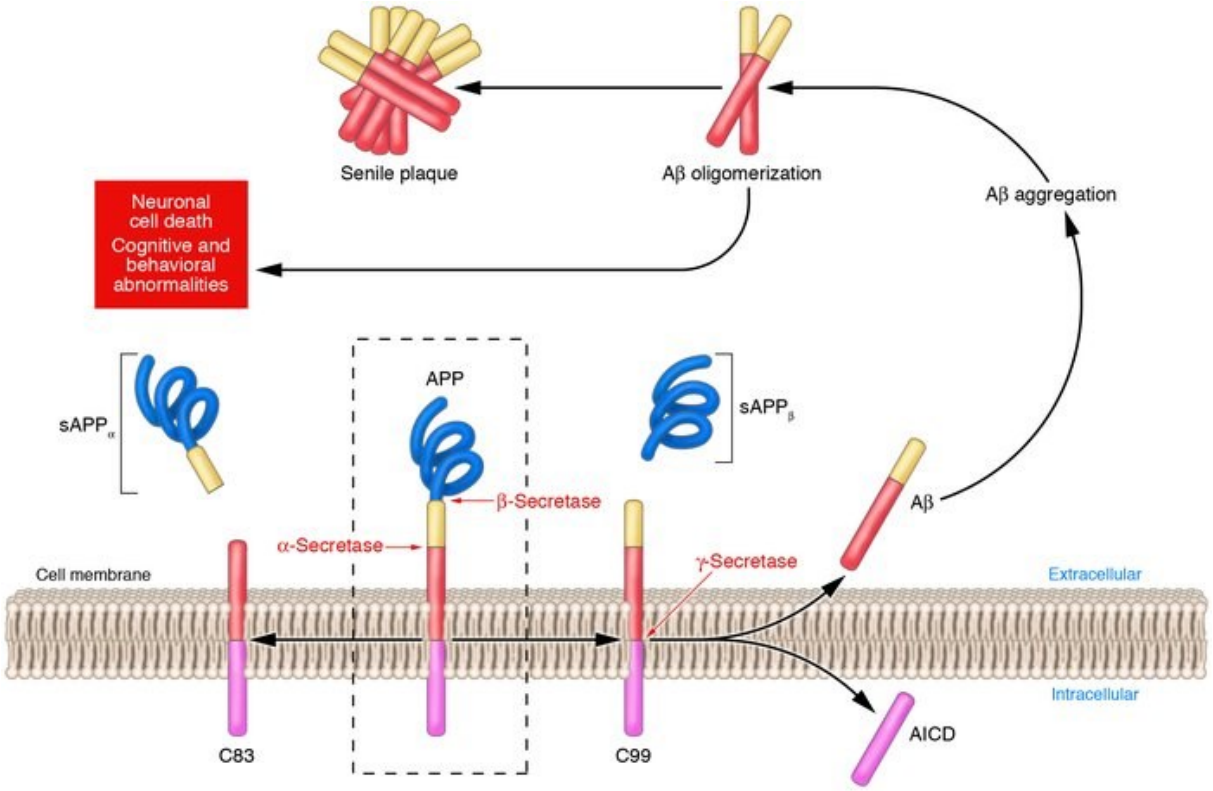

Figure 1. The processing of APP. The exact function of the amyloid precursor protein is not yet completely understood. APP is in the extracellular membrane and can be processed by α, β and γ-secretases. Cleavage of α-secretase produces C83 and cleavage of β-secretase produces C99 and sAPPβ. The C99 fragment can be further processed by γ-secretase to generate the APP intracellular

domain (AICD) and Aβ. The Aβ peptide is highly toxic, it aggregates and oligomerizes and, this process ends up in the formation of senile plaques. Source: Gandy et al., 2005 (Gandy 2005).

As the population grows older, the need for treatment and an early diagnostic tool for AD is critical. The enthusiasm that the “amyloid cascade” hypothesis created conduced to the idea that decreasing the production of Aβ in any stage could heal or at least ameliorate the symptoms of the disease. Different medications and therapeutic strategies have been probed, such as Aβ production or aggregation modulators, immunotherapy, tau protein targeting, and metabolic targeting pathways (Cummings et al. 2018), but only a few have shown a positive effect on symptoms. None have stopped or significantly modified disease progression (Han and Mook-Jung 2014).

For example, Semagacestat is the molecule affecting γ-secretase function that has advanced the most in clinical trials. However, it is not selective for APP and interferes with Notch signaling, causing several secondary side effects that include skin cancer and, in some cases, worsen the cognitive decline (Doody et al. 2013). A paper published in 2017 by Tagami et al. showed it could not be considered a true γ-secretase inhibitor because it increases the intracellular accumulation of potentially toxic γ-byproducts (Tagami et al. 2017). This study also demonstrates that other compounds including RO4229097 and MK-0752, produce the same outcome as Semagacestat. The authors explained that these substances are not specific γ-secretase inhibitors and better and more targeted molecules must be developed to stop the production of the toxic forms of the Aβ peptide.

The failure in effective therapies against AD can be attributed to different factors, from lacking truly specific γ-secretase inhibitors to the absence of reliable animal models. There is a consensus about the involvement of Aβ in AD, but, more recently, this hypothesis has been reconsidered, proposing a redefinition that takes into account other models of the disease process and not to focus on a single strategy but to combine therapies with different targets (Herrup 2015).

The contribution of other cell types must be included since AD is not a neuron-exclusive pathology. Microglia, astrocytes, and oligodendrocytes, among others, also contribute to the disease in diverse ways, which are not only a consequence of Aβ

toxicity. The role of microglia, for example, has been studied intensively in the last years and, now, it is known that activation of microglia is more relevant than just reacting with inflammation. Mutations in the gene TREM2, a type I transmembrane protein expressed in the central nervous system (CNS) on microglia, is a risk factor for the development of late-onset AD and other neurodegenerative diseases (De Strooper and Karran 2016).

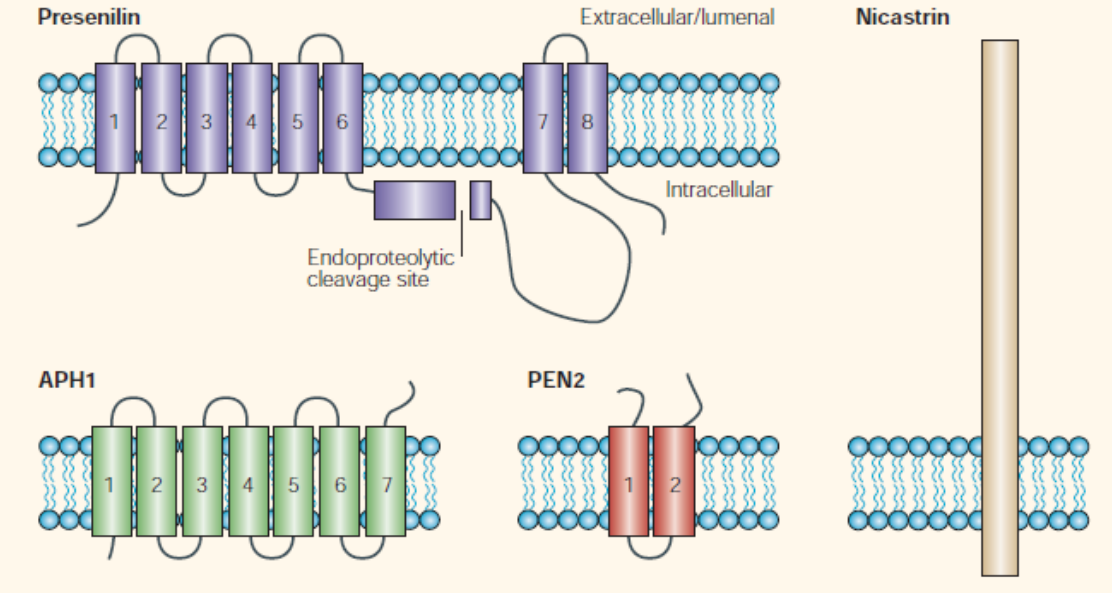

Figure 2. Representation of the components of the γ-secretase complex. The stoichiometry of the complex is likely 1:1:1:1. Presenilin is the subject of endoproteolytic cleavage as shown, one N-terminal fragment (NTF) of 35kDa and one C-terminal fragment (CTF) of 20kDa is produced, this activation step is necessary to exert its function as the catalytic core of the complex. APH1 is a 30kDa protein with seven transmembrane domains; PEN2 is a small protein of 12kDa with two transmembrane domains and nicastrin whose molecular weight is 100kDa, highly glycosylated and recruits substrates for the complex. Source: Kopan et al., 2014 (Kopan and Ilagan 2004).

Activation of microglia can be counteracted by pharmacological treatments in an APP/presenilin 1 (PS1) transgenic mouse model, which had improvements in behavior and did not show any difference in accumulation of Aβ when fed with GW2580, an CSF1R inhibitor, demonstrating thatthe removal of Aβ is not necessary to stop the progression of the disease, at least in their model (Olmos-Alonso et al. 2016).

Despite all the controversy, there is progressively more consensus about considering the disease a multi-factor syndrome than just the consequence of a single failure (Iqbal and Grundke-Iqbal 2010; Carreiras et al. 2013; Alagiakrishnan, Gill, and

Fagarasanu 2012; Sheikh et al. 2013). Aβ and tau accumulation are still central in the pathological process, but other factors are also critical, especially in the prodromal phase, and they also must be targeted to develop effective therapies.

1.2 Familiar Alzheimer´s Disease

Advances in genetic screenings have allowed the identification of around 20 genes associated with the development of sporadic Alzheimer´s disease (SAD). Despite that, only ApoE4 haplotype is established as a genetic risk factor, conferring the highest susceptibility to develop the sporadic and most common form of the disease with approximately 50% of the risk. Mutations in genes such as BIN1, PICALM, ABCA7, EPHA1, SORL1, CD2AP, and TOMM40, among others, confer only up to 10-15% of the risk to their carriers (Karch, Cruchaga, and Goate 2014). This genetic profile includes genes involved mainly in inflammation, microglia and immune control (Sala Frigerio and De Strooper 2016). It is not clear which molecular mechanisms are behind them and other factors, like the environmental and socio-economic conditions of the individual, which play a role, since the educational degree influences the occurrence of the pathology in some studies and populations (Burke et al. 2017; Zhang et al. 1990; Katzman 1993).

The discovery of genes causing the pathology was striking to the field and brought the possibility to study AD from another perspective. Less than 1% of cases in AD are inherited, and those cases are considered early-onset, or familial Alzheimer´s disease (FAD)(Van Cauwenberghe, Van Broeckhoven, and Sleegers 2016). Dementia develops before 65 years of age and mutations in APP, PS1 and presenilin 2 (PS2) are responsible for the pathology.

To date, 219 FAD-causing mutations in PS1 on chromosome 14 have been reported. Mutations in PS2 are less common, and the age of onset is widely variable, also correlated with a high clinical variation; only 16 mutations have been reported on chromosome 1 and 51 in APP on chromosome 21 **(www.molgen.ua.ac.be)**. They are fully penetrant; one mutant allele is enough to trigger the disease in the individual carrying the mutation (De Strooper, Iwatsubo, and Wolfe 2012) and most of the mutations cause an increase in Aβ production, aggregation and in the Aβ42/Aβ40 ratio (Tanzi 2012).

In this study, the mutations E280A and G384A will be examined. E280A is a mutation found in Colombian and in the Japanese population. The clinical presentation is widely variable; patients present Purkinje cell loss and an endophenotype of cerebellar ataxia (Lemere et al. 1996). With analysis of postmortem cerebella of patients carrying this specific mutation, it has been found that they have abnormal mitochondria, lower levels of expression of some Ca^{2+} channels and proteins related to mitochondrial transport (Sepulveda-Falla et al. 2014).

G384A is a mutation identified in a Japanese (Tanahashi et al. 1996) and in a Belgian family, known as family AD/B. It is located in the sixth hydrophilic loop of the transmembrane domain of PS1 (Cruts et al. 1995) (Figure 3) and *in vitro* studies have shown that the mutation impairs γ-secretase cleavage, but not the ε-cleavage, increasing the Aβ42/Aβ40 ratio. A study from Sun et al. involving the production of Aβ in 138 pathogenic PS1 mutations showed that G384A produces the highest Aβ42/Aβ40 ratio among all of them (Sun et al. 2017). Clinically and pathologically, patients with this mutation show the common SAD features with an age of onset at around 35 years (Martin et al. 1991).

1.3 Presenilin 1

PS1 is one of the three genes whose mutations cause Alzheimer´s Disease. It is a 50kDa integral membrane protein that has nine transmembrane domains (Figure 3). It is the subject of different post-translational modifications, including endoproteolysis; a necessary process to activate its function as the catalytic core of γ-secretase. The protein can be phosphorylated by different kinases (PKA, PKC, GSK3β, JNK, CDK5), ubiquitinated and cleaved by caspases (Walter 2015). Its homolog, PS2, shares 67% of the protein sequence. As a member of the γ-secretase complex, its role as the catalytic component of the complex has been widely studied (De Strooper, Iwatsubo, and Wolfe 2012; Sobhanifar et al. 2010; Fernandez et al. 2014).

PS1 expresses widespread in mouse and human tissues, but mRNA is abundant in the developing brain (Lee et al. 1996). At the cellular level, it is abundant in the

endoplasmic reticulum (ER) and the trans-Golgi network in the cell body and dendrites of neurons (Cook et al. 1996) but the γ-secretase cleavage takes place in the plasma membrane. The inconsistency between the localization of γ-secretase activity in a compartment different from which PS1 is found is also known as the "spatial paradox." For example, the C99 isoform of APP is not found in the ER or Golgi and, Aβ is generated at the cell surface and in endosomes (Cupers et al. 2001). Although the knowledge in the molecular biology of PS1 has advanced, to date the mechanism by which its mutations produce dementia is not well understood. In the case of FAD, the disease develops at an early age and, the accumulation of β-amyloid is not significant in those initial stages. The overproduction of Aβ42 has shown to be determinant for the development of neurodegeneration in transgenic mice (Kitazawa, Medeiros, and Laferla 2012), which suggests that other molecular pathways are relevant for triggering AD.

Recently, numerous studies have suggested that PSs are part of several biological events that are not linked to its catalytic function in γ-secretase (Figure 4). Those functions include stabilizing catenin in the Wnt signaling pathway, regulation of Ca^{2+} homeostasis, interaction with synaptic transmission, lysosomal function and autophagy (Duggan and McCarthy 2016).

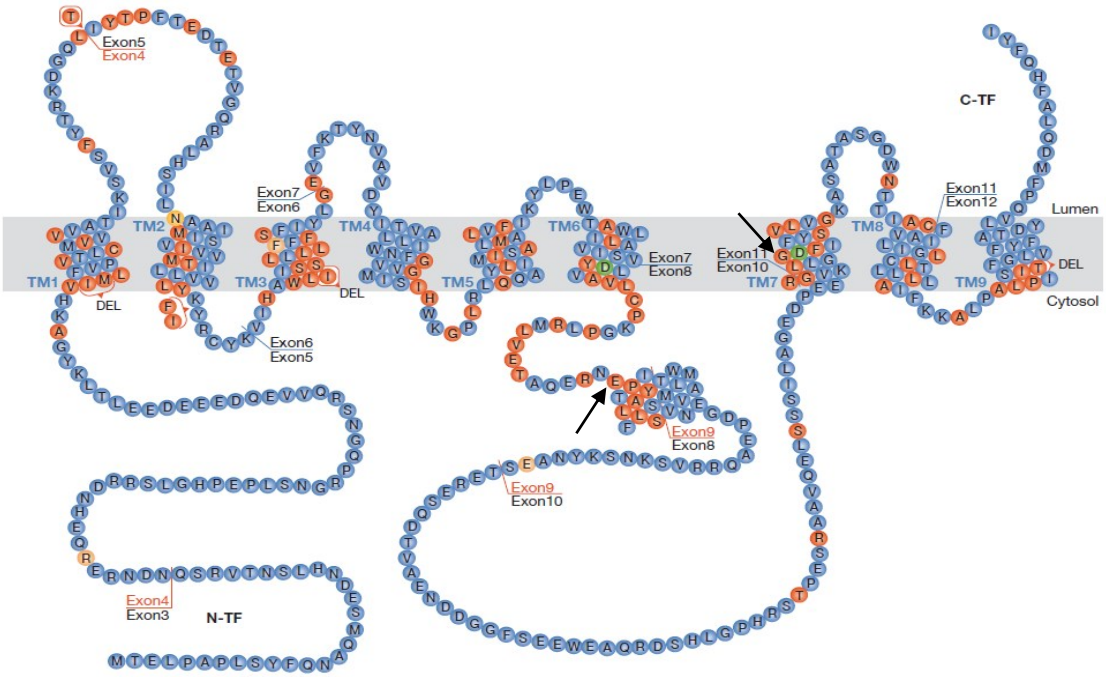

Figure 3. Presenilin 1 structure. The protein spans the membrane nine times, in red are represented the mutations that have been reported in FAD. Mutations E280A and G384A localize in exons 8 and

11, respectively (arrows pointing), as indicated in the figure. Image adapted from Hardy 2007 (Hardy 2007).

The knockdown of PSs in mice causes neurodegeneration, impairments of memory and synaptic function at two months of age and, behavioral deficits related to spatial and associative memory at six months; changes that were associated with decreased levels of the NMDA receptor (Saura et al. 2004). PSs functions were evaluated in plants lacking Notch to counteract the effect that the loss of PSs homologs could exert in the signaling of this critical receptor, and it was found that the absence of PSs in this system contributed to an abnormal phenotype, which could be rescued by the re-introduction of human PS1 (Khandelwal et al. 2007).

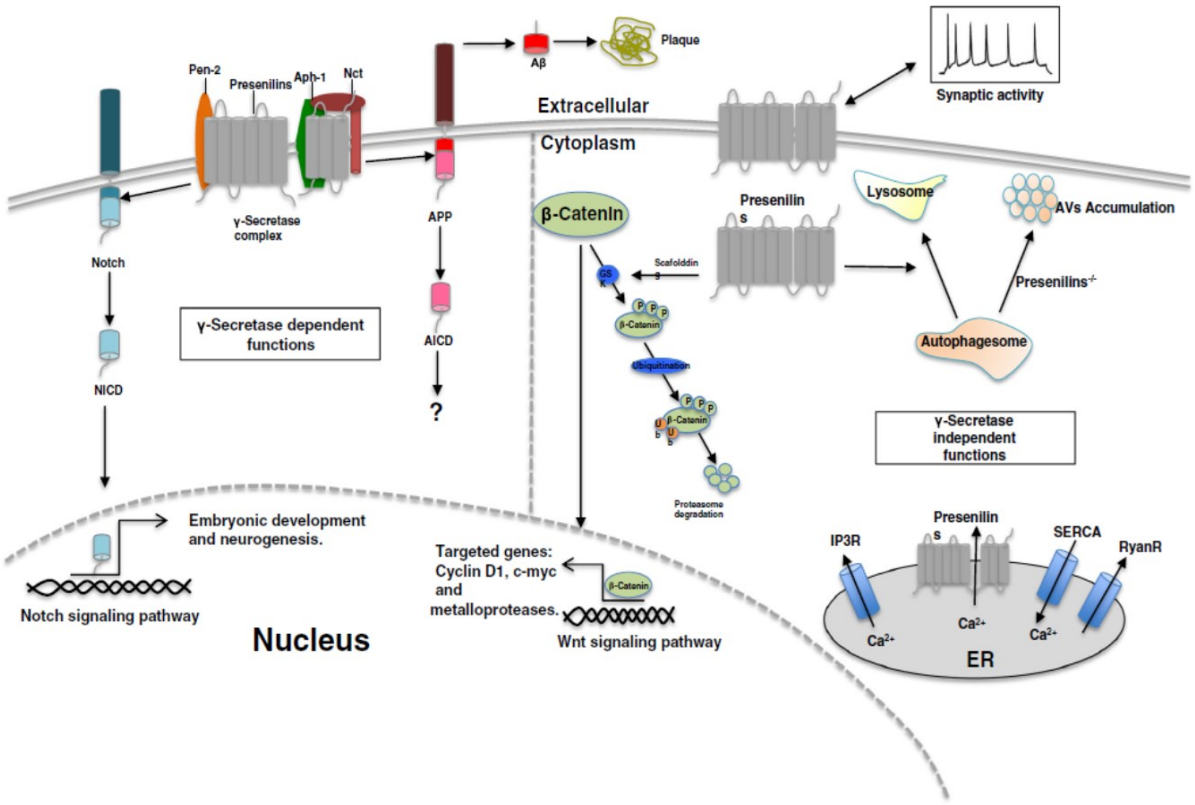

Figure 4. **Dependent and independent γ-secretase roles of PS1.** The graphic summarizes the biological functions in which PSs are involved. In the left part, it is represented the active role of PS1 in the γ-secretase complex, that executes the cleavage of Notch1 and APP, among approximately 90 other transmembrane I proteins. NICD and AICD are the products of the γ-secretase cleavage of Notch1 and APP, respectively. The Notch Signaling Pathway has been characterized thoroughly, and it is well known for its function in embryonic development and neurogenesis. The exact role of AICD remains to be determined. In the right part of the figure, γ-secretase-independent functions are represented including synaptic activity, autophagy, Ca^{2+} homeostasis regulation and, β-catenin signaling. Source: Zhang, et al., 2013 (Zhang et al. 2013).

Among the most well-characterized and interesting γ-secretase independent functions of PS1, is the alteration of autophagy function in deletion or knockdown models. In null PS1 blastocysts and neurons, macroautophagy turnover of proteins is impaired. Moreover, PS1 is necessary for lysosome acidification (Lee et al. 2010). When PSs are deleted, aggregated proteins cannot be eliminated and, the formation of autophagosomes is not observed in other cell models (N2a and fibroblasts). Furthermore, the treatment with inhibitors of γ-secretase does not affect autophagy, pointing to a mechanism independent of γ-secretase activity (Neely, Green, and LaFerla 2011). Similar results were found in human neural stem cells (Chong et al. 2018) which emphasizes the importance of this mechanism in humans and its relationship with AD. Also, mutant and wild type (WT) PS1 can rescue the turnover of β-catenin (Kang et al. 1999; Zhang et al. 2013) and interact with it via its C-terminal portion (Murayama et al. 1998), but further details about the molecular mechanism behind this function are yet to be discovered.

One of the most studied γ-secretase independent functions of PS1 is the one related to Ca^{2+} control. Ca^{2+} concentration in cells is critical and carefully controlled in different ways. Mutations in PS1 dysregulate Ca^{2+} signaling through its interaction with the IP3R channel, promoting Ca^{2+} leaking from the ER (Cheung et al. 2008). Also, PS1 was considered by some researchers as a Ca^{2+} channel itself because of its structure (Tu et al. 2006; Nelson et al. 2007), supporting the Ca^{2+} hypothesis of AD, but, later, it was challenged in a study that involved primary cortical neurons, primary PS cDKO B cells, and MEF DKO cells. In none of the models used, was ER Ca^{2+} leaking different compared to cells with WT PS1 (Shilling et al. 2012). The controversy is still open and more details into the ultrastructure of PSs could help to clarify this specific point.

1.4 Mitochondrial Dysfunction

Mitochondria are well-known for their role as the ‘power center’ of the cells, but they do have other roles: cellular homeostasis, apoptosis, iron processing, Ca^{2+} buffering and steroid synthesis, to name a few. They are versatile, dynamic and multifunctional organelles, with their own DNA. They modify their morphology and have a specialized quality control mechanism to remove damaged or non-functional

mitochondria, called mitophagy, a process in which the proteins Pink1 and Parkin play a fundamental role, by triggering the signal that targets unhealthy mitochondria and directs them to elimination, through autophagy (Friedman and Nunnari 2014).

The relationship between mitochondria and neurodegenerative diseases is widely known and has been discussed extensively (Burte et al. 2015; Chen and Chan 2009; Kawamata and Manfredi 2017). Not only metabolic abnormalities are related to those diseases but failure in synaptic transmission is another pathological condition in AD and mitochondria are central in this process (Guo, Tian, and Du 2017). Distribution of mitochondria is critical in neurons, and their high demand of energy implies great ATP production. Mitochondrial presence at the synapse is relevant to modulate Ca^{2+} signaling, which is determinant in synapse transmission (Course and Wang 2016).

Although some evidence points to an active accumulation of Aβ in the mitochondria (Caspersen et al. 2005; Lustbader et al. 2004; Devi et al. 2006; Hansson et al. 2004; Hansson Petersen et al. 2008; Chen and Yan 2010), the question about its direct production within the organelle was addressed. At least in cells, the presence of γ-secretase activity in mitochondria was challenged (Mamada et al. 2017), no colocalization of PS1 and Tom20 was found and also a very low expression of proteins such as BACE, APP, and nicastrin was detected in isolated mitochondria.

However, the role of mitochondria in neurodegeneration is complex. One of the main risks for having this type of disease relies on aging, a process closely connected with mitochondrial function. Since these organelles control the production of energy, and one of the critical features of neurodegeneration involves slow brain metabolism, also featured in aging, many researchers have proposed that mitochondrial dysfunction contributes from early stages in life to the accumulation of ROS that are potentially harmful (Manoharan et al. 2016; Huang, Zhang, and Chen 2016).

Despite this controversy, recent evidence demonstrates that mitochondria could have another relevant role concerning the removal of unfolded proteins. Experiments made in worms proved that increasing the expression of genes related to the mitochondrial unfolded protein response diminished the aggregation of Aβ (Sorrentino et al. 2017). How exactly this takes place is not known, but the importing of misfolded proteins into mitochondria presents an exciting and newly discovered

mechanism that suggests that unstable cytosolic proteins are taken into mitochondria, providing a new function for this multitask organelle, working in this case as a scavenger (Ruan et al. 2017).

The importance of mitochondria in cellular homeostasis is unquestionable, and they cannot be set aside when promoting healthy aging. To date, it is unclear if their dysfunction in neurodegeneration is a cause or a consequence but increasing evidence has shown that they are relevant in crucial cellular processes directly related to those widely documented in neurodegenerative diseases.

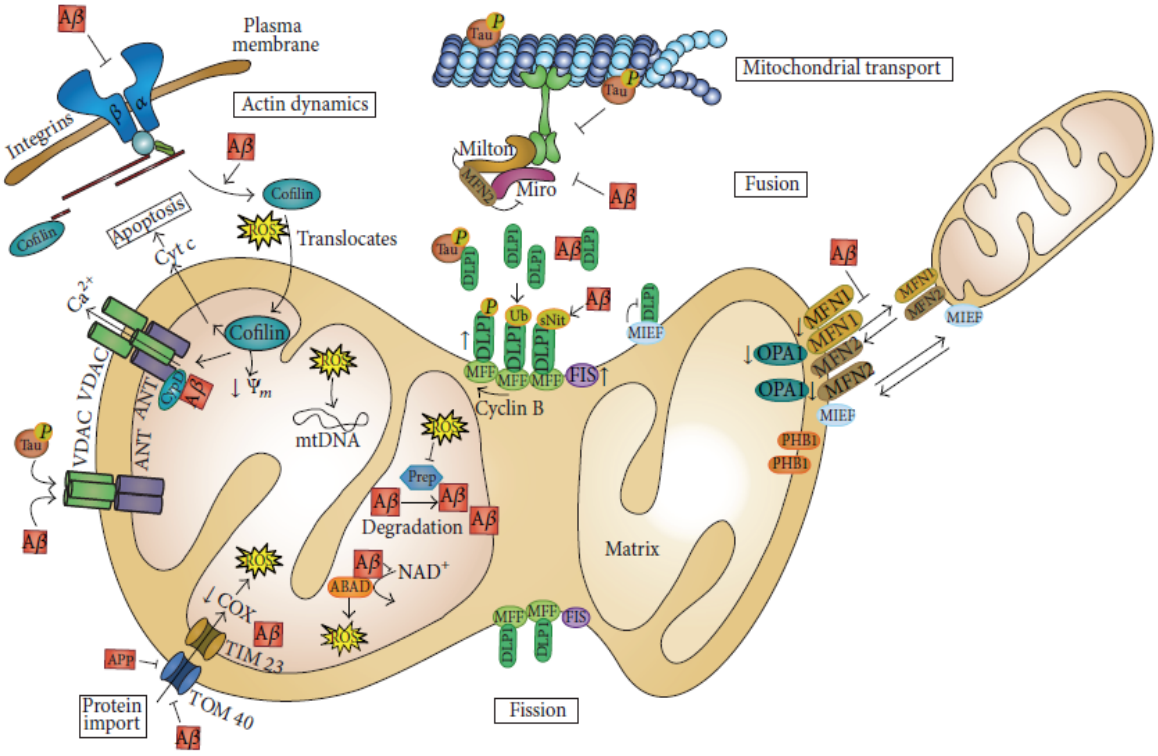

Figure 5. Schematic representation of the mitochondrial processes affected in AD. The figure summarizes the multiple cellular functions in which mitochondria have been reported affected in AD by Aβ. The accumulation of the peptide interferes with almost all the cellular functions of mitochondria from transport, apoptosis, Ca^{2+} buffering, protein import and mitochondrial dynamics (fusion and fission). Although the contribution of mitochondria to neurodegeneration could be a consequence of Aβ toxicity, the current additional functions performed by mitochondria place them in a central place, at least in the early stages of the disease. Source: García-Escudero et al. 2014 (Garcia-Escudero et al. 2013).

1.5 Presenilin 1 and its relationship with Mitochondria

PS1 has been found in very different locations inside the cell. PS1 is mainly an ER-trans-Golgi protein, but Ankarcrona et al. found PS1 also in mitochondria (Ankarcrona and Hultenby 2002). This pioneering study found PS1 localized in mitochondrial membranes through western blot (WB) and immunoelectron microscopy in rat brain. Their findings were reproduced in another study, in which other members of the γ-secretase complex were also found in this organelle (Hansson et al. 2004).

It has been shown that the deletion of PS1 and PS2 or their mutations affect mitochondria performance, although their effect is differential (Behbahani et al. 2006). PS1 lacks a mitochondrial targeting sequence, so presumably its presence there is due to interaction with other mitochondrial proteins such as FKBP38, a protein that forms macromolecular complexes with the anti-apoptotic protein Bcl-2 (Wang et al. 2005); monoamine oxidase A (Wei et al. 2012) and Bcl-X_L (Passer et al. 1999).

More recent findings indicate that PSs are enriched in ER membrane portions closely associated with mitochondria, the mitochondrial associated membranes (MAMs) (Area-Gomez et al. 2009). MAMs were first visualized by electron microscopy and, in 1973, it was reported that fractions of mitochondria were isolated together with components of the ER that were tightly associated (Lewis and Tata 1973). However, only until 1990, Vance et al. published a formal protocol to isolate specifically those membranes (Vance 1990). Initially, MAMs were found to be where lipid transport takes place with no involvement of vesicles, mainly in the import of phosphatidylserine into mitochondria, whose inner membranes are enriched in phosphatidylethanolamine (Vance 2014).

Later, the importance of the communication between the mitochondria and the ER was discovered, especially concerning the control of Ca^{2+} concentrations in the cell via IP3R and SERCA channels in the ER and the mitochondrial uniporter (MCU) (Krols, Bultynck, and Janssens 2016). Proteins like IP3Rs are found in these membranes as well as the receptor chaperone Sigma 1, which controls calcium signaling in a complex with IP3R (Hayashi and Su 2007).

MAMs are considered 'hotspots' for the signaling of Ca^{2+} (Csordas et al. 2010; Giacomello et al. 2010), a process that is vital for the cell, since the accumulation of Ca^{2+} inside the organelle leads to the liberation of cytochrome c, which triggers apoptosis (Gogvadze et al. 2001); while, basal concentrations are a signal of normal ATP production and metabolism. More functions can be attributed to the close contacts between mitochondria and ER, like lipid homeostasis, mitochondrial dynamics, autophagy, and mitochondrial biogenesis, indicating that MAMs are now considered signaling platforms (Area-Gomez 2014).

The localization of PSs in the MAMs led to the formulation of the "mitochondrial cascade hypothesis" which states that mitochondrial alterations are the initiators of AD. This hypothesis could explain some of the pathological features of the illness, especially those related to metabolism, but, of course, it has weaknesses and cannot explain all disease events. Against this hypothesis is the fact that individuals with purely mitochondrial diseases do not develop AD, besides which the mitochondrial dysfunction phenomena is shared by other neurodegenerative disorders without featuring dementia (Area-Gomez et al. 2018).

The accumulation and expression of C99 have been reported to be found in MAMs (Pera et al. 2017), without further confirmation. One key question regarding PS1 dysfunction and its impact in mitochondrial function is to what extent this might be due to loss of function of γ secretase activity and if, there is γ-secretase activity in the mitochondria or in the membranes that crosstalk with the ER.

1.6 Mouse models in FAD and SAD

Several animal models have been developed to study AD. AD transgenic mice models are very diverse, with some presenting with Aβ plaques and neurofibrillary tangles. The overexpression of both human APP and PS1 has been used and, although they show some similarities, there are considerable differences between models in terms of plaque deposition and the severity of the phenotype. Those mice are considered the first generation of AD models, but the single PS1 transgenic mice do not exhibit amyloid plaques, only when crossed with APP mutants is Aβ accumulation evident (Elder, Gama Sosa, and De Gasperi 2010).

The efforts to produce mouse models entirely resembling the pathology in humans have led to the development of transgenic animals carrying simultaneous mutations in the different genes associated with AD; these are known as second-generation mice lines. They have mutations in the endogenous APP gene (the most commonly used, the Swedish mutation K670N) and, in some cases, mutations in PS1. They produce Aβ plaques and, in specific lines, present cognitive impairment before the appearance of Aβ depositions (Sasaguri et al. 2017).

The triple transgenic mice (3x-TgAD) are produced with mutations in APP, PS1 and tau protein (Oddo et al. 2003). This model displays some of the characteristics of the disease, but those features are present at an early stage. The same problems are present in the 5xFAD mice model, which was designed with three mutations in the APP gene and two in PS1 (Oakley et al. 2006). This aggressive genotype overproduces Aβ in such a strong manner that beta-amyloid deposition impairs behavior and leads to neuronal loss at two months of age in the absence of neurofibrillary tangles.

Although most of the findings in the field could not have been achieved without these overexpression models, their limitations open questions about the physiological relevance of all the results reported in them. In general, the first-generation mice present a moderate behavioral phenotype, neuronal loss in some models and Aβ accumulation at an early stage. The disadvantages of those models are diverse, such as the random integration of the transgene, the overexpression artifacts and a mixed genetic background in some cases.

The features of the disease only have been observed when human APP is overexpressed and the levels of expression of the protein do not correspond to the physiological ones. Additionally, it is not clear to what extent the presence of plaques in mice is correlated in the same way with the plaques in humans, because humans can present cognitive decline before the appearance of depositions (Nelson, Braak, and Markesbery 2009); however, the presence of plaques is necessary for mice to observe drastic behavioral impairment (Hanna et al. 2012).

The use of the first generation of mice has provided valuable knowledge about AD. Indisputably, research in these mice provided most of the information concerning Aβ

pathology and the inhibition of γ-secretase activity as a therapeutic target. Different substances have been tested in these models to reduce Aβ levels in the brain and the cerebrospinal fluid (CSF) with success (Tucker et al. 2015), and the side effects observed in human clinical trials were predicted in mice models with APP overexpression (Van Dam and De Deyn 2011).

The so-called second generation of transgenic mice for AD was developed by the selective modification of the gene in its normal position. Although they express mutations in APP or PS1 in endogenous levels, they still do not represent the clinical presentation of human AD. For example, APP knock-in mice with Swedish mutations and with humanization of the Aβ murine sequences (murine Aβ differs in three amino acids with the human version), overexpressed Aβ42 (Reaume et al. 1996) but failed to deposit this peptide in the brain (Elder, Gama Sosa, and De Gasperi 2010). However, when crossed with the PS1 mutant, they developed Aβ plaques (Elder et al. 2010).

In general, APP and PS1 single knock-in models, present a minor behavioral phenotype, with no neurofibrillary tangles (NFT) or neuronal loss. Some discrepancies in molecular mechanisms between what has been found in first-generation mice and second-generation mice have been reported (Saito et al. 2016; Jankowsky and Zheng 2017), but many others have been confirmed (Saito et al. 2014; Sasaguri et al. 2017; Nakazono et al. 2017; Malthankar-Phatak et al. 2012; Zhang et al. 2007). These models are considered pre-clinical, such as the single overexpression ones. It should be remarked that the sequences and the isoforms of Aβ, ApoE, and tau differ between species, as well as their accumulation or potential toxicity.

Differences between the murine and human immune systems should also be considered, and even gender differences in the amyloid accumulation of transgenic mice have been reported, with females showing a higher deposition in the hippocampus compared to males (Wang et al. 2003).

In conclusion, to date, there is no perfect model for AD that fully represents the human disease. Each model has limitations, and, for that reason, there is no common use of a specific one and special care must be taken when interpreting the

data. Despite this fact, transgenic mice continue as the primary tool for research and the understanding of neurodegenerative diseases such as Alzheimer´s. Although very sophisticated worms, flies and yeast can solve molecular or cellular questions, from the neuropathological point of view, those models are far from representing what it is observed in humans.

2. Objectives

This project focuses on the study of the role of PS1 point mutations in mitochondria morphology, function and biology, beyond the well-characterized role of PS1 in the γ-secretase complex.

The project was divided in three parts, which are the aims of this study:

1. The characterization of the phenotype of two transgenic mice with single mutations in human PS1.
2. The study and the analysis of the mitochondrial biological changes after impaired function of human PS1.
3. The investigation of the molecular mechanism behind the modulation of mitochondrial function by PS1 mutations.

3. Materials and methods

3.1 Cell Culture and Transfection

Murine Neuroblastoma N2a cells were stably transfected with pcDNA 3.1 Zeo + vector using 5 µg of 4 different plasmids: mock (empty vector), human PS1WT, PS1E280A and PS1Δ9 (PS1 exon 9 deletion). Transfection was performed with lipofectamine™ 2000, according to the manufacturer's instructions. The clones were established by selection with Zeocin (Invitrogen, Carlsbad, CA, USA). The dose used for selection was 200 µg/mL. Positive clones were isolated after approximately 30 days. Overexpression of PS1 was assessed via WB and quantitative polymerase chain reaction (qPCR) for human PS1. Cells were cultured in Dulbecco's Modified Eagle Medium (DMEM) supplemented with 10% fetal bovine serum (FBS) and kept in a 5% CO_2 incubator at 37°C.

3.2 Transgenic Mice

Two different transgenic mouse lines were used: ps45 (B6, D2-Tg (Thy1Ps1)45/18Npa mice) and ps68 (B6-Tg (Thy1-PSEN1*E280A)68Npa mice), expressing human PS1 (hPS1) with the point mutations G384A and E280A, respectively. Both lines were kindly donated by Dr. Matthias Staufenbiel. The transgenes were introduced under the control of the Thy-1 promoter in both lines; therefore, the expression of hPS1 is restricted to neurons (Caroni 1997). Breedings were done on a C57BL/6 background. Littermates were used as “normal” controls. Biopsies were taken from tails or ears, and standard PCR was performed to genotype each animal, primers used are listed in Table 1. For experiments, mice were anesthetized with 2-Bromo-2-Chloro-1,1,1-Trifluoroethane and euthanized via decapitation. All procedures were approved by the *Behörde für Gesundheit und Verbraucherschutz Hamburg* in accordance with the German Animal Welfare Regulations.

3.3 RNA extraction and qPCR

Total RNA was isolated from cells with the RNeasy Mini Kit (Qiagen, Hilden, Germany) according to the manufacturer’s instructions. The isolated RNA was then treated with DNase I (Invitrogen, Carlsbad, CA, USA). 500 ng of total RNA was

reverse transcribed with RevertAid H Minus First Strand cDNA Synthesis kit K1632 (Thermo Fisher, Waltham, MA, USA) using OligodT´s. cDNA templates were diluted ten-fold before performing qPCR. The primers used for hPS1 are listed in Table 1 (Greenough et al. 2011); qPCR was performed on a RotorGeneQ (Qiagen, Hilden, Germany) with Maxima SYBR Green/Fluorescein qPCR Master Mix K0242 (Thermo Fisher, Waltham, MA, USA). Results were analyzed using the ΔΔCt method (Kubista et al. 2006; Livak and Schmittgen 2001).

Table 1. Sequences of the primers for PS1 and Actin used in this study.

Gene of Interest	Primer Sequence
hPS1 forward for qPCR	5'-CTGGTGAAGACCCAGAGGAA3'
hPS1 reverse for qPCR	5'-AAACAAGCCCAAAGGTGATG-3'
β-actin forward	5´-GCTTCGCTGTCTACTTTCCA-3'
β-actin reverse	5´-CAGCCCGACTACTGCTTAGA-3´
PsenSe1 for genotyping	5´-CTCATGGCCCTGGTGTTTAT-3´
PsenAse1 for genotyping	5´-GGAAAGTTCCTGGACAGCAG-3´

3.4 Murine Aβ 1-40 and Aβ 1-42 ELISA assay

Sandwich enzyme-linked immunosorbent assay (ELISA) for murine Aβ40 and Aβ42 was performed as recommended by the manufacturer (kits KMB3481 and KMB3441, Thermo Fisher Scientific, Schwerte, Germany). N2a cells overexpressing hPS1 and mock transfected cells were harvested and lysed with lysis buffer (50mM Tris-HCl, 150mM NaCl, 1mM EDTA, 10% glycerol, 1% NP-40 and sodium azide). Protein concentration was determined with the bicinchoninic acid assay (BCA) method, and equal amounts of protein were used for Aβ peptides concentration assessment. Protein lysates were collected and tested with the ELISA kit for each antigen. Samples were measured at 450 nm in a Bio-tek mQuant spectrophotometer (Winooski, VT, USA) and expressed as ng/mg of total protein.

3.5 Primary cell culture

Primary neurons were grown in co-culture with astrocytes for immunofluorescence experiments.

3.5.1 Cultivation of astrocytes

Primary astrocytes were prepared from post-natal day 0 or post-natal day 1 (P0-P1) mice. Mice were decapitated, and brains were taken and placed in dissection

medium (DM). The hippocampus and cortex were separated, and the tissue was incubated with Trypsin 0.25% for 15 min. The trypsinization process was stopped by the addition of glial growth medium (GGM). The tissue was washed with GGM and centrifuged at 1,000 x g during 5 min and triturated to obtain single cells. The suspension was then passed through cell strainers of 70 µm, and the cells were counted and seeded in 75 cm^2 flasks. The astrocytes were kept in culture approximately one month to reach maturation (Jones, Cook, and Murai 2012).

3.5.2 Cultivation of neurons

Neurons were prepared following a modified version of the Banker´s protocol (Banker and Cowan 1979). The experimental procedure was like the one used for astrocytes. Primary cortical and hippocampal neurons were prepared from P0-P1 mice. Mice were decapitated, and brains were taken and placed in DM. The hippocampus and cortex were separated, and the tissue was incubated with Trypsin 0.25% for 15 min. The trypsinization process was stopped by the addition of neurobasal medium (NBM). The tissue was washed with NBM and centrifuged at 1,000 x g during 5 min and triturated to obtain single cells. The suspension was then passed through cell strainer of 70 µm, and the cells were counted and seeded in plates or coverslips previously coated with PLL 1X. Fifty thousand cells were seeded in 24 well/plates for immunofluorescence (IF). For RNA extraction, 600,000 cells per plate were seeded in 6 well/plates. Neurons were grown until day 18 for IF and until day 7 for respiration and RNA extraction.

3.6 Long term potentiation assay

All LTP experiments were performed and analyzed blind to genotype. Mice were anesthetized in 80% CO_2 / 20% O_2 and decapitated. The brain was rapidly removed from the skull and immersed in ice-cold solution containing in mM: choline chloride 110, $NaHCO_3$ 25, D-glucose 25, sodium L-ascorbate 11.6, $MgSO_4$ 7, NaH_2PO_4 1.25, KCl 2.5, $CaCl_2$ 0.5, pH 7.4, 310 to 315 mOsm/kg, saturated with 95% O_2 / 5% CO_2. Ventral side down the cerebellum was trimmed away, and a thin slice of tissue was removed from the lateral surfaces at an angle of approximately 20° from the sagittal plane. After cutting away the prefrontal cortex and dividing the hemispheres along the midline, the cut lateral surfaces were glued with cyanoacrylate to the support of a

Compresstome (VF-200-0Z Microtome, Precisionary Instruments) and filled with 1.2% warm (42°C) low-melt agarose. After rapid cooling, 350 µm sections were cut.

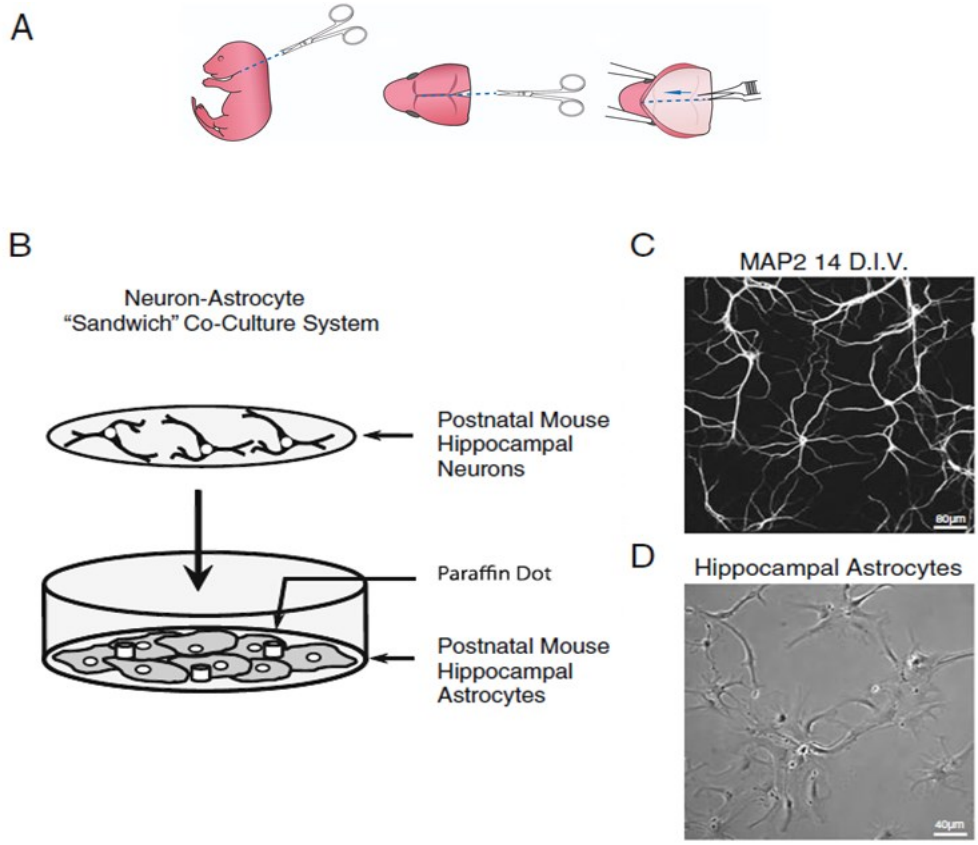

Figure 6. Diagram showing the preparation of primary neurons with astrocytes. Pups from P0 or P1 were sacrificed and their brains extracted as shown in **A**. Drawing adapted from Lian et.al, (Lian, Roy, and Zheng 2016). **B.** The hippocampus was isolated and maintained in DMEM+Glucose to grow astrocytes for thirty days or seeded on coverslips in NBM medium to have neurons in the same plates. Micrographs of neurons in **C.,** and astrocytes in culture in **D**. Sketch modified from Jones et.al, (Jones, Cook, and Murai 2012).

Excess agarose was removed from the sections containing the dorsal hippocampus. Slices were allowed to recover at 33 °C for 15 min in artificial cerebrospinal fluid (ACSF) containing in mM: NaCl 124, $NaHCO_3$ 26, D-glucose, $MgSO_4$ 1, NaH_2PO_4 1, KCl 4, $CaCl_2$ 2.4, pH 7.4, 302-305 mOsm/kg saturated with 95% O_2 / 5% CO_2. The temperature was reduced to 30 °C and the slices were allowed to recover for a further 45 min. The slices were then transferred to the submerged type recording chambers of a 4 chamber Synchroslice (Lohmann Research Equipment) where they

were perfused top and bottom with ACSF with a flow rate of 2.5 mL/min at 30°C for 45 min. Two concentric stimulation electrodes were placed in stratum radiatum on either side of a bipolar recording electrode placed in radiatum near the border with stratum pyramidale.

Electrode position and stimulation intensity were adjusted to evoke field excitatory postsynaptic potentials (fEPSPs) of about 2 mV amplitude. Stimuli (200 μs) were applied every 30 s on each electrode with a 1 s delay between electrodes for 10 min. Input-output responses were obtained, and the stimulus intensity adjusted for each stimulation electrode to evoke a fEPSP of half maximum amplitude. Stimuli were evoked for 20 min. At the end of the 20 min, stimulation intensity was readjusted if necessary, prior to obtaining the baseline.

Responses were recorded at 30 s intervals for 30 min (baseline). To induce potentiation, theta burst stimulation (10 bursts 5 Hz, each burst 5 pulses 100 Hz, repeated three times 30 s intervals) was applied to one stimulation electrode of each slice while the other electrode (control pathway) remained unstimulated. Responses were then recorded for a further hour. The fEPSP slope (10-90%) was measured for each response. The “base” fEPSP slope is the mean of 10 min immediately before TBS, “2” is the mean of 2 min immediately following TBS and “LTP” was assessed 50-60 min after TBS. The tail tips were collected, and re-genotyping was performed to confirm the original assignment of each animal. Unblinding occurred after a final decision was made to include or exclude any data from the analysis.

3.7 Western Blot

Cells were harvested after 24 hours and lysed with a buffer containing 50mM Tris-HCl, 150mM NaCl, 1mM EDTA, 10% glycerol, 1% NP-40 and sodium azide. Total protein brain lysates were prepared after homogenization of the tissue in a douncer and centrifugation at 1,300 x g in sucrose containing buffer. Protein concentration was determined with the BCA method, and equal amounts of protein were loaded into a 12% SDS-PAGE gel and transferred to a PVDF membrane. Membranes were blocked with 5% nonfat milk in TBST for 1 hour and then incubated with specific primary antibodies overnight at 4°C (Table 2). Afterward, blots were incubated with secondary antibodies for 1 h and detected by chemiluminescence.

Table 2. List of antibodies used in this study.

Protein	Reference Number	Dilution	2° antibody	Size (kDa)
NeuN	Millipore MAB377	1:50	Mouse	46/48
Nicastrin	Thermo Fisher PA1-758	1:500	Mouse	110
β-actin	Cell Biolabs	1:5000	Mouse	43
APP	Millipore 171610	1:5000	Rabbit	110
PS1 human	Millipore MAB1563	1:500	Rat	55-35
MAP2	Sigma Aldrich M9942	1:500	Mouse	280
Synaptophysin	Abcam Ab32594	1:250	Rabbit	34
IP3R I/II/II	SantaCruz sc-377518	1:100	Mouse	313/260/ 250
Opa1	BD Biosciences	1:500	Mouse	80-100
KDEL	Enzo 10C3	1:500 (1:100 for IF)	Mouse	94/78/55
FACL4	Thermo Fisher PA5-12225	1:1000	Rabbit	75
Grp-75	Thermo Fisher A305-256AM	1:1000	Rabbit	75
ERO1	Thermo Fisher PA1-46120	1:1000	Rabbit	57
VDAC	Millipore AB10527	1:500	Rabbit	35
Sigma 1-R	SantaCruz sc-137075	1:200	Mouse	30
Tom 20 (for IF)	SantaCruz sc-11415	1:100	Rabbit	20
PS1 (unspecific)	Cell Signaling 3622	1:500	Rabbit	55/22
PS1 (for IF)	Abcam ab-15456	1:50	Mouse	28
GM130	Abcam ab-52649	1:50	Rabbit	112
Lamp1	Thermo Fisher 14-107182	1:50	Rat	120
Mrpl22	Thermo Fisher PA5-38961	1:500	Rabbit	20

Mrpl32	Thermo Fisher PA5-49942	1:500	Rabbit	20
NDUFB6	Abcam ab-110244	1:500	Mouse	15
NDUFB8	Abcam ab-110242	1:500	Mouse	22
Cyt C	Cell Signaling 4272	1:500	Rabbit	14

3.8 Immunohistochemistry

The animals were sedated and perfused with paraformaldehyde (PFA) 4% pH 7.4. Fixed brains were embedded in paraffin and sections of 3-5 µm were cut. The sections were deparaffinized, and antigen retrieval was performed with citrate/EDTA. After hydration and blocking with serum, the sections were incubated with primary antibody against NeuN overnight at 4°C. Sections were rinsed with TBST and incubated with secondary antibody for 30 min at RT. After rinsing and dehydration, sections were mounted on coverslips.

3.9 Electron Microscopy

Electron microscopy was performed in order to analyze mitochondrial ultrastructure and mitochondria and ER contacts. Tissue blocks were fixed in PFA 4%, 0.25% glutaraldehyde in DPBS1X (pH 7.4), cut in 1 µm sections and post-fixed in 1% osmium tetroxide. After that, the tissue was dehydrated in different concentrations of ethanol and embedded in Epon 812 (Serva Electrophoresis, Heidelberg, Germany).

Thin sections were cut and stained with Toluidine Blue, and ultrathin sections of 60 nm were obtained and collected onto grids. Finally, the grids were stained with uranyl acetate and observed under a LEO EM 912AB electron microscope (Carl Zeiss AG, Oberkochen, Germany). Mitochondria were classified as abnormal if they presented discontinued cristae or their entire absence. Morphological analyses were done blinded to genotype.

3.10 Subcellular fractionation of mitochondrial associated membranes

MAMs isolation was performed and standardized from whole mouse brain tissue, following protocols published by Wieckowski et al., and Annunziata et al. (Wieckowski et al. 2009; Annunziata, Patterson, and d'Azzo 2013). Brains were homogenized with 12 passages of a pestle, and the crude mitochondrial fraction (13,800 x g pellet) was subjected to separation on a 30% self-generated Percoll gradient. A low-density band (the MAMs fraction) and a high-density band (mitochondrial fraction) were collected and analyzed by immunoblotting against IP3Rs, KDEL, as ER markers, Grp75 and FACL4 (as MAMs markers), VDAC (as a mitochondrial marker) and Na^+/K^+ ATPase as plasma membrane marker (Table 2). MAMs were collected from 4 months old mice.

3.11 Subcellular fractionation of enriched mitochondrial fractions

Whole brains were dissected from male mice at different age groups (1, 6 and 12 months). The cerebellum was removed, and the tissue was homogenized by 12 passages of a pestle in mitochondrial isolation buffer (MIB, 320 mM sucrose, 1mM EDTA, 10 mM Tris-HCl and protein inhibitors, pH 7.4) and centrifuged at 1,300 x g during 3 min. The pellet was resuspended in MIB, homogenized and centrifuged again. This step was repeated 2 times, and the collected supernatants were combined and centrifuged at 21,000 x g for 10 min. The resulting pellet was dissolved in 15% Percoll in MIB and placed on top of a gradient composed of Percoll at 23% and 40%. After centrifugation at 90,000 x g for 30 min, the interface between 40% and 23% Percoll was recovered, washed with MIB buffer and subjected to centrifugation at 20,000 x g for 20 min to obtain the final mitochondrial pellet. The samples were dissolved in lysis buffer and kept at -80°C until analyses.

3.12 Proteomics

3.12.1 Tryptic digestion

The mitochondrial fraction was prepared for protein analysis using a filter aided sample preparation (FASP) tryptic digestion protocol (Manza et al. 2005).

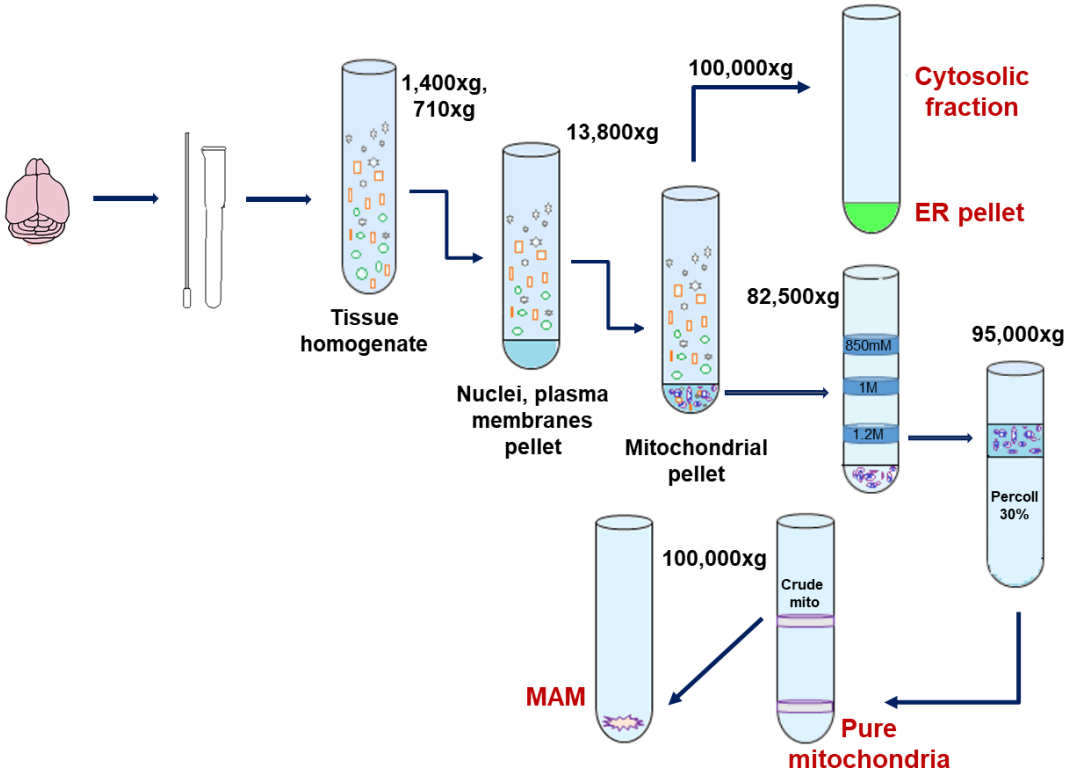

Figure 7. **Schematic representation of MAMs isolation from mice brains.** The graphic represents all the steps involved in the separation of mitochondrial associated membranes in mouse brains. The procedure includes two gradients, the first one using three different concentrations of sucrose and the next one in which Percoll at 30% is used to isolate mitochondrial membranes further.

Briefly, 30 µg of protein were loaded into a 10 kDa centrifugal filter (Merck, Darmstadt, Germany) and denaturated adding two times 400 µL of 6M Urea. The sample was concentrated to a volume of 50 µL by centrifugation (12,000 x g for 10 min). Reduction and alkylation were performed adding 1.3 µL of 100 mM dithiothreitol (DTT) for 10 min at 56 °C followed by 1.3µL of 300 mM iodacetamide (IAA) for 30 min in the dark.

The sample was diluted with 425 µL of 100 mM NH_4HCO_3. For digestion, 0.5 µg trypsin (Promega, Madison, USA) were added to the sample and incubated overnight at 37 °C. Tryptic were recovered by centrifugation at 12,000 x g for 20 minutes. The samples were evaporated to complete dryness with a vacuum concentrator (SpeedVac™, Thermo Scientific, Bremen) and stored at -20 °C awaiting liquid-chromatography/mass spectrometry (LC-MS/MS) analysis.

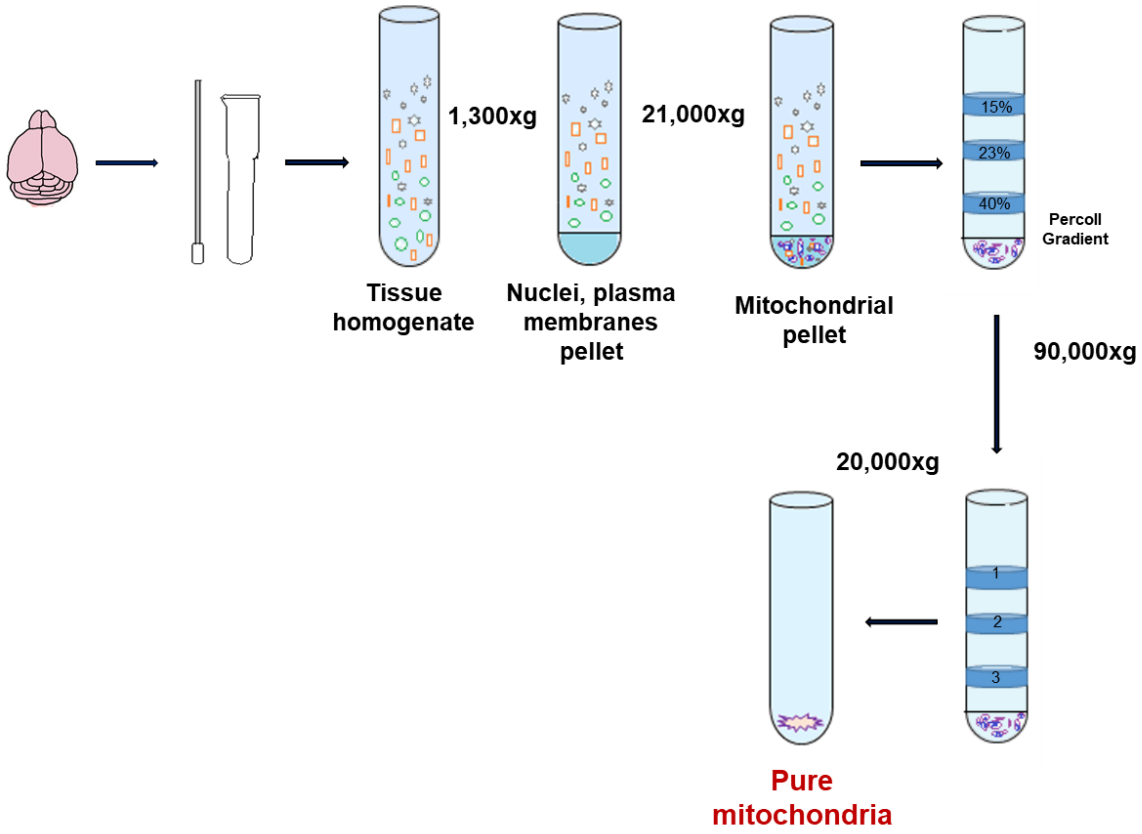

Figure 8. **Schematic representation of the isolation of enriched-mitochondrial fractions from mice brains.** The graphic represents all the steps involved in the isolation of intact mitochondria from mouse brains. The procedure includes a Percoll gradient of 3 different concentrations; mitochondria remain in the 40% phase and must be subjected to an extra centrifugation step at 20,000 x g to obtain an enriched mitochondrial fraction.

3.12.2 LC-MS/MS analysis

Tryptic peptides were resuspended in 30 µL of 0.1% formic acid (FA) and analyzed by LC-MS/MS on a nano-liquid ultra-pressure chromatography system (Dionex ultimate 3000 RSLCnano, Thermo Scientific, Bremen, Germany) coupled to a linear trap quadrupole orbitrap tandem mass spectrometer (Orbitrap Fusion, Thermo Scientific, Bremen, Germany) via nano-electrospray ionization-source (NSI); 2 µL of each sample were loaded onto a trapping column (Symmetry C18 Trap Column; 100 Å, 5 µm, 180 µm x 20 mm, Waters, Eschborn, Germany) and washed with 3% buffer B (99.9% Acetonitrile, 0.1% FA) for 5 min. The peptides were eluted onto a reversed phase capillary column (Acclaim PepMap® RSLC, 75 µm x 500 µm, C18, 2 µm, 100 Å, Thermo Scientific, Bremen, Germany) and separated with a linear gradient from 3 to 22% buffer B in 105 min and from 22 to 32% in 15 min (0.3 µL/min).

Eluting peptides were ionized by NSI (I.D. 10 µm, New Objective, Woburn, USA) at a capillary voltage of 1,800 V. The maximum injection time was 120 ms for an AGC target of 2e5. MS1 was recorded at an m/z range from 400 to 1,300 Da with a resolution of 120,000 FWHM at m/z 200. Data-dependent acquisition was performed in Top Speed mode, fragmenting the most intense precursor ions with an intensity greater than 1e4 with a normalized HCD collision energy of 30 % and a dynamic exclusion of 20 s. Fragment spectra were recorded with a maximum injection time of 60 ms in the ion trap with the first mass set to m/z 120. HPLC-grade water and acetonitrile were obtained from Merck (Darmstadt, Germany). Urea, DTT, IAA, and NH_4HCO_3 were purchased from Sigma-Aldrich (Munich, Germany). FA from Honeywell Fluka (Bucharest, Romania).

3.12.3 Protein identification

LC-MS/MS data were analyzed with Max Quant (Version 1.5.8.3) (Cox and Mann 2008). Protein identification was performed with Andromeda search engine against the Murine (*mus musculus*) SwissProt database (**www.uniprot.org**). The parameters were set as follows: precursor mass tolerance was set to 10 ppm, the fragment mass tolerance was set to 0.4 Da, and two missed cleavages were allowed for peptide identification; a maximum of 5 modifications per peptide and a false discovery ratio (FDR) of 1% were allowed. The carbamidomethylation of the cysteine residues and the oxidation of methionine residues were set as fixed and variable modifications, respectively. The data were analyzed to identify a Gaussian distribution and normalized according to the number of detected proteins. A second normalization step was performed against the mitochondrial proteins Ndufs3, Sdhb, Cytc1, mt-Co2, and Atp5h, commonly expressed in all experimental groups. The package ProStaR 1.12.18 from R software was used to do t-test analyses (Wieczorek et al. 2017) and volcano plots were generated in GraphPad. The website STRING (**https://string-db.org/**) was used to create the protein-protein interaction networks.

3.13 Intracellular Ca^{2+} Imaging

PS1 N2a stably transfected cells were used to measure intracellular Ca^{2+} concentrations using targeted aequorins (AEQs). Fifty thousand cells were grown on

coverslips and transfected with 0.5 µg aequorin-cDNA construct directed to different cellular compartments: cytosolic (cytAEQ), mitochondria (mitAEQ) and ER (ERAEQ). Mitochondrial and cytosolic responses were induced by addition of 100 µM bradykinin (Sigma Aldrich, Munich, Germany) which raises the internal Ca^{2+} levels (Table 3). ER Ca^{2+} re-uptake was measured in Ca^{2+} depleted cells. Cells were reconstituted for 2h at 37°C and 5% CO_2, then the coverslips were placed in a thermostat at 37°C, washed with Ca^{2+}-free Krebs Ringer Buffer (KRB, 135 mM NaCl, 5 mM KCl, 0.4 mM KH_2PO_4, 1mM $MgSO_4$, 20 mM HEPES, 5.5 mM glucose pH 7.4) solution and then stimulated with bradykinin. Cells were lysed with a 10 mM Ca^{2+} and 0.1% Triton containing buffer at the end of the experiment to estimate the efficiency of transfection (Bonora et al. 2013; Coussee et al. 2011). The same experiment was repeated in cells previously treated for 30 min with 250 nM of N-[N-(3,5-Difluorophenacetyl)-L-alanyl]-S-phenylglycine t-butyl ester (DAPT, Sigma-Aldrich, Hamburg, Germany) and 100µM of 2-Aminoethoxydiphenyl borate (2-APB, Sigma-Aldrich, Hamburg, Germany).

3.14 Ca^{2+} imaging

N2a stably transfected cells were used to measure Ca^{2+} concentration using Fluo-4 AM. Fifty thousand cells were grown on coverslips and loaded with 2µM of Fluo4-AM. The experimental chamber was placed on the stage of an upright confocal microscope (LSM 510, Carl Zeiss AG, Oberkochen, Germany) equipped with a water immersion lens (Achroplan 40×, NA 0.75; Zeiss, Oberkochen, Germany) with 2mm working distance, and the preparation was continuously superfused with ARCF. Ca^{2+} recordings started with Ca^{2+} containing buffer, and after 3 min a buffer free of Ca^{2+} was added, then 50 µM of Cyclopiazonic acid (CPA) was applied to inhibit the entry of Ca^{2+} to the endoplasmic reticulum through the SERCA pump. After 10 min of stimulation, the Ca^{2+} free buffer was re-applied, and then the buffer containing Ca^{2+} was reintroduced.

Table 3. List of reagents used in Ca^{2+} and mPTP assays

Name	Company	Mode of action
Bradykinin	Sigma-Aldrich	Bradykinin receptor agonist, stimulates intracellular Ca^{2+} activity, GPCR activation, IP3-dependent Ca^{2+} ER release
CPA	Sigma-Aldrich	SERCA pump inhibitor
Ionomycin	Sigma-Aldrich	Ca^{2+} ionophore
FCCP	Sigma-Aldrich	Oxidative phosphorylation uncoupler

Oligomycin	Agilent-Technologies	Inhibits ATP synthase by blocking its proton channel (F0 subunit)
Rotenone	Agilent-Technologies	Inhibitor of mitochondrial respiratory complex I
Antimycin A	Agilent-Technologies	Inhibitor of electron transfer at complex III. Induces apoptosis
DAPT	Sigma-Aldrich	Inhibitor of γ-secretase, blocks Notch signaling
2-APB	Sigma-Aldrich	IP_3 receptor antagonist. TRP channel modulator, stimulates store-operated Ca^{2+} (SOC) release at low concentrations (< 10 μM) and inhibits it at higher concentrations (>50 μM), Modulator of TRP channels.
Calcein acetoxymethyl ester	Sigma-Aldrich	Cell-permeable dye, fluorescence of calcein is quenched by Co^{2+} in the cytosol but not in mitochondria
Cyclosporin A	Sigma-Aldrich	Calcineurin inhibitor
Compound W	Tocris Bioscience	Inhibitor of γ-secretase; causes a decrease in the released levels of Aβ42 and notch-1 Aβ-like peptide 25 (Nβ25).

3.15 Mitochondrial membrane potential measurement

Mitochondrial membrane potential ($\Delta\Psi_m$) was measured by loading cells with 10 nM Tetramethyl Rhodamine Methylester T-668 (TMRM; Life Technologies, Carlsbad, CA, USA) for 30 min at 37°C. Images were taken on an inverted microscope (NikonLiveScan Swept Field Confocal Microscope (SFC) Eclipse Ti equipped with NIS-Elements microscope imaging software (Nikon Instruments, Melville, NY, US). TMRM excitation was performed at 560 nm, and emission was collected through a 590 to 650 nm band-pass filter. Images were taken every 5 s with a fixed 20 ms exposure time. Carbonyl cyanide p-trifluoromethoxyphenylhydrazone 10 μM (FCCP) an uncoupler of oxidative phosphorylation, was added after 5 min acquisitions to collapse the electrical gradient established by the respiratory chain completely.

3.16 Assessment of mitochondrial permeability transition pore (mPTP) opening

3.16.1 Calcein-Co^{2+} quenching assay

Permeability transition pore complex opening was assayed as previously described (Bonora et al. 2016). Briefly, cells were loaded with 1 mM calceinacetoxymethyl ester and Co^{2+} as instructed by the Image-IT® LIVE Mitochondrial Transition Pore Assay Kit (Thermo Fisher Scientific, Waltman, MA, USA). Cells were then imaged based on 490 ± 20 nm excitation, and 525 nm long pass emission filters on an Axiovert 200M

fluorescence microscope equipped with a 40X water immersion objective (N.A. 1.2, from Carl Zeiss AG, Oberkochen, Germany, LLC). Finally, images were analyzed with MetaMorph® (Molecular Devices, San Jose, California, USA), and quenching rate was calculated as the slope of the fluorescence trace over a period of 60 s after stimulation. This experiment was repeated with cells treated with DAPT, 2-APB (as described before), 1.6 μM Cyclosporin A (CsA) for 30 min and additionally with 10μM of Compound W (Tocris Biosciences, Bristol, England), as a pre-treatment for 48h.

3.16.2 Mitochondrial transmembrane potential

$\Delta\Psi_m$ was assayed as previously described (Bonora et al. 2016). Briefly, cells were loaded with 10 nM TMRM (Life Technologies, Carlsbad, CA, USA) in KRB buffer supplemented with 250 μM sulfinpyrazone, then placed in a humidified chamber at 37°C and imaged with a LiveScan Swept Field Confocal Microscope (Nikon Instruments, Melville, NY, US) equipped with a 60× oil immersion (N.A. 1.4, from Nikon Instruments, Melville, NY, US) every 30 s for 30 min. TMRM fluorescence was analyzed by means of the NIS Elements software package (Nikon Instruments, Melville, NY, US), and depolarization rate was calculated as the slope of the fluorescence trace over a period of 10 min after stimulation.

3.17 Immunofluorescence and mitochondrial morphology

Primary hippocampal and cortical neurons were fixed with pre-warmed 4% PFA + 4% Sucrose for 10 min, then washed three times with PBS 1X for 5 min and permeabilized with Triton X-100 0.25% in PBS 1X for 10 min. Blocking buffer (1% BSA, 2% NDS and Triton X-100 0.25% in PBS 1X) was added for 1 h. Then cells were incubated overnight with primary antibodies. The primary antibody was washed with PBS1X 3 times for 5 min. The secondary fluorescent antibody (Alexa Fluor 555 goat anti-rabbit IgG, 1:500, A-11079 Invitrogen, Carlsbad, CA, USA and Alexa Fluor 488) was added for 2 h. Then the cells were washed again, and one drop of Fluoromount-G™ was applied to each slide. Images were acquired on LCS-SP5 (Leica Microsystems, Wetzlar, Germany) confocal microscope, with an HCX PL APO Lambda blue 63x/1.4 Oil UV objective under illumination with a HeNe laser at 488 nm and 561 nm. Pictures were obtained by using z-stacks of images separated by 0.5 μm along the z-axis. Colocalization was analyzed using Image J software 1.51d (National Institutes of Health, USA). For morphology analyses, the images obtained

by confocal microscopy were contrast optimized and converted to 8-bit images. Mitochondrion was marked to analyze morphological characteristics such as area, perimeter and major and minor axes. Based on these parameters, the Aspect Ratio (AR; the relationship between major and minor axes of the ellipse) of a mitochondrion and its Form Factor (F/F; perimeter 2/4π * area) were calculated (Figure 9). A numeric cut off was applied to divide mitochondria into two groups: fragmented and tubular (Marchi et al. 2017).

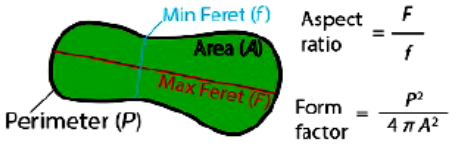

Figure 9. Form Factor and Aspect Ratio. Representation of the meaning in morphological terms of the Aspect Ratio and the Form Factor. Source: Marchi et al., 2017 (Marchi et al., 2017).

The subcellular colocalization of PS1 was addressed also by immunofluorescence in N2a cells with the same protocol described before. Cells were incubated overnight with the following antibodies: PS1 ab-14456; KDEL PA1-013 as an ER marker; Tom20 sc-11415, as a mitochondrial marker; GM130 ab-52649 as a Golgi marker and Lamp1 (Millipore as a marker for lysosomes, Table 2).

3.18 Respiration assays

Assessment of respiration was performed with the use of the Seahorse XF Cell Mito Stress Kit 103015-100 (Agilent Technologies, Santa Clara, CA, USA). Oxygen consumption rate (OCR) and extracellular acidification rates (ECAR) were measured in an XF96 Extracellular Flux analyzer (Seahorse Bioscience, MA USA). Fifty thousand hippocampal neurons were seeded per well 7 days before the experiment on Seahorse XF-96 plates and neurobasal media supplemented with 2% B27 serum. The day of the respiration assay neurobasal medium was replaced for XF Base Medium supplemented with pyruvate, glucose, glutamine and incubated during 1h in a non-CO_2 incubator at 37°C. In all experiments, the medium assay was adjusted to pH 7.4, and the measurements of basal OCR and ECAR were recorded 3 times for 12 min before each injection. 1μM of Oligomycin (ATP synthase inhibitor), 2μM pf FCCP (mitochondrial uncoupler) and a mixture of 1μM of Rotenone/Antimycin

(inhibitors of the complex III of the electron transport chain, ETC) were injected sequentially, and three measurements were taken during 21 min. After completion of each assay, cells were lysed, and the total amount of protein was quantified for normalization. A total of 4 independent experiments were performed.

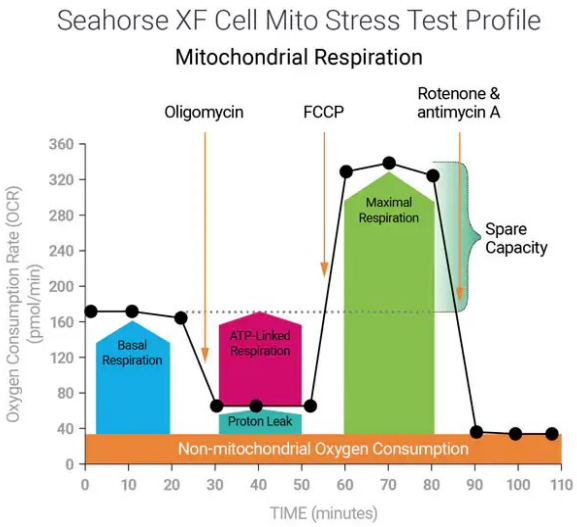

Figure 10. Graph depicting the Seahorse Assay. Oxygen consumption is measured under different conditions. Source: www.agilent.com.

3.19 Statistical Analysis

Data were analyzed by GraphPad Software (La Jolla, CA, USA) using t-tests, one-way or two-way ANOVA, when required, followed by Tukey, Dunn´s or Holms-Sidak post-hoc correction; values are given as mean ± standard error of the mean (SEM). Differences with P-value<0.05 were considered significant.

4. Results

4.1 hPS1E280A and hPS1G384A transgenic mice display a mild phenotype

4.1.1 hPS1E280A and hPS1G384A mice do not show neuronal loss

Despite not exhibiting the complete range of characteristics of the disease, PS1 FAD mice can display a phenotype that differs between mutations. For that reason, it was necessary to characterize the models used here for a better understanding and a more precise interpretation of the results. In this study, we used as controls the littermates of both mice lines that did not carry the transgenes. Neuronal loss is one of the characteristics of dementia, although it depends on the brain region according to the specific diagnosis (Bowen et al. 1979; V. N. Mukhin 2017). Freshly dissected brain tissue obtained from mice at different ages was stained with a neuron-specific nuclei protein (Neu N), and the number of cells, the area that they occupied and neuronal densities in the CA1 hippocampal region and the temporal cortex were quantified (Figure 11). No differences were found between mice lines, at any of the ages considered.

4.1.2 Long term potentiation is enhanced in hPS1G384A mice

Learning and memory are severely affected in AD (Jahn 2013). Deficits in LTP in transgenic mouse models for AD and APP have been reported (Nalbantoglu et al. 1997; Hwang et al. 2017; Chapman et al. 1999; Jacobsen et al. 2006; Balducci et al. 2011) but other researchers have found no significant differences (Fitzjohn et al. 2001; Volianskis et al. 2010; Brown et al. 2005). Hippocampal slices were prepared as described in 3.6 for control, hPS1G384A and hPS1E280A mice of 6 months of age. Quantification of the slope of the fEPSP, the amplitude of the fiber Volley and input/output curves were done. As shown in Figure 12, only the mice carrying the hPS1G384A mutation showed an enhancement in LTP; on the other hand, no difference was found in basal conditions in hPS1E280A mutants.

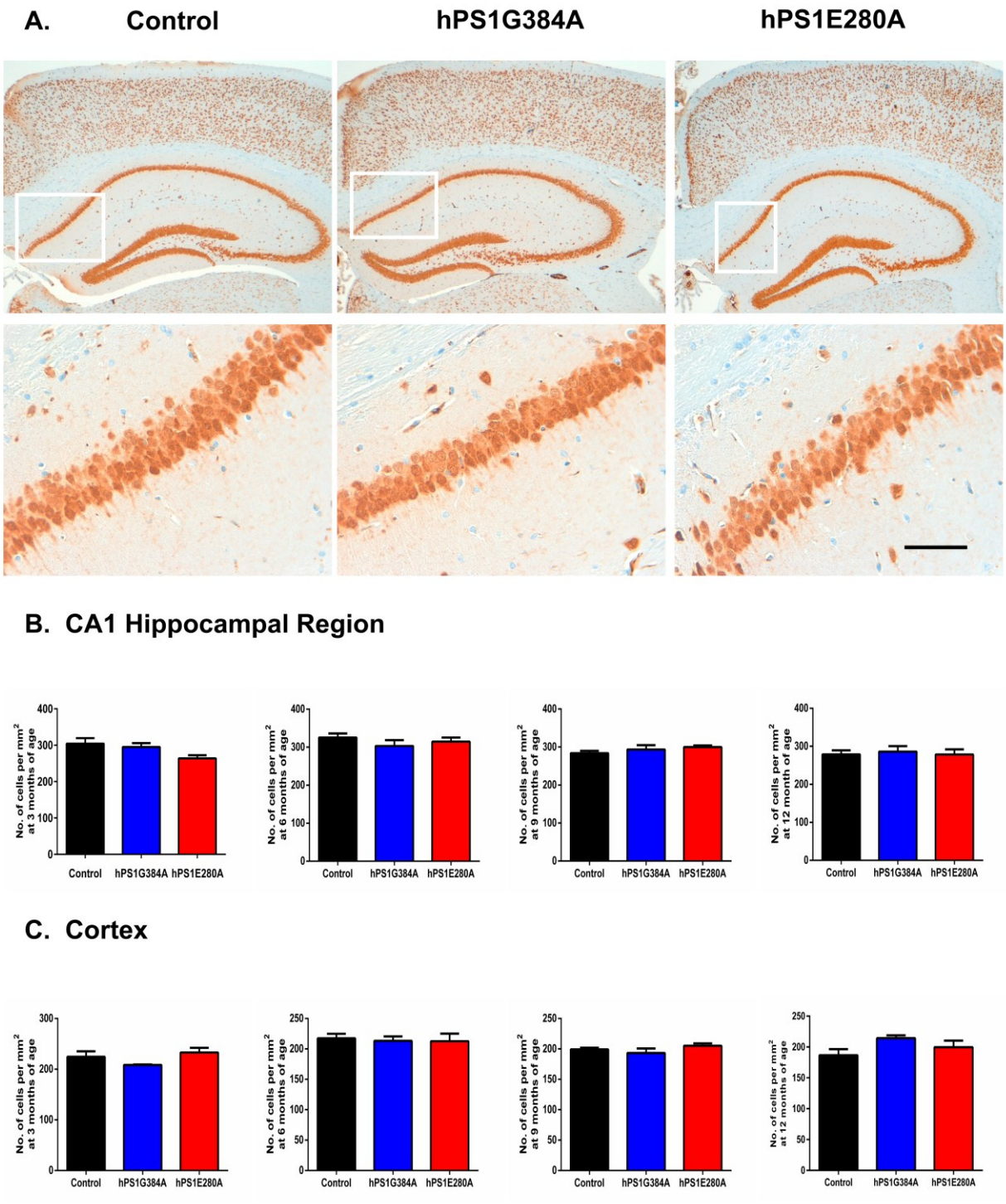

Figure 11. **NeuN immunohistochemistry of the brains of hPS1 transgenic mice. A.** Representative images of the brain regions used to do the counting. Squares represent the areas chosen to quantify the neurons. CA1 hippocampal (**B**) and cortex (**C**) neuronal density in littermates (Control), hPS1G384A and hPS1E280A mice at 3, 6, 9 and 12 months of age. NeuN staining revealed no differences in hippocampal and cortical density, measured as the total number of neurons per mm^2. Data are represented as mean SEM, N=5. Scale Bar: 100μm.

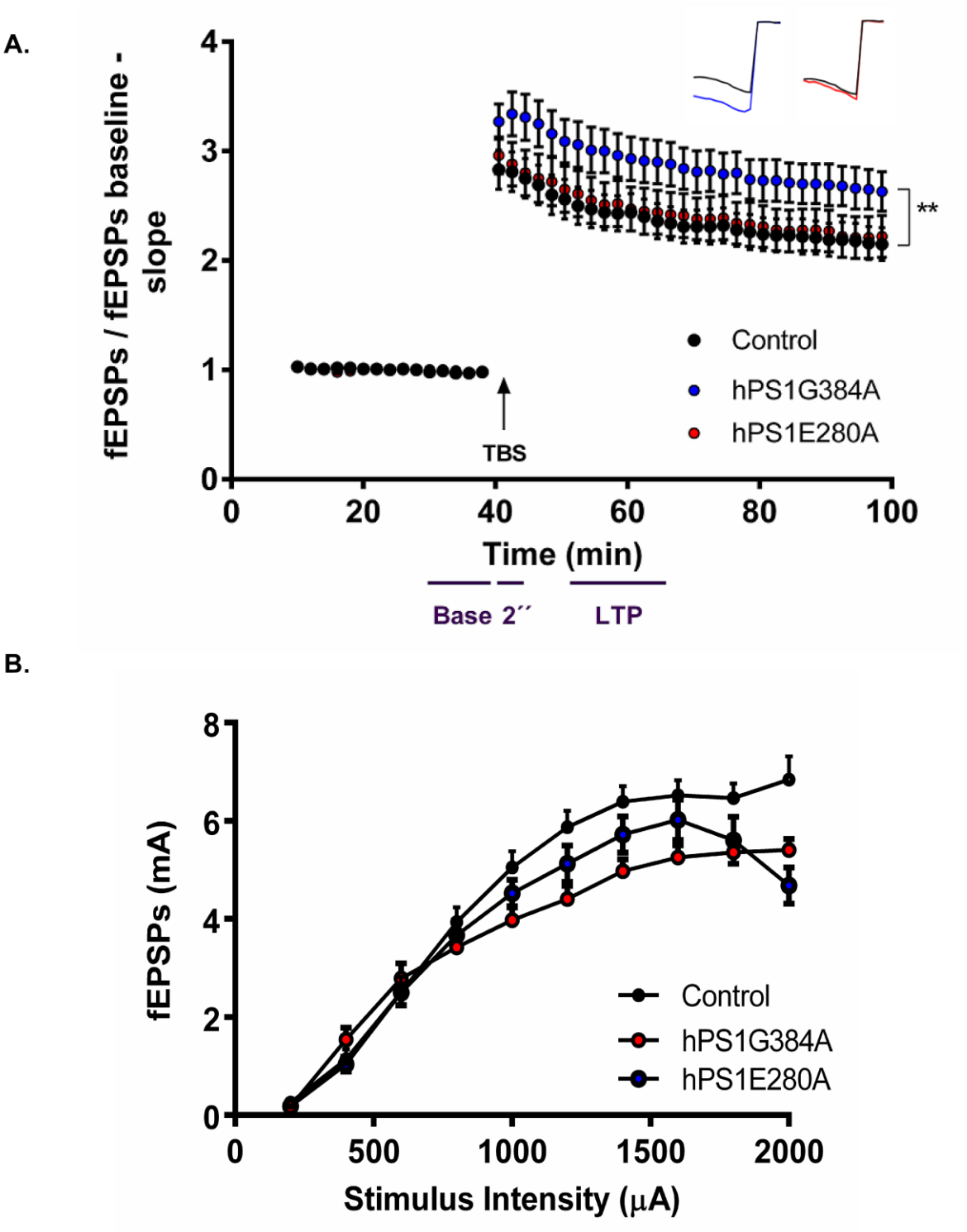

Figure 12. Long term potentiation in hPS1E280A and hPS1G384A transgenic mice. A. Normal synaptic transmission was detected in transgenic mice with the mutation E280A in animals of 6 months of age, but LTP was enhanced in the mice carrying the G384A mutation at the same age. **B.** Input and Output curves. All data are represented as means ± SEM. The number of hippocampal slices and mice was 20 for Controls, 24 for hPS1G384A and 16 for hPS1E280A. The time course is plotted as mean ± SEM normalized to baseline. Statistical analyses (non-parametric) were performed using GraphPad Prism.

4.1.3 Overproduction of Aβ 42 in hPS1G384A mice

Most of the FAD mutations have shown to increase the levels of Aβ42 and to accelerate APP cleavage (Xu et al. 2016; Li et al. 2016; Sun et al. 2017). The expression of some of the proteins that compose the γ-secretase complex was assessed as well as the production of two Aβ isoforms, 40 and 42 (Figure 13). Also, the expression of hPS1 in the mice was confirmed using a human-specific antibody against PS1 (Figure 13A). Both mutations presented an elevation in the Aβ42 levels (Figure 13B), but no effect was detected for the Aβ40 isoform (Figure 13C), the ratio Aβ42/Aβ40 was also calculated (Figure 13D). For both, Aβ42 levels and Aβ42/Aβ40 ratio, elevated values in the hPS1G384A mutation were statistically significant when compared to controls and hPS1E280A mutation. The total amount of protein was quantified and used to normalize the levels of the Aβ peptides.

4.1.4 Decreased number of dendritic spines in transgenic mice

Memory is generated from changes in synaptic structure and strength. The study of synaptic protein turnover is crucial because the proteins responsible for such connections are renovated, with different half-life times (Heo et al. 2018) changing the composition of synapses (Cohen and Ziv 2017). Such proteins accumulate in protrusions called dendritic spines that serve as biochemical compartments for the neurons to regulate plasticity (Nimchinsky, Sabatini, and Svoboda 2002).

Primary hippocampal and cortical neurons were prepared and stained with MAP-2 and Synaptophysin to label dendritic spines after 18 days of differentiation in co-culture with primary hippocampal astrocytes. Previously, the overexpression of hPS1 from day seven after seeding was evaluated with qPCR using human-specific sequences for the gene (Supplemental Figure 1). With the help of the software SynPAnal (Danielson and Lee 2014), three different axons were selected per neuron, and the total number of dendritic spines was quantified (Figure 14). Ten neurons per group and three independent replicates were done, for a total number of 30 cells analyzed in basal conditions. Hippocampal neurons from both PS1 mutant lines showed fewer dendritic spines compared to controls.

Specifically, the number of synaptic puncta was decreased drastically in hippocampal neurons from hPS1E280A mice, with approximately 94% fewer spines compared to controls. The decrease in synaptic puncta was also significant for neurons with the hPS1G384A mutation, in this case showing a reduction of 66% (Figure 14B). These results were validated with the quantification of the intensity of the signal given by Synaptophysin (Figure 14C), showing again less intensity of the signal for both transgenic mice compared to the control and with a more drastic decrease in primary neurons with the hPS1E280A mutation.

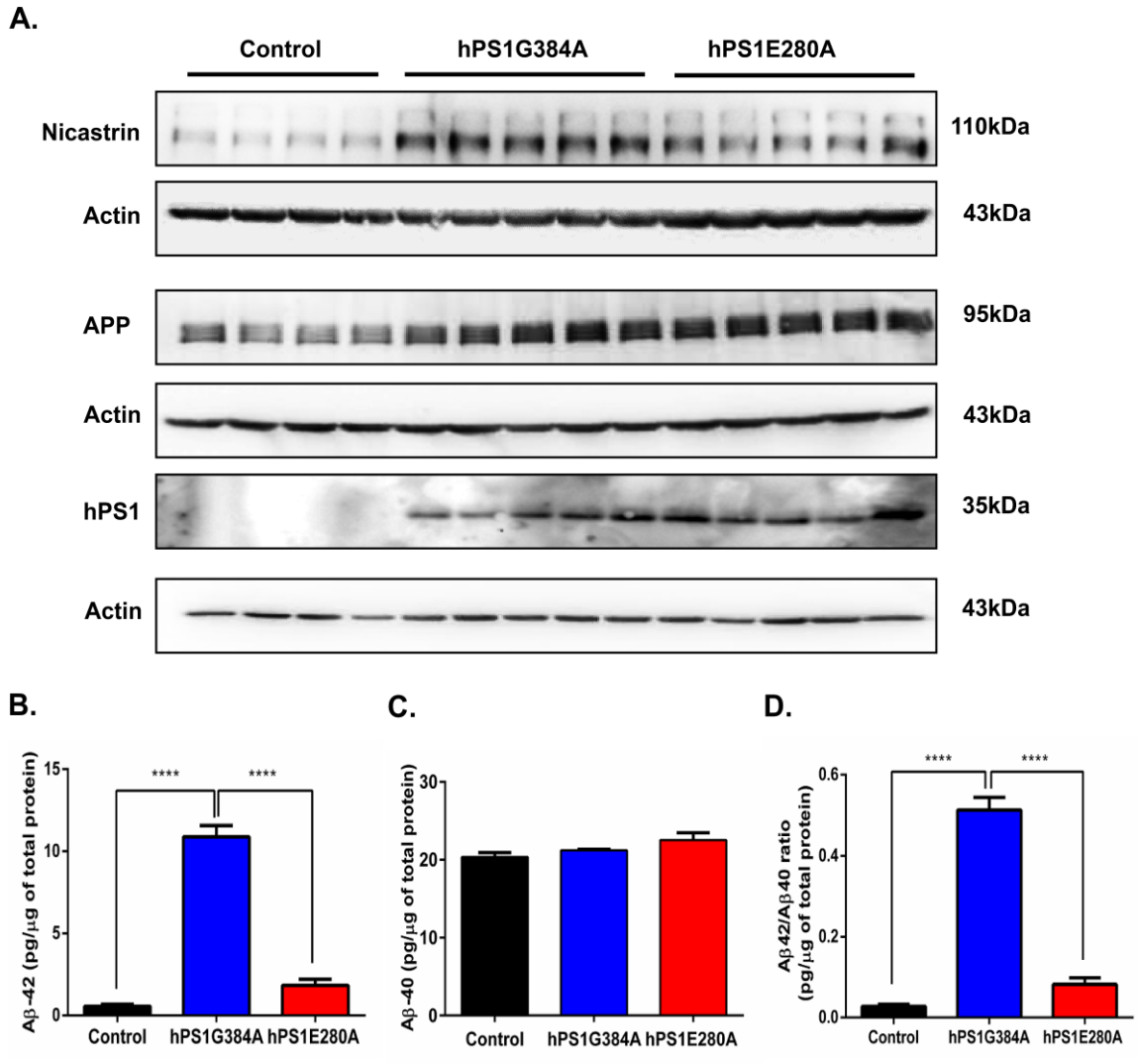

Figure 13. **Expression of some components of the γ-secretase complex and Aβ40-Aβ42 production in transgenic mice. A.** WB of nicastrin, APP, and hPS1 of total protein lysates from brain mice. Actin was used as loading control. The overexpression of hPS1 is apparent for transgenic mice. **B.** ELISA was performed to quantify the levels of Aβ42 and Aβ40 (**C)** in total brain lysates from control and transgenic mice. **D.** The ratio Aβ42/Aβ40 was also calculated. N=5, all data are represented as means ± SEM. One-way ANOVA was used and Tukey as a post-hoc test, *P<0.05.

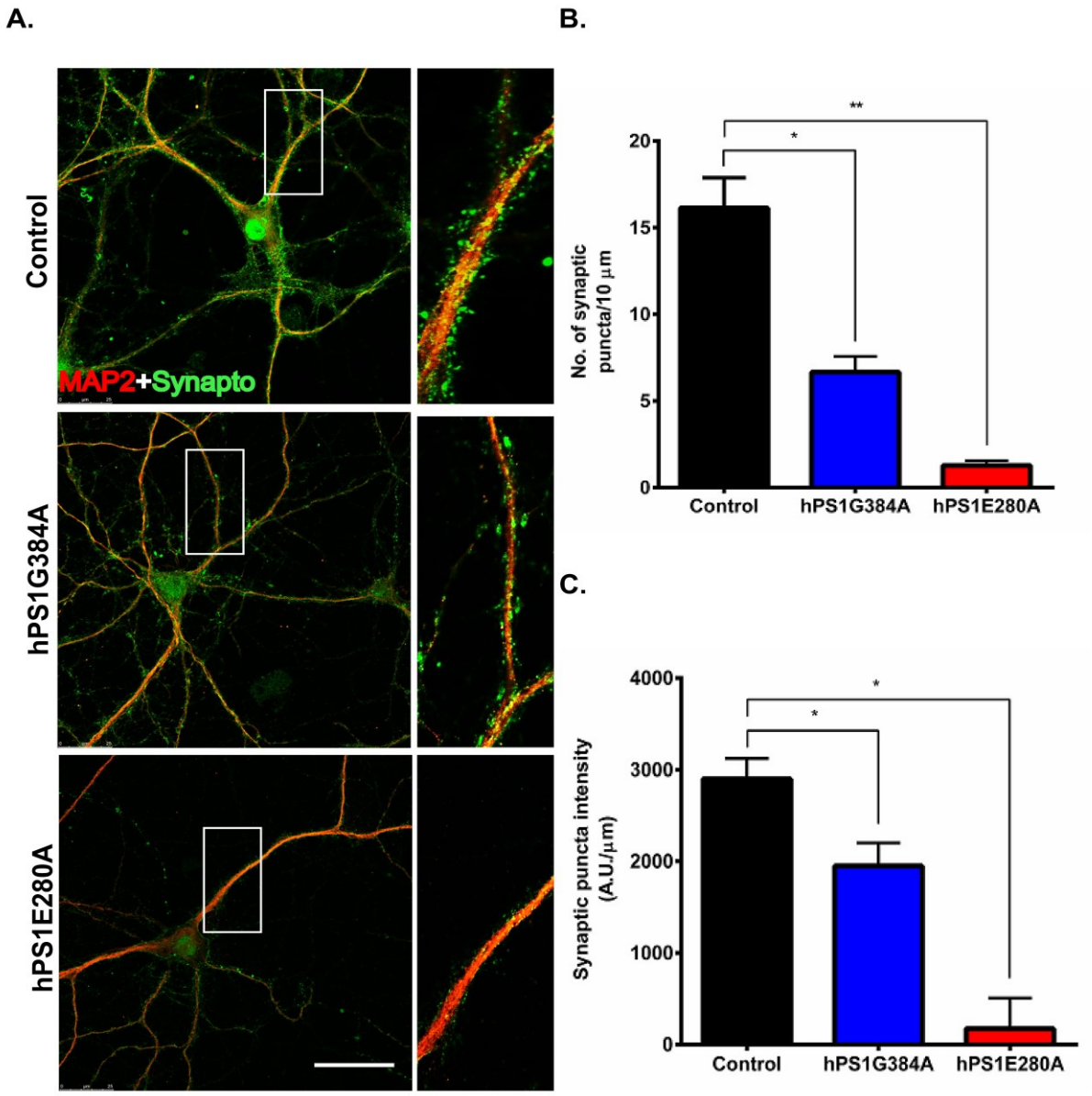

Figure 14. Dendritic spine counting in primary hippocampal neurons. Primary hippocampal neurons were prepared from P0-P1 pups and cultivated together with astrocytes until reaching 18 days in co-cultured to have fully differentiated neurons. **A.** Representative images of selected neurons showing the staining with MAP2 (as a neuronal marker) and Synaptophysin (as the major integral membrane glycoprotein of synaptic vesicles). **B.** Quantification of the number of synaptic puncta expressed as the number of puncta per 10μm in the three different groups. **C.** Quantification of the puncta intensity or signal intensity of Synaptophysin expressed as the number of puncta per 10μm. Three independent experiments were performed; ten cells per group were quantified in 3 different axons. Data are represented as mean ± SEM, *P<0.05, **P<0.01, N=30. One-way ANOVA (non-parametric, Dunn´s post-hoc test) Scale Bar=30 μm.

4.2 Abnormal mitochondrial morphology and function in hPS1E280A mice

4.2.1 Abnormal mitochondrial morphology in the brains of adult hPS1E280A mice

Considering that abnormal mitochondria were previously identified in the cerebella of human brains carrying the E280A mutation (Sepulveda-Falla et al. 2014), electron microscopy was used to study mitochondrial morphology in the brains of the transgenic mice at four months of age. Given that alterations in dendritic spines number were identified in primary hippocampal neurons, both temporal cortex and hippocampal regions were analyzed. Three adult animals per line were sacrificed and decapitated; the brain was cut first in a sagittal way and then in the coronal plane to visualize the cortex and the hippocampus and to further prepare the samples for electron microscopy. Mitochondria were classified as normal or abnormal depending on the morphology of the cristae. Only in the hippocampus of the hPS1E280A line was around 75% of the mitochondrial content found to be abnormal, compared to controls and hPS1G384A (Figure 15 A-B). Interestingly, the defect was not found in cortical mitochondria (Figure 15 C).

4.2.2 Abnormal mitochondria in hPS1E280A mice are not associated with defects in mitochondrial associated membranes

As the resolution of electron microscopy allows to measure close contacts, like the ones between mitochondria and ER, it was also possible to count the number of mitochondria that were in close apposition with ER. For that reason, only distances between 15-25 nm were considered as points of contacts between the two organelles (Figure 16 A). No statistical differences were found between groups (Figure 16 B-C). For the connections, rough and smooth ER were considered.

According to several studies, PS1 is bound transiently in the ER and trans-Golgi network (Busciglio et al. 1997). Nevertheless, PS1 has been reported to be localized in mitochondrial associated membranes. MAMs isolation was performed and standardized from whole mouse brain tissue, following protocols published by

Wieckowski et al. and Annunziata et al. (Wieckowski et al. 2009; Annunziata, Patterson, and d'Azzo 2013). The enrichment of each fraction was evaluated by western blot for each experimental group, as shown in Figure 17A, for several cytosolic, ER, mitochondrial, and MAMs markers.

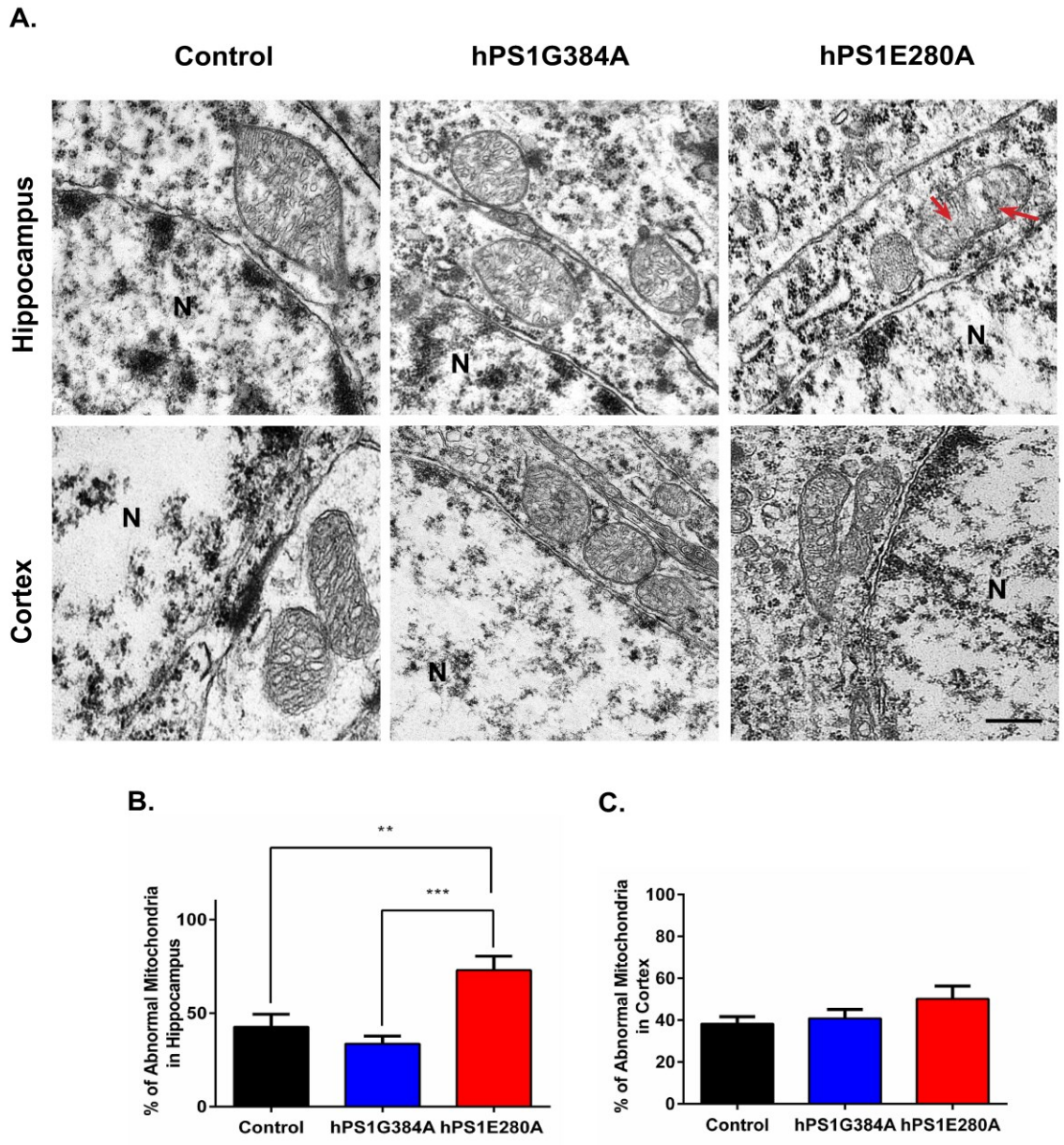

Figure 15. **Abnormal mitochondria in the hippocampus of transgenic mice carrying the E280A mutation.** Brains from 4 months old mice were dissected and cut with a vibrotome to further preparation of samples. The cuts were done in the sagittal and coronal plane to visualize hippocampus and cortex in the same sample. **A**. Representative electron microscopy images of mitochondria in cortex and hippocampus from the two transgenic lines and littermates or controls. Abnormal mitochondria were considered those in which cristae were absent or having unusually large sizes; red arrows point to abnormal cristae; N=nuclei. **B**. Percentage of abnormal mitochondria found in the hippocampus of the three experimental groups; 3 mice per line; 10 cells were imaged per

animal, between 93-158 mitochondria were analyzed in total; **P<0.01; ***P<0.001. One-way ANOVA (Holms-Sidak´s post-hoc test). Only perinuclear mitochondria were considered. **C.** Percentage of abnormal mitochondria found in the cortex of the three experimental groups. No statistical differences were found.

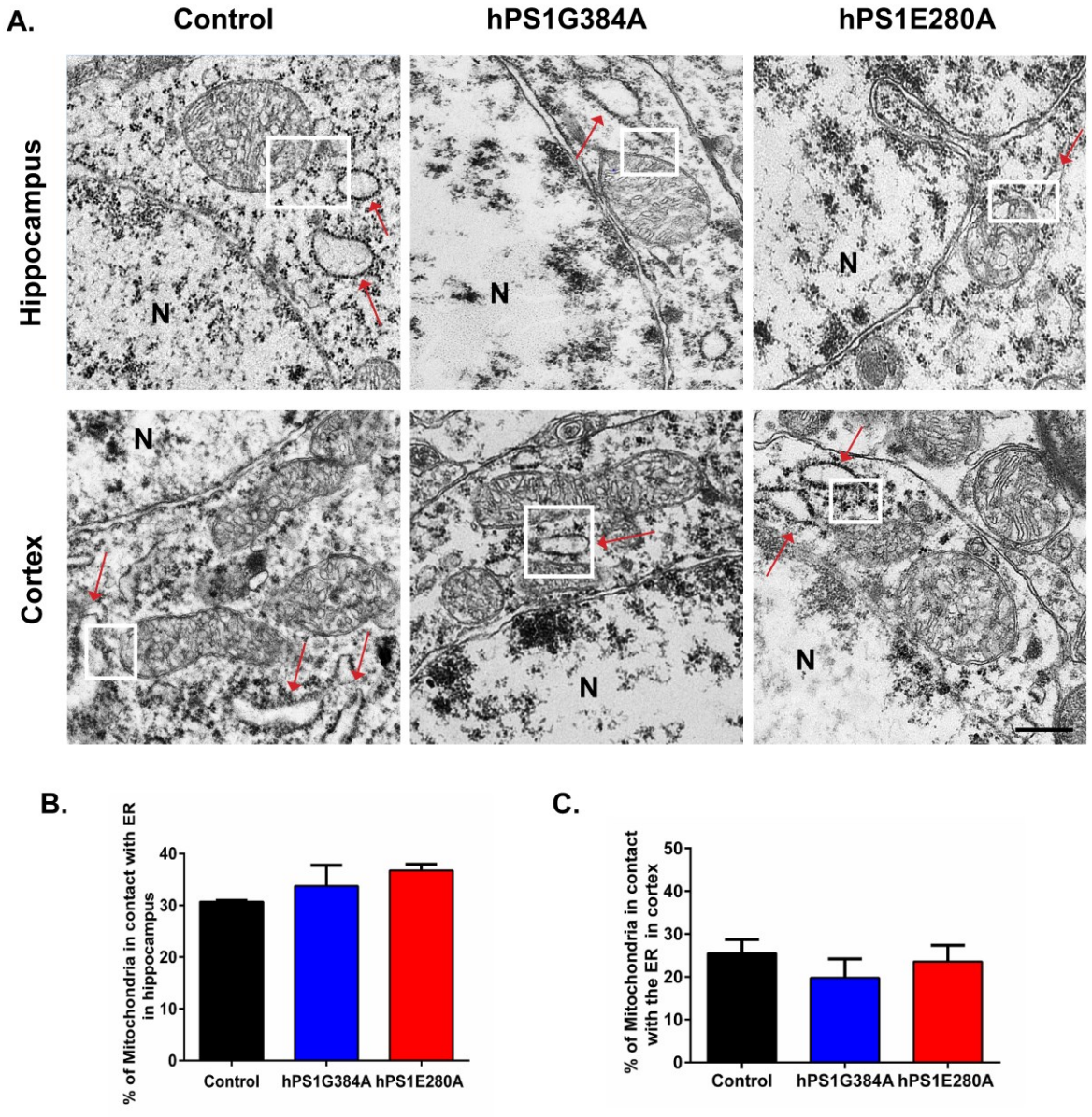

Figure 16. **ER-Mitochondrial contacts are not affected in the brains of transgenic mice.** Brains from 4 months old mice were dissected. **A**. Representative electron microscopy images of mitochondria in cortex and hippocampus from the two transgenic lines and littermates or controls. The distance between the ER and the mitochondria was measured to establish mitochondria-ER contacts. A range between 10-25 nm was considered as a point of contact (white boxes indicating ER membranes in proximity to mitochondria, red arrows pointing to ER membranes), N=nuclei. **B.** Percentage of mitochondria in contact with the ER in the hippocampus. **C.** Percentage of mitochondria in contact with the ER in cortex. Three mice per line were used, and ten cells were imaged per animal,

between 93-158 mitochondria were analyzed in total. Only perinuclear mitochondria were considered. No statistical differences were found.

Proteomic profiles in MAMs reported between 991 and 1239 unique peptides which were classified in very different biological processes, including mitochondrial dysfunction, oxidative phosphorylation, Ca^{2+} signaling, and PKA signaling, among others (Zhang et al. 2011; Huang et al. 2017; Poston, Krishnan, and Bazemore-Walker 2013). MAMs proteins like ERO1, FACL4, and VDAC were detected. The enrichment of this fraction was further tested with electron microscopy (Figure 17 B) in which the membrane structure was evident, while the mitochondrial fraction was enriched in these organelles.

ELISA was performed in order to assess the levels of Aβ42 and Aβ40 in these membranes. Both peptides were detected with this sensitive assay and, similarly to what was found in whole brain lysates, the levels of Aβ40 remain unchanged in all experimental groups (Figure 17 C). The levels of Aβ42 were low and interestingly displayed a similar concentration with the ones found in whole brains, with low levels in the control mice; meanwhile, the transgenic mice exhibited a higher expression. These values were also normalized to the total number of proteins found in the MAMs fractions. There were not statistically significant differences among groups.

4.2.3 Early mitochondrial defects in primary neurons from transgenic mice

Mitochondria are dynamic organelles that continuously change their shape and distribution inside the cell. They also are transported to axons to reach long distances, as far as the energetics of the cell requires. For that reason, their morphology adapts to different stimuli and provides information about cellular processes, such as apoptosis (Youle and Karbowski 2005). The constant shape change of mitochondria is called mitochondria dynamics and involves fusion and fission processes. Mitochondria fuse to form networks, to repair their damage and to share genetic information. They also undergo fragmentation in response to apoptosis signaling (Ishihara et al. 2009).

All those functions are performed by specific mitochondrial proteins that are involved in neurodegenerative diseases. Using primary neurons obtained from transgenic mice at post-natal day 0 or 1 in co-culture with astrocytes, their mitochondria were stained with Tom-20 and MAP-2 and their morphology was analyzed as described by Dagda et al. (Dagda et al. 2009). With this protocol, differentiated and healthy neurons were prepared, which constitute an ideal model to study mitochondrial morphology and dynamics.

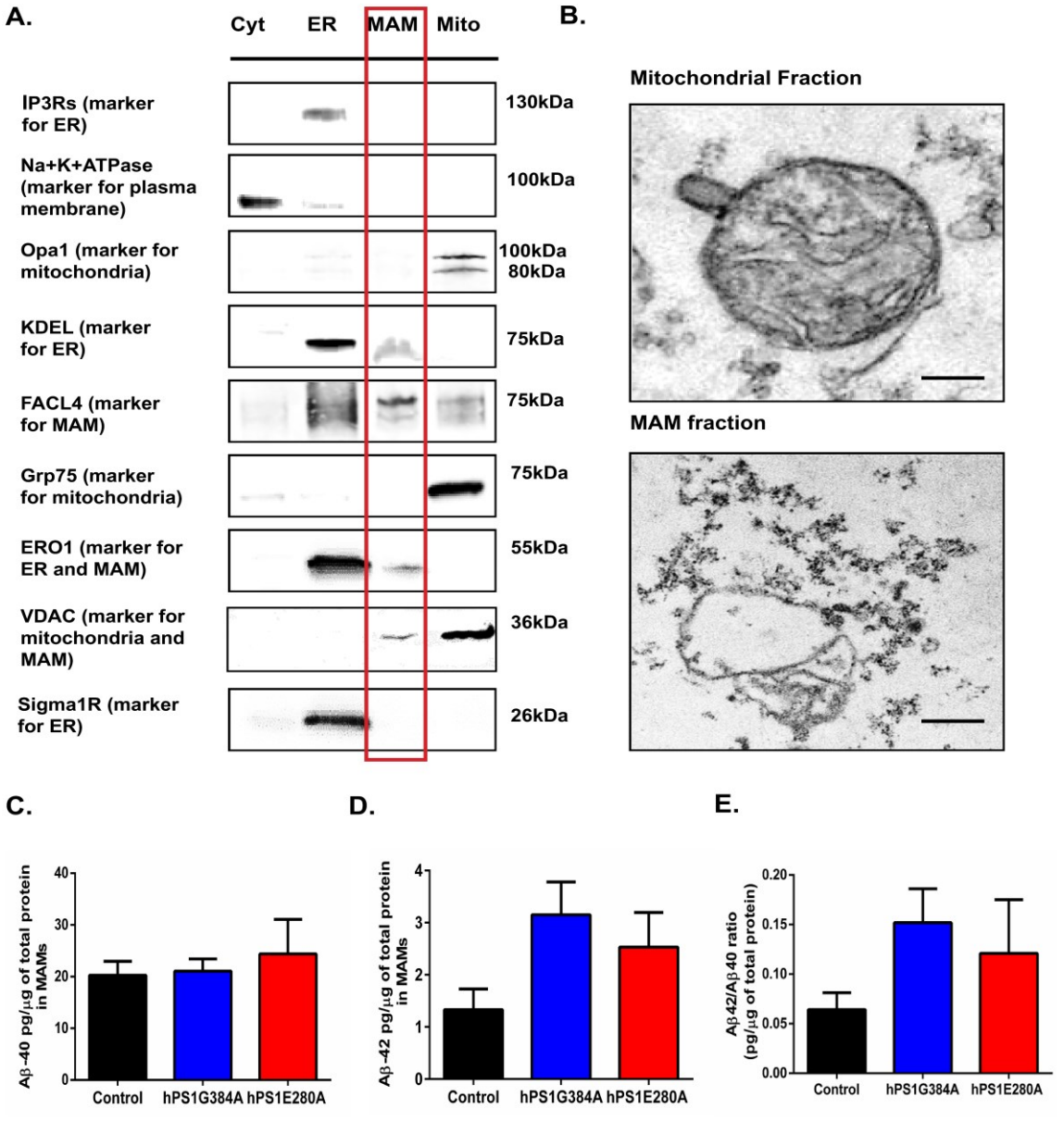

Figure 17. **Aβ40 and Aβ42 are detected in mitochondrial associated membranes**. **A.** MAMs subcellular fractionation from fresh brain tissue from 6 months old C57BL/6 mice as controls and transgenic mice. MAMs fraction outlined in red, none of the MAMs markers are expressed exclusively in that fraction. **B.** Ultrastructural analysis of ER-mitochondria junctions of the MAMs and the mitochondrial enriched fraction. **C.** Quantification of the concentration of Aβ40 and Aβ42 (**D**), obtained

with ELISA. **E.** The ratio of Aβ42/Aβ40 was also calculated. The data were normalized with the total protein concentration. Data are represented as mean ± SEM, N=3. One-way ANOVA. No statistical differences were found. Scale Bar=1μm.

Extensive and complex networks were found in neurons. The pictures were taken in soma and dendrites, and the Aspect Ratio, which represents the size of the particles (it is the number obtained after dividing the maximum Feret´s diameter between the minimum Feret´s diameter) and the Form Factor were calculated (Figures 10 and 18 A).

Mitochondria from the hPS1E280A and hPSG384A groups tended to be more fragmented both in dendrites and axons, but the most significant change was observed in dendritic prolongations (Figure 18 B). Although controls and hPS1G384A neurons also have fragmented mitochondria, larger particles or more associated mitochondria were identified in these two groups when the particles analyzed were divided into tubular mitochondria (Supplemental Figure 2).

4.2.4 Mitochondrial functional impairment in hPS1E280A primary neurons

Mitochondrial morphology can be considered a qualitative parameter to measure mitochondrial health. To assess whether the impairments in morphology are connected to the function of the organelle, the oxygen consumption rate was measured before and after the addition of different inhibitors to analyze the state of components of the electron transport chain. The quantity of primary hippocampal neurons seeded for the experiment was previously standardized (Supplemental Figure 3) to determine that 50,000 was the ideal number of cells to obtain a good response after each stimulus.

Mitochondrial respiration has been found impaired in 3x-Tg AD mice of 12 months of age (Walls et al. 2012; Yao et al. 2009) and fibroblasts from FAD patients (Gray and Quinn 2015). Here, it was found that ATP production, maximal respiration as well as basal respiration were affected in mice with the hPS1E280A mutation (Figure 19 A, C-E), but no effect was detected for hPS1G384A mutation (Figure 19 B). These

results point to a mutation-specific effect on mitochondrial form and function, in this case, being more drastic for the E280A mutation.

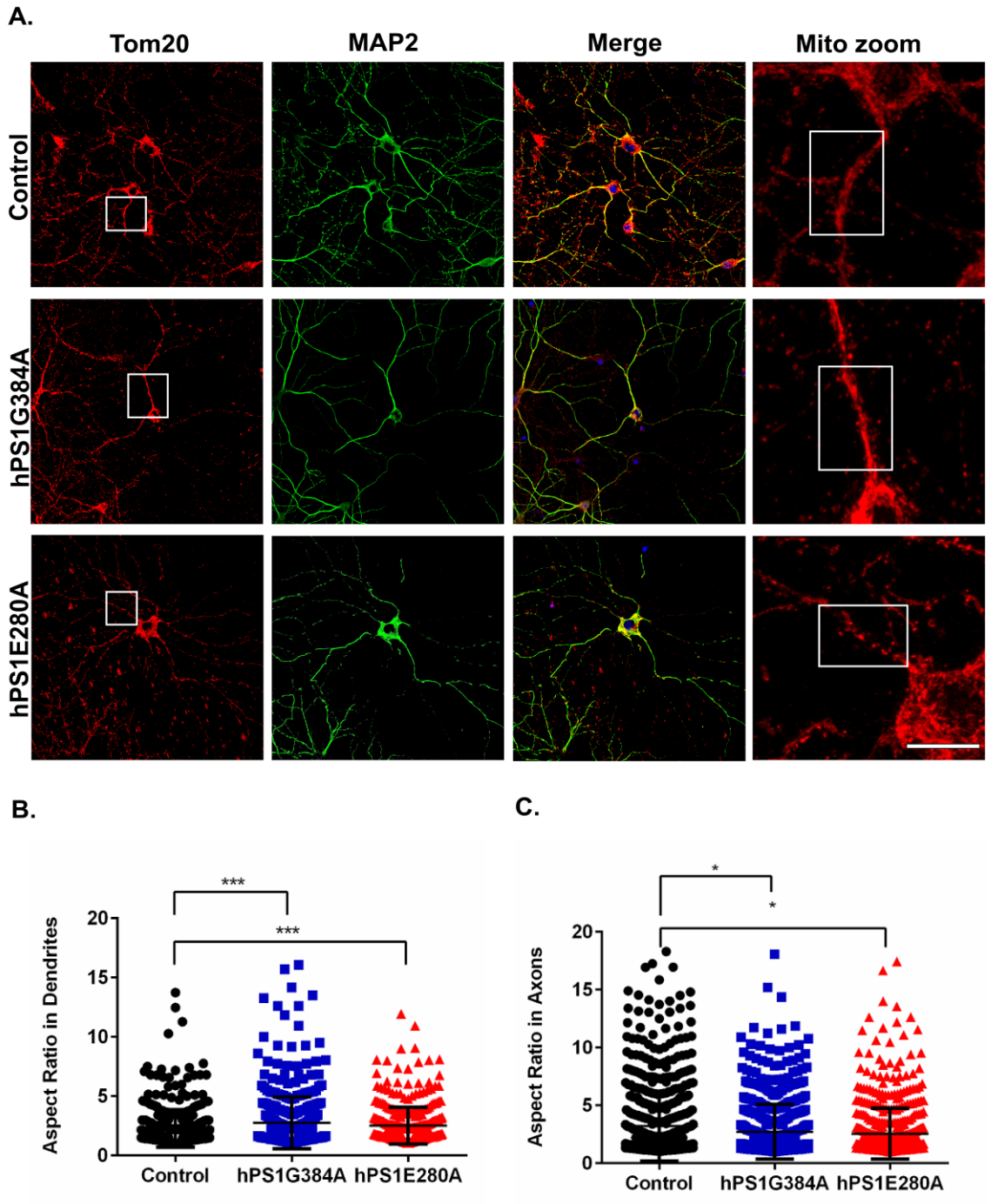

Figure 18. **Primary hippocampal neurons from transgenic mice have more fragmented mitochondria. A.** Mitochondrial morphology was assessed in primary hippocampal neurons from transgenic mice and controls. Cells were fixed and stained against Tom20 as a mitochondrial marker and MAP2 as a neuronal marker. Axons and dendritic prolongations were selected and imaged as shown in the representative pictures. **B.** Quantification of the Aspect Ratio in dendrites and axons (**C**). Data -are represented as mean ± SEM, *P<0.05, ***P<0.001, three independent experiments were

performed. A total number of 30 neurons per experimental group were considered in the study. One-way ANOVA (Kruskal-Wallis test). Scale Bar=30 μm.

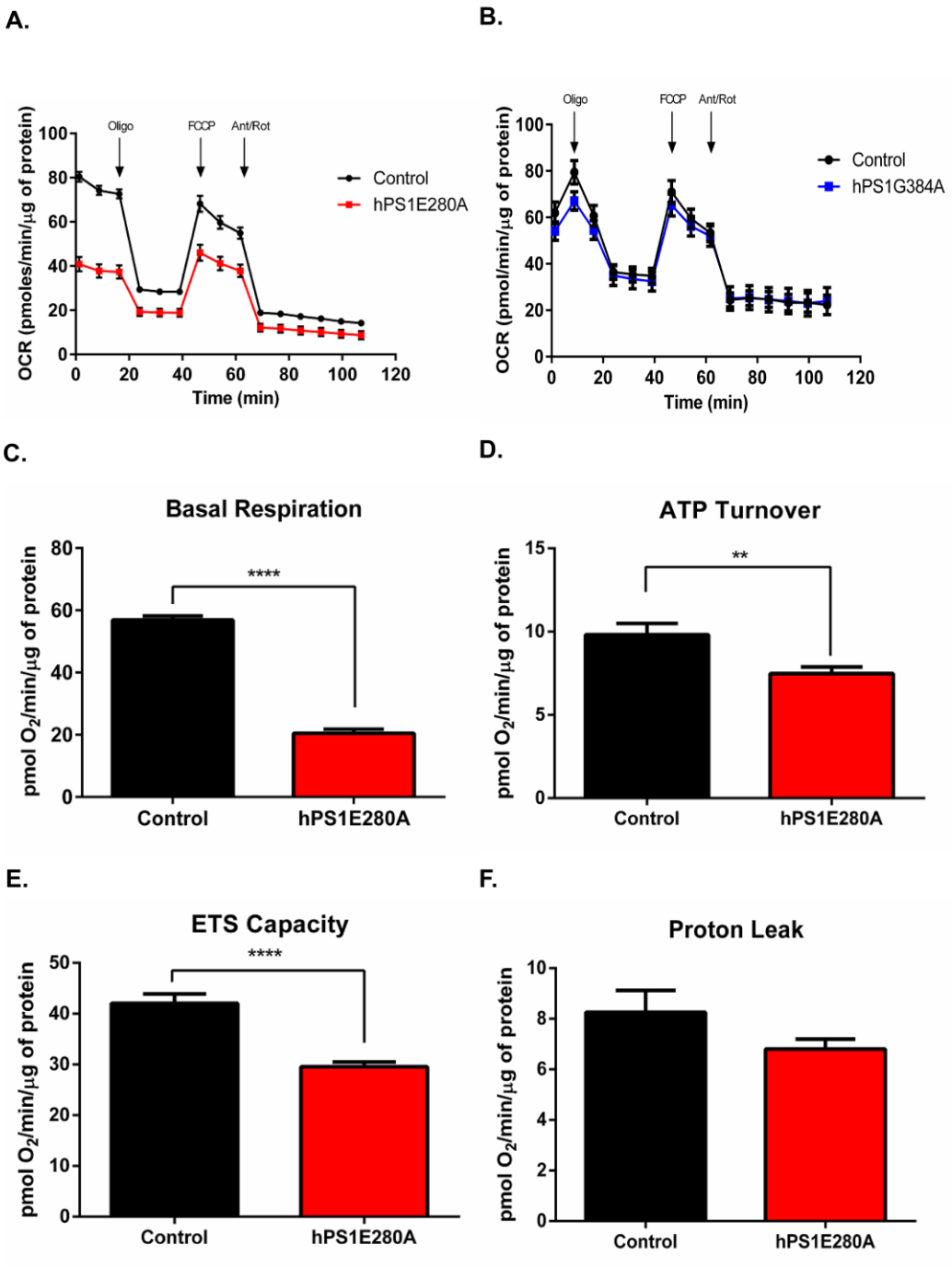

Figure 19. **Mitochondrial respiration is affected in primary hippocampal neurons from hPS1E280A transgenic mice.** The capacity of the oxidative phosphorylation (OXPHOS) was evaluated through oxygen consumption**. A.** OCR was determined with the Seahorse assay**;** dotted lines represent the time points in which each of the injections of Oligomycin, FCCP and Rotenone/Antimycin were applied in hPS1E280A and hPS1G384A neurons (**B). C.** Basal respiration was obtained as well as the ATP production **(D);** the maximal respiration **(E)** and the proton leak **(F)**

for hPS1E280A neurons. Values are given in pmol/min and were normalized to the total number of proteins as calculated with the BCA assay. **P < 0.01, ****P < 0.0001. Data are mean ± SEM, Unpaired T-tests, Mann-Whitney tests (N=14-18, from 4 independent experiments).

4.2.5 Brain mitochondrial proteome characterization of hPS1E280A and hPS1G384A mice

To establish if mutations in hPS1 affect the expression of mitochondrial proteins at different ages, enriched mitochondrial fractions were extracted from whole mice brains at one, six and 12 months of age and two independent experiments were performed at each age with a total number of four animals per group. As described before, these mice do not show a strong phenotype, but the results presented here point to an early mitochondrial impairment that is detected in primary hippocampal neurons. Following this, at one month of age, from a total of 823 mitochondrial proteins recognized, 651 were identified as common between the experimental groups. Expression was different for 16 proteins when hPS1G384A and controls were compared, while expression of 27 proteins differed between controls and hPS1E280A (Figure 20 A-B); volcano plots represent the statistical validation of the proteins considered.

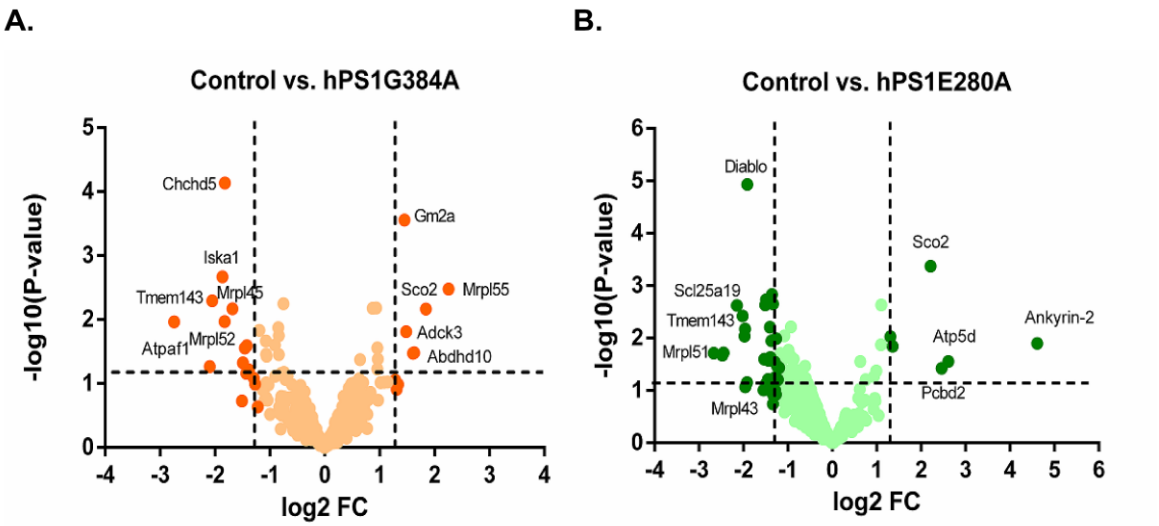

Figure 20. **Mitochondrial proteomic profile of brain mice at one month of age**. **A.** Volcano plots showing the magnitude and the significance of the protein´s comparisons between Controls and hPS1G384A and between Control and hPS1E280A (**B**). The -log10 or P value is plotted against the log2 FC (fold change) value. Abbreviations in Supplemental Tables 4 and 5. Two independent experiments were performed, N=4. Independent two-sample T-test, P≤0.05 and FC of ±1.2.

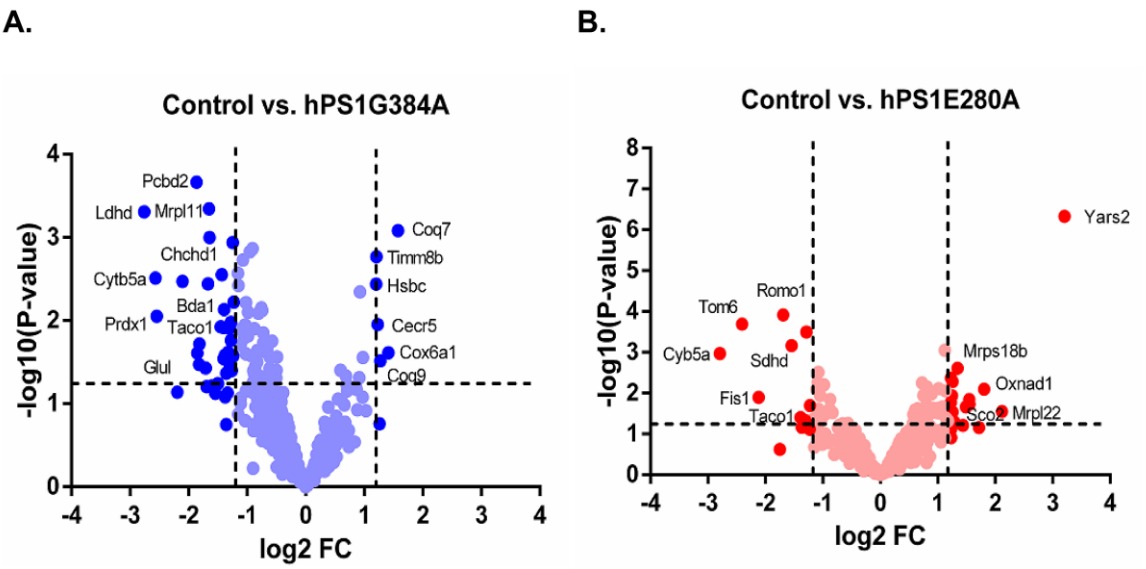

Figure 21. **Mitochondrial proteomic profile of brain mice at six months of age**. **A.** Volcano plots showing the magnitude and the significance of the proteins comparisons between Controls and hPS1G384A and between Control and hPS1E280A (**B**). The -log10 or P value is plotted against the log2 FC (fold change) value. Abbreviations in Supplemental Tables 7 and 8. Two independent experiments were performed, N=4. Independent two-sample T-test, P≤0.05 and FC of ±1.2.

Only five proteins were up-regulated, and 11 were downregulated in hPS1G384A samples (Supplemental Table 4), while six were up-regulated and 21 downregulated in hPS1E280A carriers (Supplemental Table 5); according to the cut-off's values established by a P-value≤0.05 and FC of ±1.2. The biological cluster analysis concluded that these proteins belong to respiratory and mitochondrial RNA function (Supplemental Figure 5). At this age, there are three common proteins dysregulated between the two mutations, Sco2, Tmem143 and Mrpl52 (Supplemental Table 6).

The brain mitochondria from adult mice (six months of age) presented an increased number of dysregulated proteins for the mutation G384A, with a total number of 34 proteins whose expression were different in comparison with controls (Figure 21 A-B). For the mutation E280A, 21 mitochondrial proteins diverge, and their biological functions belong to respiration and RNA function, as was found with the younger animals. Interestingly, most of the proteins dysregulated in hPS1E280A were found to be upregulated, but, in contrast, from the 34 proteins found dysregulated for hPS1G384A, 26 were found to be downregulated (Supplemental Tables 7 and 8). In these groups, Mrpl22 was found as a commonly dysregulated protein, upregulated in

the group hPS1E280A; a result validated with western blot (Supplemental Figure 4). Fis1, a protein involved in mitochondrial fission, has a low expression compared to the controls only for the E280A mutation. Meanwhile, both mutations present a decreased abundance in cytochrome b 5.

In older animals, the mutation E280A presents differences in the expression of 36 proteins compared to controls (Figure 22 A-B), from which 29 of them were upregulated (Supplemental Table 10). Although for mutation G384A, 25 proteins were found to be dysregulated, there was a balance between the number of proteins up and downregulated (Supplemental Table 11). The copper metallochaperone Sco2 was the only protein found to present a higher abundance at all ages in mutation E280A. For this mutation, different isoforms of the mitochondrial ribosomal proteins (Mrpls) were detected to be downregulated at a young age, but higher abundances were identified in adults and old mice brains. Figure 23 shows the clusters of proteins whose expression changed significantly at all ages in the E280A mutation. Commonly dysregulated proteins between mutations at six and 12 months of age are reported in Supplemental Tables 9 and 12, as well as their respective interaction networks (Supplemental Figures 6 and 7).

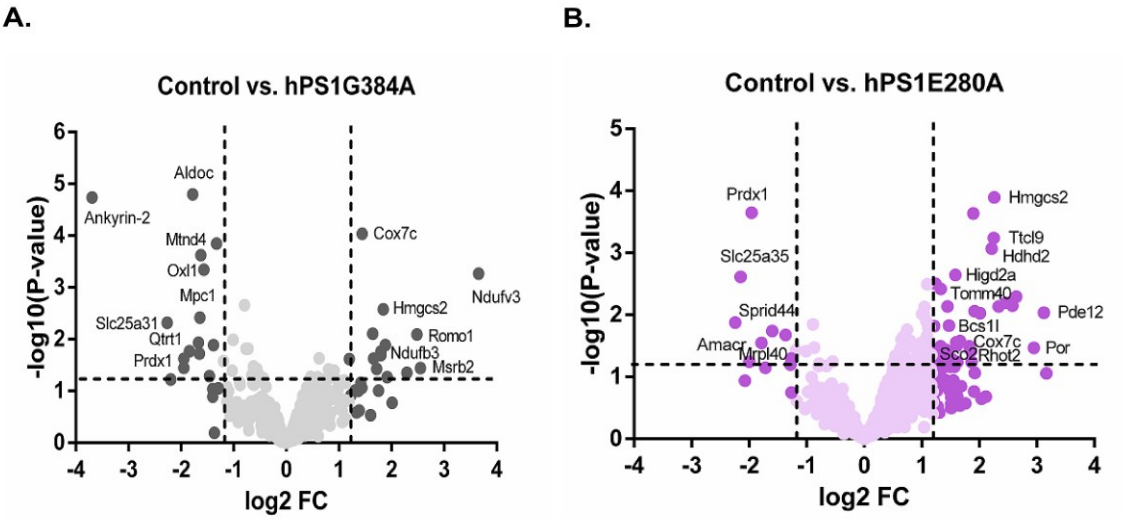

Figure 22. **Mitochondrial proteomic profile of brain mice at 12 months of age**. **A.** Volcano plots showing the magnitude and the significance of the proteins comparisons between Controls and hPS1G384A and between Control and hPS1E280A (**B**). The -log10 or P value is plotted against the log2 FC (fold change) value. Abbreviations in Supplemental Tables 10 and 11. Two independent experiments were performed, N=4. Independent two sample T-test, P≤0.05 and FC of ±1.2.

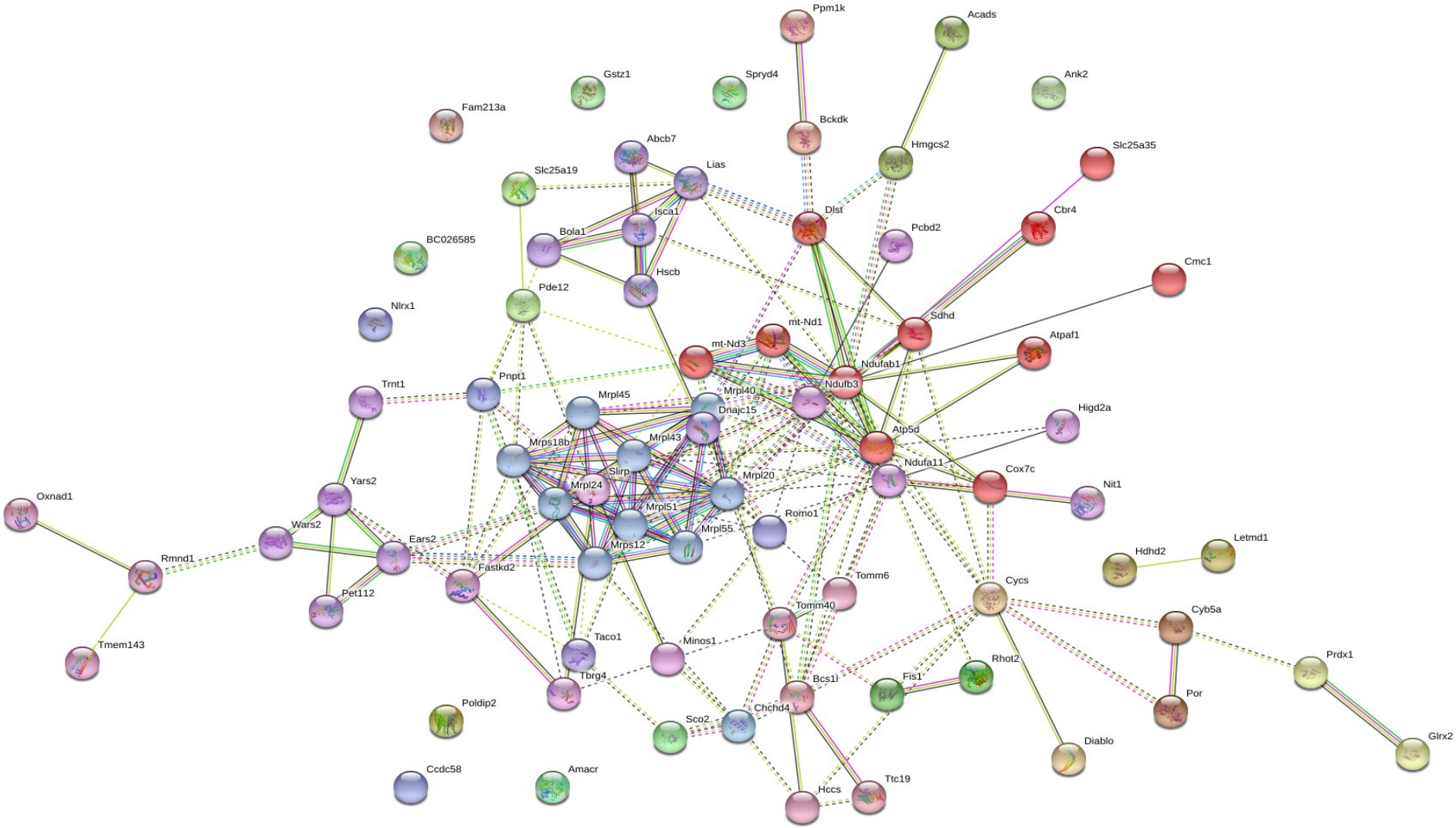

Figure 23. **Interaction network of the proteins dysregulated in the brains of hPS1E280A mice.** Mitochondrial RNA and Respiration proteins were dysregulated at all ages evaluated.

4.3 hPS1 mutations impact the opening of the mitochondrial permeability transition pore in N2a cells

N2a cells were transfected to generate cells overexpressing hPS1E280A, hPS1Δ9, hPS1WT, and mock cells. Cultures were tested for the overexpression of PS1 with WB and with qPCR. PCR products were also sequenced to verify the expression of the mutations (Figure 24). PCR products were also sequenced to verify the expression of the mutations (Figure 24). Since mutation Δ9 deletes a complete exon, proteolytic cleavage takes place there, and only full-length PS1 is detected (Figure 24 A). The expression of APP and the production of Aβ40 and Aβ42 was also assessed in this model, as shown in Figure 24 E. In different cellular types, overexpression of PS1 has induced changes in the localization of the protein (Sannerud et al. 2016). For that reason, cells were fixed and stained with a PS1 antibody and KDEL, Tom20, GM130, and Lamp1 to trace the subcellular localization of PS1 in the N2a mutants and WT model. PS1 was mainly found colocalizing with the ER marker KDEL in all four cell lines (Figure 25 A-B).

4.3.1 Abnormal Ca^{2+} homeostasis in hPS1 overexpressing N2a cells

One the best-characterized functions of the communication between the ER and the mitochondria come from all the studies that show that this connection is necessary to regulate the intracellular Ca^{2+} concentrations to control mitochondrial dynamics, function, division, and apoptosis (Rowland and Voeltz 2012). Specifically, Ca^{2+} uptake is driven by the electron potential in the inner mitochondrial membrane and by the MCU (Schrader et al. 2015). The importance of Ca^{2+} signaling for mitochondria also deals with its positioning and distribution, since a Ca^{2+} binding protein called Miro mediates the halt of mitochondria in axons (Jeyaraju, Cisbani, and Pellegrini 2009) and promotes mitochondrial division (Cho et al. 2017). Numerous proofs are showing the central role that PS1 plays in Ca^{2+} signaling (Begley et al. 1999; Lee et al. 2017; Wu et al. 2013), from its interaction with Ca^{2+} channels to the proposal that PS1 is a Ca^{2+} channel itself (Bezprozvanny 2013). Although, the last point is not clear, what is evident is that mutations in PS1 impact Ca^{2+} intracellular concentrations.

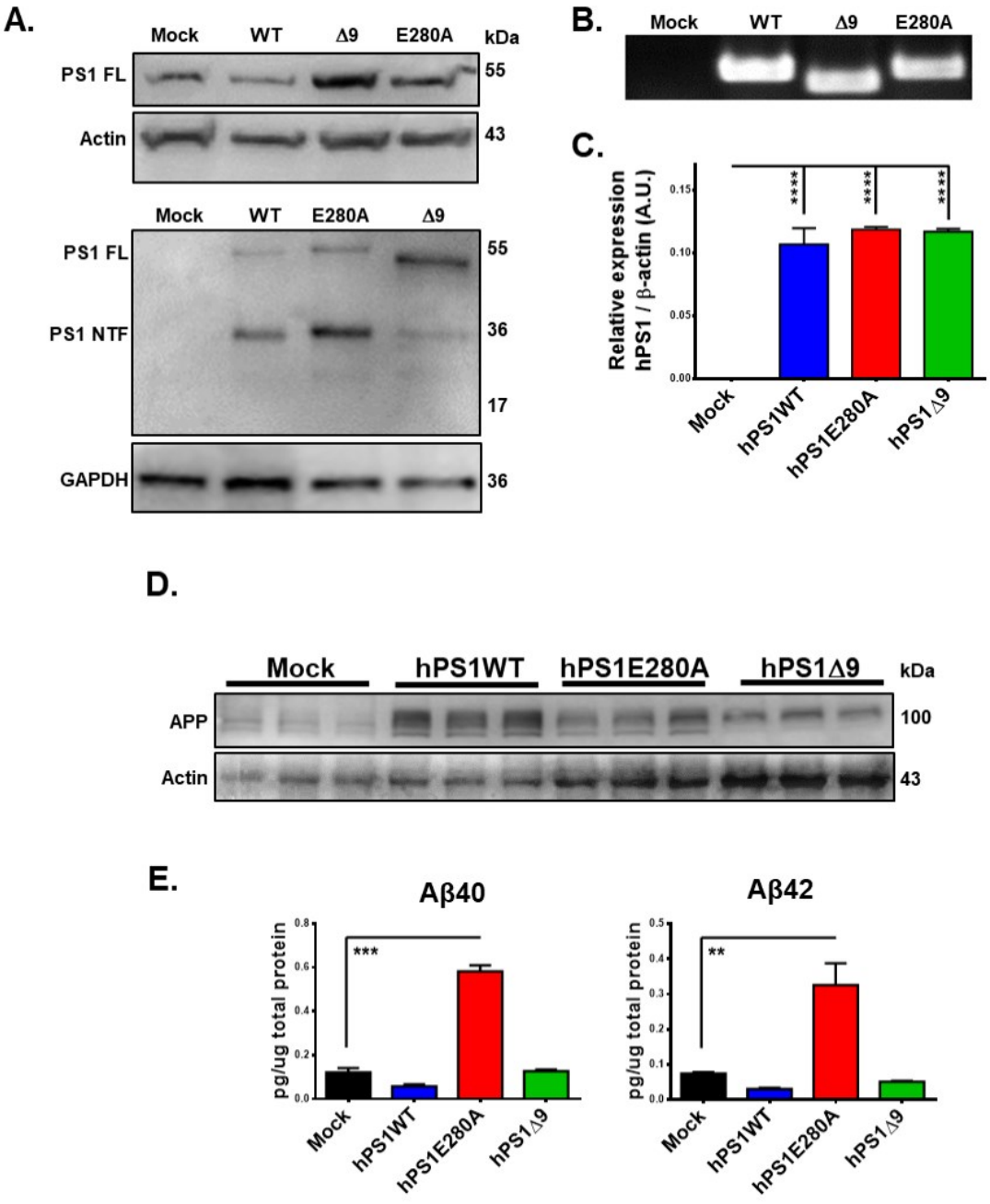

Figure 24. **WT and mutant PS1 overexpression in N2a cells**. **A**. Western blot for hPS1 levels in stably transfected N2a cells assessed using two different PS1 antibodies (Cell signaling #3622, unspecific and Millipore MAB1563, human-specific) Specific expression of human PS1 is visible in all stably transfected cell lines. **B.** Agarose gel electrophoresis for PCR products using human PS1 primers in stably transfected N2a cells. **C.** Human PS1 expression in stably transfected N2a cells was also tested by qPCR. **D.** Western blot for APP levels in mock and stably transfected N2a cells. **E.** ELISA assays for murine Aβ40 and Aβ42 in stably transfected N2a cells. Only hPS1E280A cells show significantly increased levels when compared to mock cells. **P < 0.01, ***P < 0.001. Data are mean ± SEM, One-Way ANOVA.

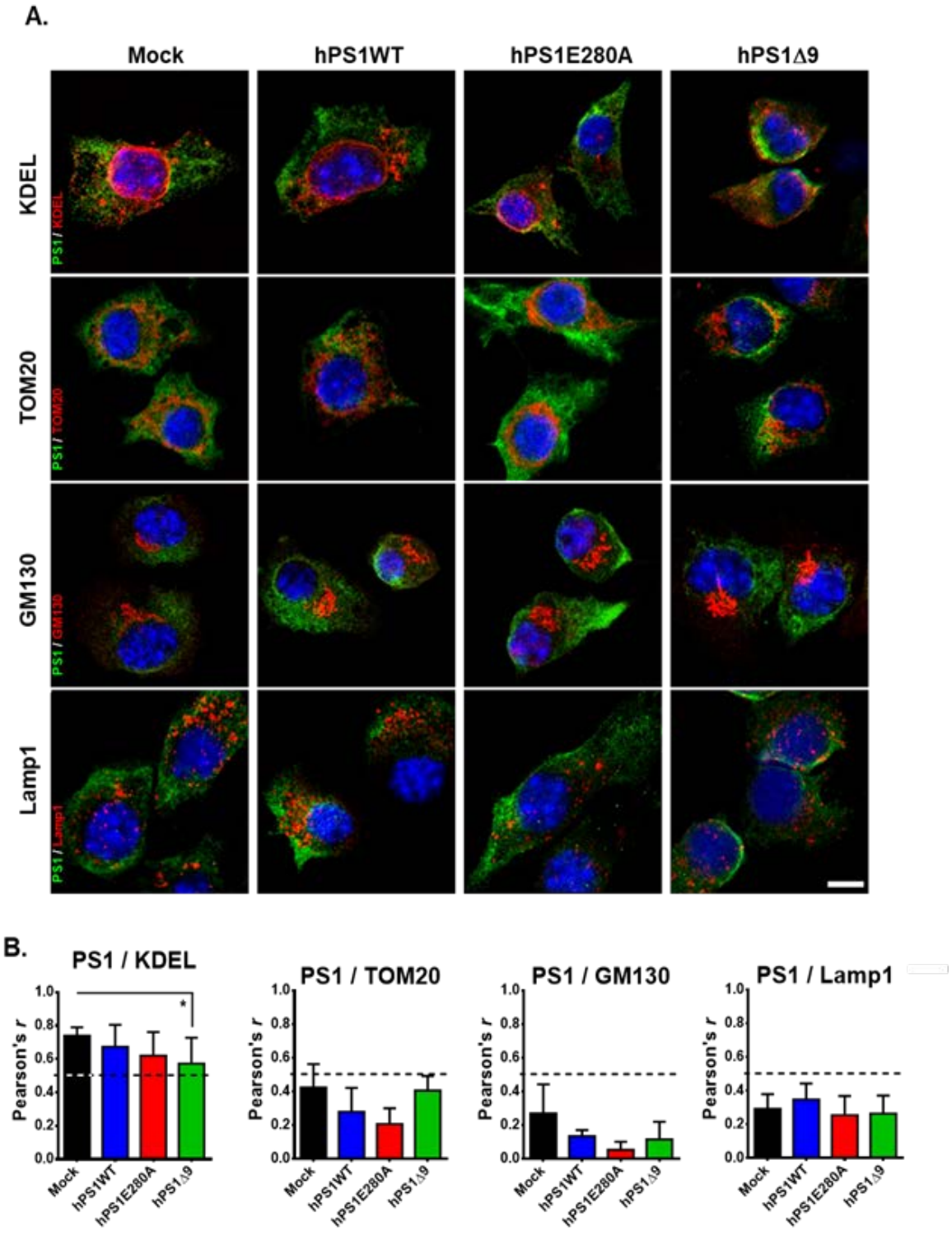

Figure 25. **PS1 localization in N2a cells**. **A.** Representative confocal microscopy pictures of Mock, hPS1WT, hPS1E280A and hPS1Δ9 N2a cells assessing PS1 (red) colocalization with markers (in green) for ER (KDEL), mitochondria (Tom20), Golgi (GM130) and lysosomes (Lamp1). **B.** Signal was quantified in 3 independent experiments in at least 10 cells per experiment and cell line. Pearson's coefficients showed significant differences for PS1-KDEL colocalization between mock and hPS1Δ9 N2a cells. Dotted lines represent colocalization thresholds. *P < 0.05. Data are mean ± SEM, Two-Way ANOVA. Scale Bar = 20 μm.

With the previous evidence that mitochondrial dysfunction and Ca^{2+} abnormalities are present in the cerebellum of FAD patients carrying the PS1E280A mutation (Sepulveda-Falla et al. 2014), N2a cells stably transfected with this mutation and with the ∆9 mutation were used to examine intracellular Ca^{2+} concentrations in basal conditions. In effect, cytosolic Ca^{2+} levels were significantly increased in hPS1WT and hPS1E280A, when compared to mock N2a cells. hPS1∆9, in contrast, did not show a significant increase in cytosolic Ca^{2+} concentration (Figure 26 A-B). On the other hand, ER Ca^{2+} concentration was significantly higher only in hPS1WT N2a cells when compared to the others (Figure 26 C-D); and mitochondrial Ca^{2+} concentration was increased considerably in all hPS1 overexpressing cells when compared to mock cells (Figure 26 E-F).

Although increased ER Ca^{2+} in hPS1WT could be attributed to PS1 overexpression, cells overexpressing mutant hPS1 did not present that effect. Cytoplasmic and mitochondrial Ca^{2+} levels showed a similar trend in which hPS1E280A Ca^{2+} levels were significantly increased in both compartments. While increased mitochondrial Ca^{2+} levels can result from increased ER Ca^{2+} levels in hPS1WT cells, increased mitochondrial Ca^{2+} in hPS1E280A cells can be associated with a mitochondria-specific alteration in this mutation. The results obtained with aequorin transfection were validated with a single cell method employing Fluo4-AM. Ca^{2+} dysregulation in cells carrying FAD mutations has been attributed to attenuated store-operated Ca^{2+} entry (Tong et al. 2016); for that reason, an experiment was performed in order to test the refilling of the ER Ca^{2+} stores (Figure 27 A).

A significant increase in Ca^{2+} concentration (area under the curve) was found in hPS1WT and hPS1E280A, while the cells with the ∆9 mutation showed a significant decrease when compared to mock cells (Figure 27 A). The hPS1∆9 cells showed substantial differences in the Ca^{2+} re-entry amplitude, which could be related more to the properties of the plasma membrane. The hPS1∆9 and hPS1E280A Ca^{2+} signals were opposite, and, although the hPS1E280A cells did not show a statistically significant difference, they tended to accumulate more Ca^{2+}, and their response to the CPA stimulus was faster compared to the other groups (Figure 27 C). These results agree with recent investigations in which other PS1 mutants were evaluated (Toglia et al. 2016). Taken together, these findings indicate that Ca^{2+} imbalance in

mutant PS1 affect different cellular compartments and can have a direct impact in Ca^{2+} mediated mitochondrial functions.

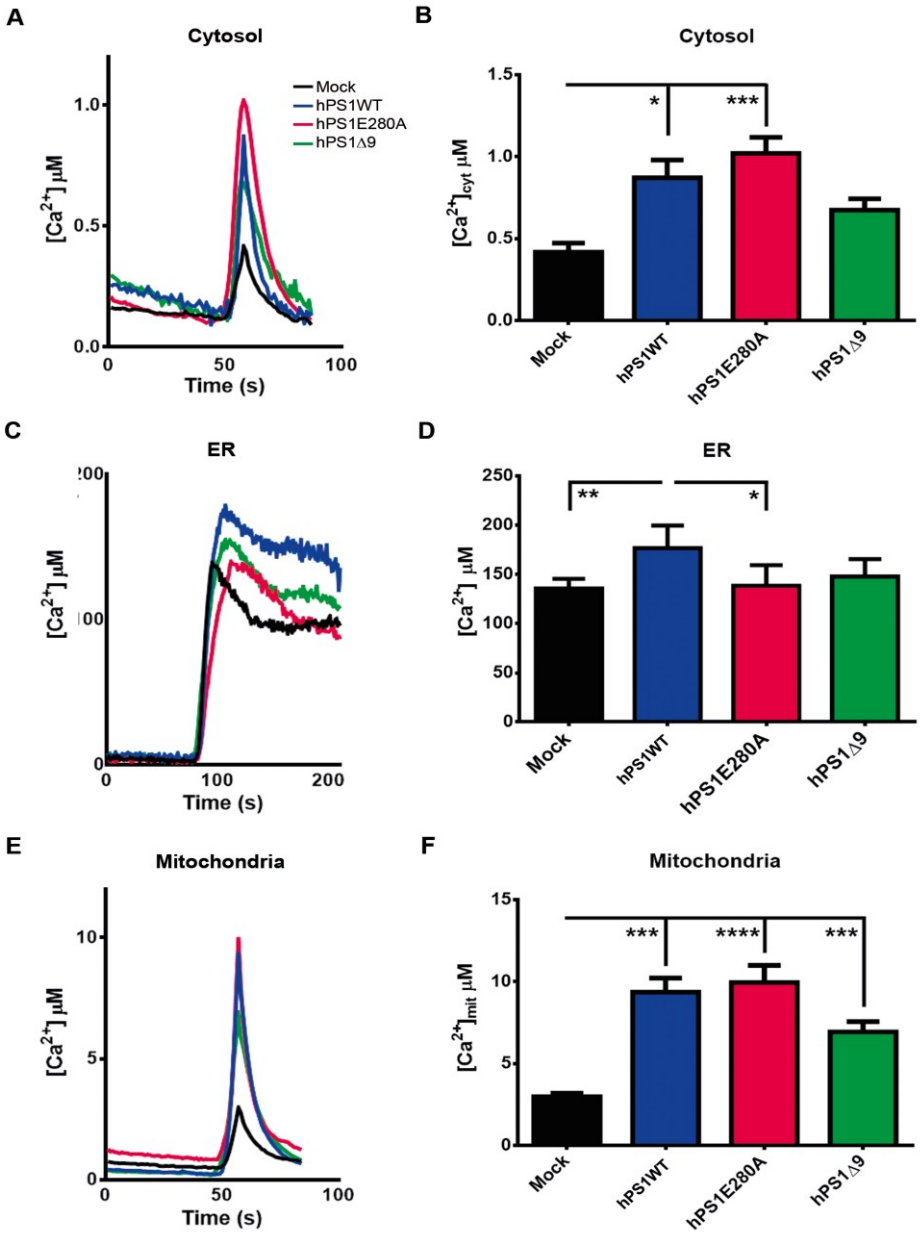

Figure 26. **Abnormal Ca^{2+} concentration in cellular compartments of N2a cells overexpressing WT and mutant hPS1.** N2a stably transfected cells overexpressing hPS1WT, hPS1E280A and hPS1Δ9 were used to measure intracellular Ca^{2+} concentrations using transient transfection of compartment-specific aequorin constructs. **A.** Representative averaged recordings of cytosolic Ca^{2+} in the different cell lines, showing the maximum Ca^{2+} level reached after bradykinin addition. **B.** Bar graphs of the maximum cytosolic Ca^{2+} concentration showing an increased in hPS1WT and hPS1E280A cells. **C.** Representative averaged recordings of ER Ca^{2+} in N2a mock and hPS1 overexpressing cells. **D.** Bar Graphs of maximal Ca^{2+} concentration detected in the Endoplasmic Reticulum, hPS1WT showed increased Ca^{2+} levels in the ER. **E.** Representative averaged recordings

of maximal mitochondrial Ca^{2+} concentration in the different cell lines. **F.** Bar graphs of the maximal mitochondrial Ca^{2+} concentration after bradykinin addition; mean and ±SEM are presented for all experiments, Two Way ANOVA, *P<0.05, **P<0.01, ***P<;0.001, ****P<;0.0001, N=3.

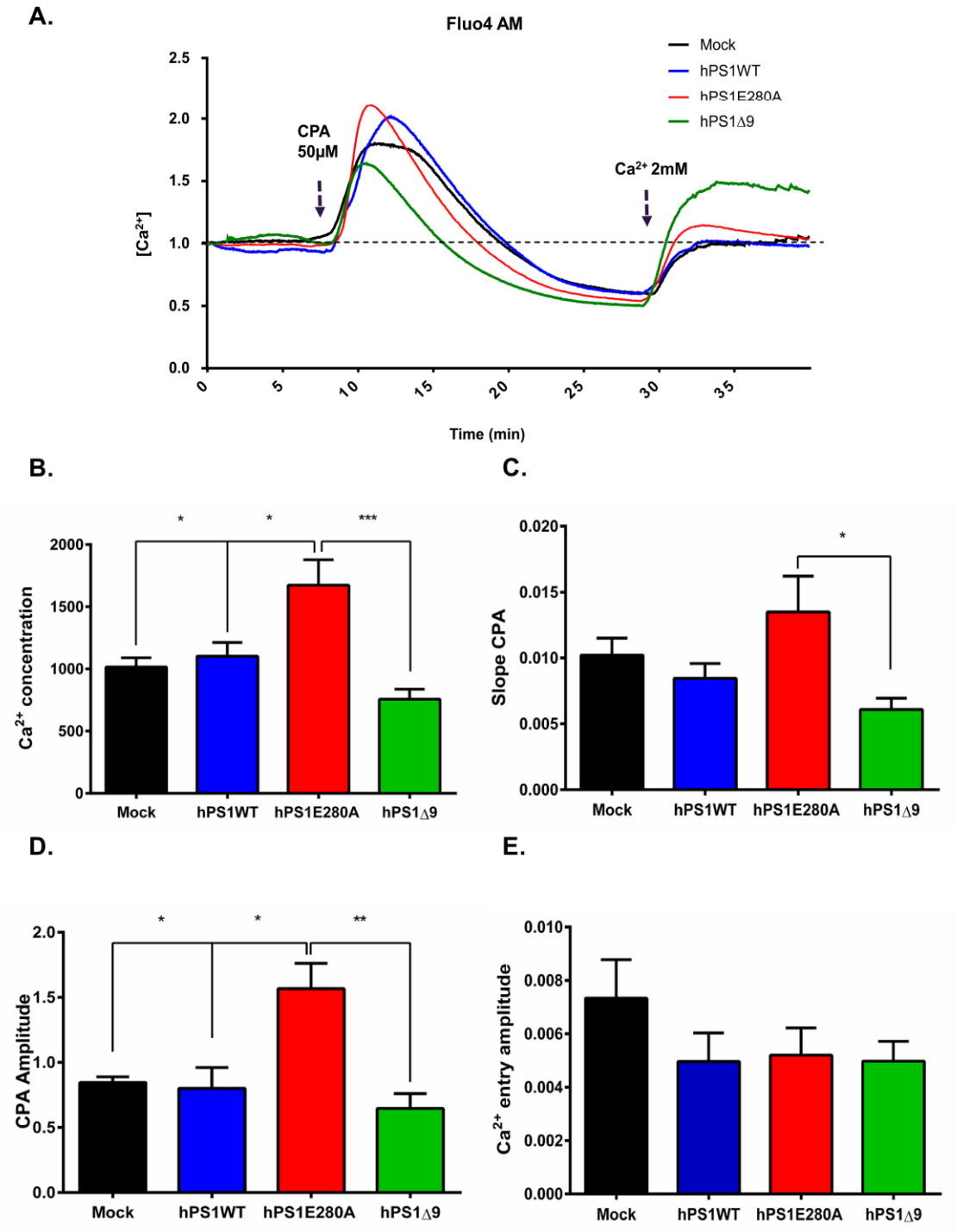

Figure 27. **Ca^{2+} imaging in N2a stably transfected cells loaded with Fluo4-AM. A.** Representative curves showing the Ca^{2+} response in ARCF solution and after the addition of CPA; **B.** Bar graphs showing the area under the curve calculated to obtain the concentration of Ca^{2+} in intracellular stores after depletion with CPA in all experimental groups; **C.** The speed of the increase in Ca^{2+}

concentration in the cytosol was measured after the addition of CPA; **D.** The rate of Ca^{2+} re-entry was calculated as well as the total Ca^{2+} accumulation (**E**) for all cell lines. Mean, and ±SEM are presented for all experiments, One-Way ANOVA, ***P<;0.001, five independent experiments were performed. The total number of cells was 108 for Mock, 112 for hPS1Wt, 110 for hPS1E280A and 123 for hPS1Δ9.

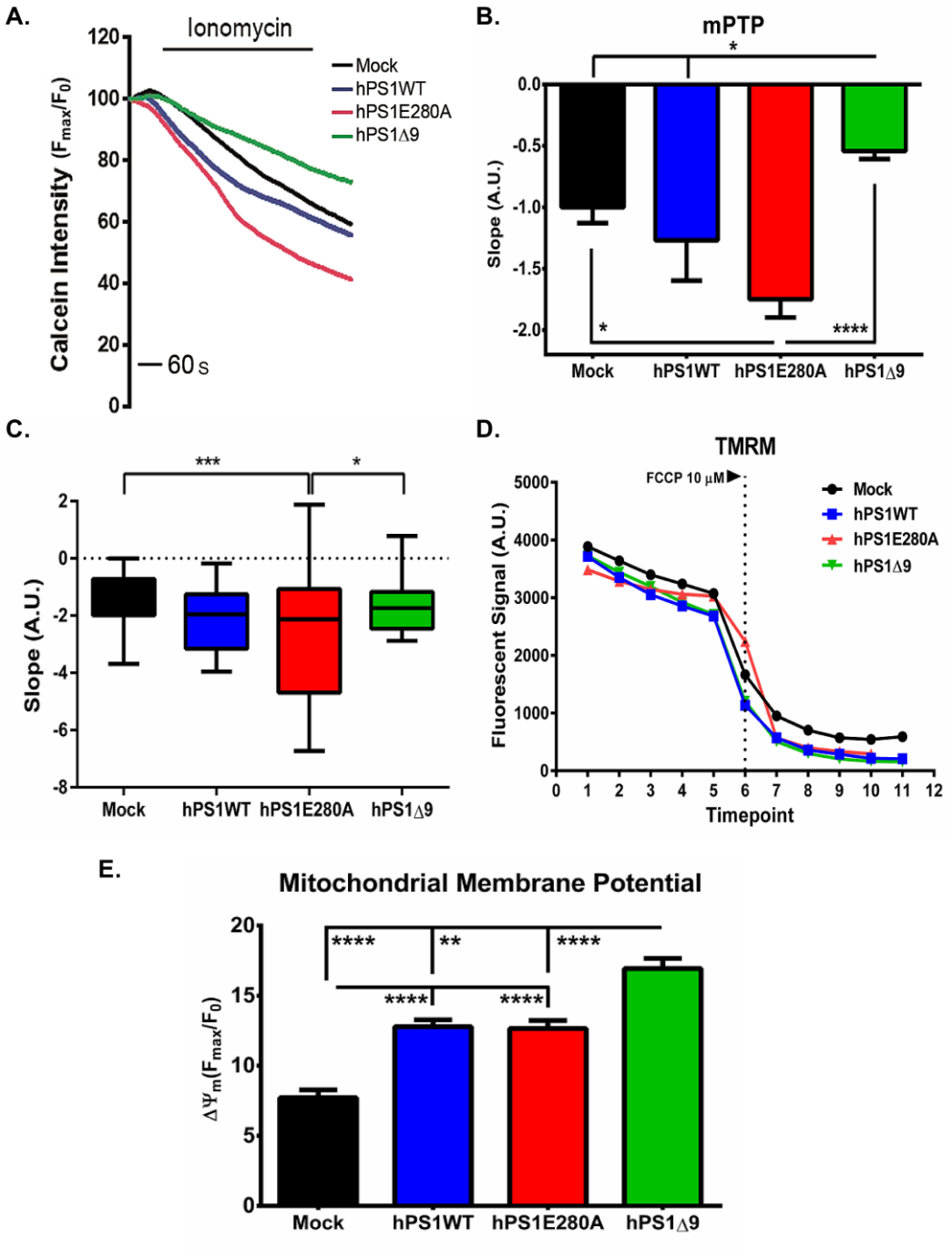

Figure 28. **hPS1E280A cells showed an accelerated opening of the mitochondrial transition pore.** Live cell imaging was used to measure the opening of the mitochondrial transition pore in N2a cells with the calcein-Co^{2+} assay; **A.** Cells were challenged with 1µM ionomycin (Sigma-Aldrich, Hamburg, Germany) to induce mPTP opening and quenching of the calcein signal. Representative

timeline of calcein intensity quenching after the addition of ionomycin in hPS1 overexpressing and mock N2a cells. **B.** PS1 mutant cells showed altered mPTP opening, accelerated in hPS1E280A and inhibited in hPS1Δ9 cells; **C.** Cells were challenged with H_2O_2 500μM to induce mPTP opening and to depolarize mitochondria, hPS1E280A mPTP opening was accelerated compared to mock. SEM, **P<0.01, ***P<0.001, four independent experiments were performed, the total number of cells was between 118-180; **D.** TMRM response curves after addition of FCCP for all cell lines. **E.** Bar graphs represent TMRM intensity as the measurement of $\Delta\Psi_m$ during live imaging. All hPS1 overexpressing cells showed increased potential compared to mock, and hPS1Δ9 displayed increased potential when compared to all other cell lines. Measurements were made from three independent cell cultures, n=19-72. All data are mean ± SEM, One-Way ANOVA, *P<0.05, **P<0.01, ***P<;0.001, ****P<;0.0001, N=3.

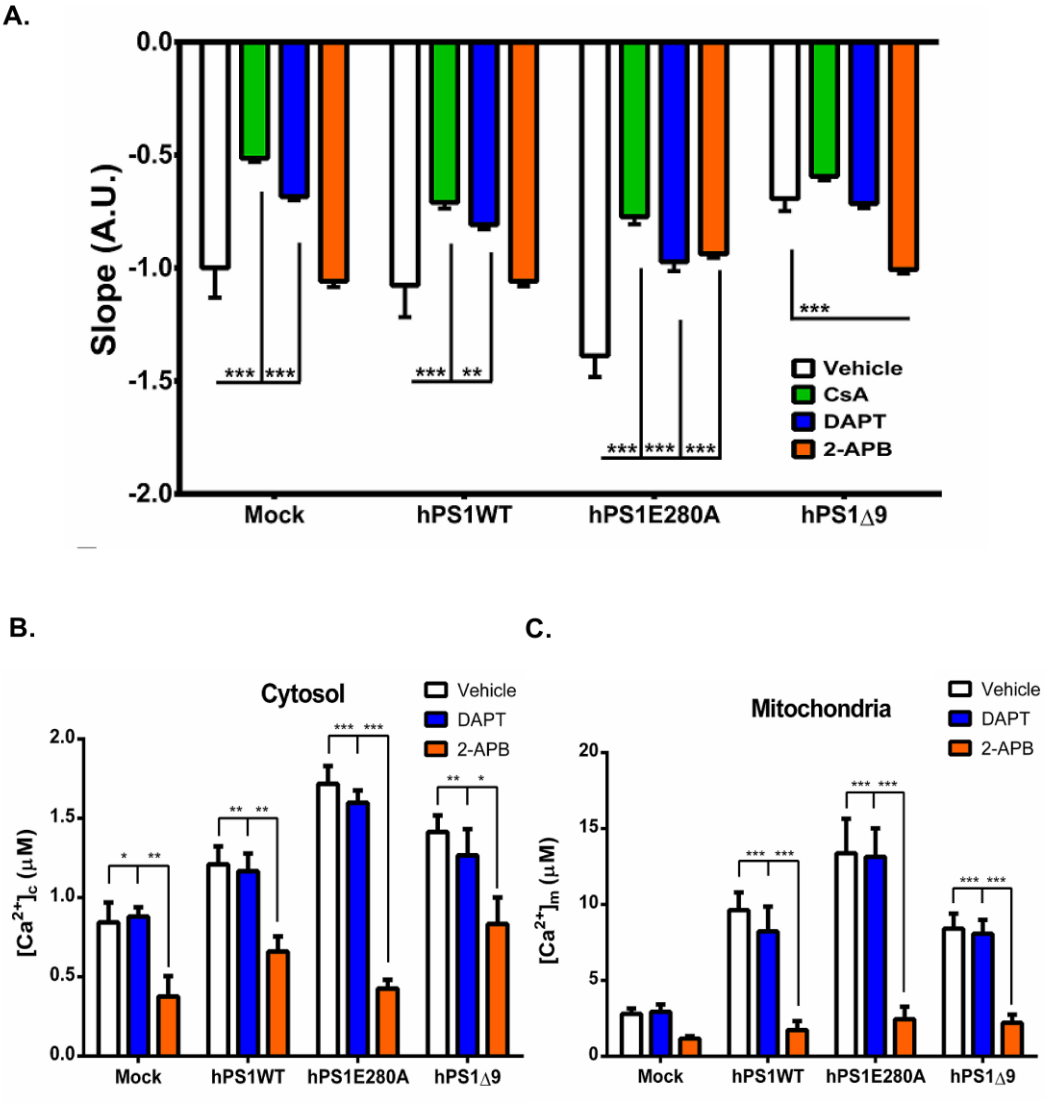

Figure 29. γ-Secretase dependent response in hPS1E280A cells. A. Mock-transfected, hPS1WT, hPS1E280A, and hPS1Δ9 N2a cells were challenged with 1μM ionomycin to induce mPTP opening and quenching of the calcein signal. Cells were treated with CsA, DAPT, or 2-APB. CsA and DAPT inhibited mPTP opening in mock, hPS1WT, and hPS1E280A cells while 2-APB only showed an effect in PS1 mutants, inhibiting mPTP opening in hPS1E280A cells and accelerating it in hPS1Δ9 cells. **B.**

Bar graphs of maximum cytosolic Ca^{2+} concentration and **(C)** mitochondrial Ca^{2+} concentration in the different N2a cell lines, with and without DAPT and 2-APB treatment for 16h. 2-APB decreased mitochondrial Ca^{2+} levels in PS1 overexpressing cells and cytoplasmic Ca^{2+} levels in all cells. *P < 0.05, **P < 0.01, ***P < 0.001. Data are mean ± SEM, Two-Way ANOVA.

4.3.2 Mutations in PS1 modulate the opening of mPTP in N2a cells

Increased mitochondrial Ca^{2+} concentrations suggest a possible activation of mitochondrial permeability transition pore (Elrod et al. 2010; Bernardi and Petronilli 1996), but other researchers have found no correlation (Eriksson, Pollesello, and Geimonen 1999; Wei et al. 2011; De Marchi et al. 2014). The mPTP opening was assessed in mock and PS1 overexpressing N2a cells using two different methods. The evaluation of mPTP-dependent alteration of the mitochondrial transmembrane potential showed that hPS1E280A cells accelerated mPTP opening (Figure 28 A). By using the calcein-quenching assay, it was found that only PS1 mutants, hPS1E280A, and hPS1Δ9 cells, presented with significantly accelerated and delayed mPTP openings, respectively, when compared to mock cells (Figures 28 B-C).

Both results indicate a PS1 mutation-dependent effect on mPTP activity in N2a cells. Basal mitochondrial membrane potential ($\Delta\Psi_m$) in mock and stably transfected hPS1N2a cells was evaluated as a measurement of mitochondrial health. The hPS1 overexpressing cells were hyperpolarized, presenting a significant increase in $\Delta\Psi_m$ when compared to mock and hPS1Δ9 cells showed higher $\Delta\Psi_m$ when compared to hPS1WT and hPS1E280A cells (Figure 28 D-E). In summary, mitochondrial health findings support a role for PS1 in mitochondrial homeostasis with PS1 mutations potentially leading to mitochondrial stress characterized by abnormal mPTP opening in basal conditions.

4.3.3 γ-Secretase dependent and independent mitochondrial phenotypes in hPS1E280A overexpressing cells

The opening of the mPTP was evaluated using DAPT, a γ-secretase inhibitor and 2-APB, an ER Ca^{2+} channel´s inhibitor. Firstly, the efficacy of DAPT in inhibiting γ-secretase was tested by measuring the production of the Aβ40 and Aβ42 peptides in

all cell lines (Supplemental Figure 8A) and it was found that the ratio Aβ42/Aβ40 was decreased by almost 50% for mutant cell lines, except for hPS1ΔE9 as expected, because this mutation causes a complete lack from γ-secretase activity. Similar to Cyclosporin A, a well-described mPTP inhibitor, DAPT was able to significantly inhibit mPTP opening in mock hPS1WT and hPS1E280A cells but not in hPS1ΔE9 cells. On the other hand, 2-APB only affected mPTP opening in PS1 mutants, inhibiting it in hPS1E280A cells and accelerating it in hPS1ΔE9 cells (Figure 29A).

The effect of γ-secretase inhibition on mPTP opening was confirmed by using another γ-secretase inhibitor, Compound W, in mock hPS1WT and hPS1E280A cells (Supplemental Figure 8B). Given the possible effect of mitochondrial Ca^{2+} levels to drive the opening of mPTP, mitochondrial and cytoplasmic Ca^{2+} concentration under DAPT and 2-APB treatments in hPS1 overexpressing cells were evaluated. As expected, only 2-APB had an impact in Ca^{2+} levels in both, mitochondria and cytoplasm, although mitochondrial Ca^{2+} levels were unaffected by 2-APB in mock cells (Figure 29 B-C). These results indicate that γ-secretase activity influences mPTP opening and that this role is affected by PS1 mutations while the intracellular Ca^{2+} regulation is a PS1 γ-secretase independent role.

5. Discussion

5.1 hPS1 transgenic mice phenotype

PS1 mutations have been found in screenings for FAD in chromosome 14. PSs are better known for their role as the catalytic component of the γ-secretase complex, and different mouse models have been developed with the mutations identified in humans, but, to date, there has been no ideal mouse model that fully represents what has been reported in human patients (Elder et al. 2010). There is wide variability in the severity of the damage produced by PS1 mutations in murine models but most of the studies showed that single transgenic mice present with impaired neurogenesis and several pathological features including age-related neuronal and synaptic loss at later ages (Elder et al. 2010), which is in accordance with findings in humans because the time course of the disease can last 20 or even more years (Bateman et al. 2012; McDade et al. 2018).

Neuronal and synaptic loss are considered hallmarks of AD (Scheff, Neltner, and Nelson 2014), but a recent study conducted in human samples at different stages of AD demonstrated that the levels of expression of synaptic markers in total homogenates of neocortical Brodmann area 9 were not significantly affected by dementia (Poirel et al. 2018). However, Aβ toxicity has been proposed as the main effector for neuronal death in patients (Morishima et al. 2001), and a good model should include this feature. In transgenic mice, the results are variable. Aged mice (older than 13 months) PS1-FAD models present neurodegenerative changes and neuronal loss (Chui et al. 1999) and, to date, only in one knock-in mouse with the mutation I213T, NFT-like inclusions were found (Tanemura et al. 2006).

In general, single mutation transgenic models do not exhibit any behavioral or cognitive impairment (Hall and Roberson 2012), or at least a very mild one. In the models used in this study, neurons from the CA1 region were chosen for neuronal counting, because the most noticeable damage observed in patients has been localized in the CA1 and CA3 (Padurariu et al. 2012) hippocampal regions. However, both controls and transgenic mice presented the same number of neurons at every age evaluated (Figure 11), confirming previous studies in which these kinds of

models do not exhibit this characteristic (Irizarry, McNamara, et al. 1997; Irizarry, Soriano, et al. 1997; Chui et al. 1999), in the ages studied here.

The absence of plaques could contribute to these observations, since neuronal loss has been attributed to the accumulation of Aβ, because the peptide induces cell death in different *in vitro* models (Liu et al. 2017; Shaked et al. 2006; Reifert, Hartung-Cranston, and Feinstein 2011; Wei, Wang, and Kusiak 2002). However, in humans, the situation is different; plaques are found in non-demented individuals (Maarouf et al. 2011; Zolochevska et al. 2018), which implies that the deposition of proteins is part of the normal aging process that does not necessarily means dementia or, specifically, AD. Additionally, there is a low correlation between the burden of plaques and the degree of dementia (Arriagada et al. 1992; Nelson, Braak, and Markesbery 2009).

Most of the PS1 transgenic models show an elevated production of Aβ42 (Kitazawa, Medeiros, and Laferla 2012; Richardson and Burns 2002). Here, as expected, it was found that Aβ40 is more abundant than Aβ42 in mice brains, but the hPS1G384A mutation presented the highest production of the more hydrophobic and more prone to aggregation peptide Aβ42 (Figure 13), this was also demonstrated by the higher Aβ42/Aβ40 ratio present in the brains of these mutants. It is important to emphasize that these mice do not produce plaques and in general, the Aβ produced in mice differs in three amino acids from its human homolog, and it is less amyloidogenic (Chui et al. 1999).

In the case of mutations for hPS1 it is widely accepted that there is an increase of toxic oligomers, but, in APP, there is controversy around the effects of the different mutations. For example, a study by Jonsson et al. (Jonsson et al. 2012), proposes that the Iceland mutation APPA673T does not cause AD, on the contrary, it is protective because it decreases the production of Aβ

A study published by Xia et al. (Xia et al. 2015), with knock-in mice homozygous for mutations L435F and C410Y in hPS1, recapitulates the phenotype observed in the PS1 knockout model, demonstrating that both single mutations abolished the γ-secretase activity, impaired Notch signaling, and neurogenesis. This research

suggests that the loss of function of PS1 must be responsible for the pathological effects and that it should be reconstituted rather than inhibited to treat the disease. Currently, it is clear that the biological role of PS1 in AD is more complex and goes beyond being the catalytic portion of a larger complex. Mutations, like substitutions for proline, lead to aggregation (Ben-Gedalya et al. 2015) but the role of the other mutations is still the subject of numerous studies.

The synaptic transmission can be recorded through electrophysiological methods. In old Tg2576 mice, probably the most well-characterized and one of the widely used AD models, LTP is severely affected in CA1, and dentate gyrus (Chapman et al. 1999) and dendritic spine loss and behavioral impairment accompanied this phenotype (Lanz, Carter, and Merchant 2003). Even so, conflicting results have also been published in which no alteration of synaptic transmission was detected in APPSwe/PS1Δ9 transgenic mice (Volianskis et al. 2010) nor APPK670N-M671L/PS1A246E (Fitzjohn et al. 2010), both studies were performed in aged mice.

In this study, ex-vivo brain slices were prepared and, as expected, no difference was found in the mice carrying the hPS1E280A mutation. However, interestingly, the brains with the hPS1G384A mutation presented an enhancement in LTP (Figure 12). The mice used were adults, of six months of age. The same phenomenon was also identified in knock-in PS1M146V mice in early LTP with animals of three months of age, but not in older animals (Auffret et al. 2010).

Similar results were also found in transgenic mice with another PS1 mutation, the A246E (Parent et al. 1999) when theta burst stimulation was applied (a form of stimulus more efficient in the induction of LTP (Larson and Munkacsy 2015)) like the one used the present study. Auffret et al. discussed that early-LTP is the most common form of LTP measured in FAD and SAD models, but the same research also shows that late-LTP decreases with age in the same knock-in mice used. Late LTP is related to long term memory in which protein synthesis takes place. Those results agreed with the findings shown here and demonstrated once again that experiments performed in physiological rodent models reproduced the results obtained in transgenic overexpression mice. The present results do not allow to establish the mechanism by which this increase in LTP is taking place, but it is clear that the

overexpression paradigm is not affecting the early synaptic response in these adult transgenic mice.

A remarkable decrease in the number of dendritic spines was also identified in both transgenic lines (Figure 14). Shape and number of spines can be affected for different factors in AD, such as Aβ accumulation, microglia activation and tau hyperphosphorylation (Dorostkar et al. 2015). It is of importance to note fewer protrusions in these cells, since they were evaluated in basal conditions, with no addition of toxic substances. What is intriguing is that this effect was not strong enough to induce behavioral impairment in adult animals, so it means it is not persistent or chronic, but, as with other cellular processes, the change of morphology of the spines is dynamic and adapts to different cellular conditions (Izeddin et al. 2011; Berry and Nedivi 2017).

The changes in dendritic spines imply increased formation (associated with motor learning) and, in this task, some of those spines are permanent. However, for other purposes, the synaptic spines are in constant turnover, producing and eliminating prolongations according to environmental factors. Loss of spines is another feature in neurodegenerative disorders associated with impairment of many signaling pathways (Herms and Dorostkar 2016).

Taken together, these findings demonstrate that the transgenic mice used here are a pre-clinical model, characterized by subtle phenotypic differences. Also, both hPS1 mutants showed early impairment in primary neurons in the absence of human APP expression and amyloid pathology, unrelated to the overproduction of Aβ42. These differences should be taken into consideration when using PS1 animal models for Alzheimer's research.

5.2 Early mitochondrial defects hPS1E280A transgenic mice

Early prevention and detection have the highest importance in neurodegenerative diseases. In AD it is critical since it is complicated to treat the symptoms after postmitotic neurons degenerate irreversibly. It is well established that the pre-clinical phase of AD is so long that it is considered a disease to prevent, not to cure

(Sasaguri et al. 2017; Zahs and Ashe 2010). Additionally, the long phase between the first symptoms and the cognitive decline is crucial and convenient to intervene to stop progression.

Although the influence of the β-amyloid cascade in AD is undeniable, recent discoveries point to a broader spectrum in the development of the disease, in which not only the accumulation of toxic proteins plays a role. AD is a multifactorial pathology in which several cellular functions are impaired before the appearance of protein deposits. PS1 not only has to deal with the production of the different isoforms of Aβ, but it is also implied in many other critical cellular processes that have the potential to contribute to disease states by their own, not only depending on the toxic factors that accumulation of proteins cause (Pimplikar et al. 2010).

While the role of mitochondria in different neurodegenerative disorders is clear, especially in the ones whose mitochondria genes are directly involved, in the case of AD it is less evident if they cause part of the disease or are just being affected by cellular pathways triggered by Aβ. Despite that some researchers proposed the presence of PS1 and γ-secretase in this organelle almost 20 years ago, many questions remain open on this subject.

The results presented here demonstrate that neurons from adult hPS1E280A mice have a significantly increased number of abnormal mitochondria. Near 75% of mitochondria in hPS1E280A adult brain mice present absence of cristae (Figure 15) and additionally, primary neurons present more fragmented mitochondria and defects in oxygen consumption (Figures 18 and 19). Surprisingly, the quantification of mitochondria and ER contacts gave no difference (Figure 16), contrary to what has been published in some studies in which increased ER-mitochondria connectivity was detected in MEF mutant PS1 cells, in human fibroblasts from individuals with FAD mutations in PS1 (Area-Gomez et al. 2012) and also in primary hippocampal neurons (Hedskog et al. 2013). This discrepancy can be explained by the fact that those studies used different transgenic mice, not the ones used here, carrying multiple mutations. Furthermore, the hPS1E280A mutation has been shown to reduce points of contact between ER-mitochondria in human cerebellar tissue and cell models (Sepulveda-Falla et al. 2014). Additionally, the communication between the ER and

the mitochondria is a dynamic process, one that changes frequently, and, with the electron microscopy, it is not possible to address such a changing phenomenon in adult brains. Filadi et al. suggest that only PS2 and Mfn2 are necessary to establish the contacts between these organelles and that PS1 and Mfn1 are not essential in the process (Filadi et al. 2016).

MAM isolation was done to test the concentrations of the 40 and 42 isoforms of Aβ. Both peptides were identified, in levels similar to the ones detected in a previous research (Schreiner et al. 2015), with the transgenic mice more prone to express higher amounts of the Aβ42 isoform. This finding corroborates the presence of Aβ in these membranes, which could be indicative of a γ-secretase PS1 associated function. However, the mere presence of members of this complex does not guarantee their activity, and technical reasons also interfere, because it is almost impossible to obtain completely 'pure' fractions that could also explain why PSs have been found in different locations within the cell, including nuclei and cytoplasm, apart from the ER and the Golgi apparatus.

APP, PSs, Aβ and γ-secretase activity are enriched in lipid rafts (Vetrivel et al. 2004; Urano et al. 2005) and the MAMs are considered membranes with such characteristics. The catalytic activity of γ-secretase in MAMs can influence cholesterol ester synthesis (Area-Gomez et al. 2012), but Aβ has been detected in such membranes in another mouse model (Schreiner et al. 2015) with ELISA. As shown in this study, the concentration of Aβ40 remained unchanged between groups, but a higher level of Aβ42 was evident for the brains with the hPS1 mutations.

Aβ has also been reported in mitochondria in an *in vitro* assay (Cha et al. 2012), and it has been suggested that its accumulation impacts ER-mitochondria communication in biopsies of human brains with plaques and neurofibrillary tangles (Leal et al. 2018). It is not surprising to detect PS1 and Aβ in MAMs. In the spots where ER and mitochondria communicate, multiple signaling and relevant functions take place. In those membranes, molecular chaperones, lipid enzymes, apoptosis-related proteins and proteins involved in protein degradation, among others, meet (Fujimoto and Hayashi 2011).

The ER is an organelle in constant communication with mitochondria, and they are connected physically and biochemically (Hayashi et al. 2009). PS1 as an ER protein can be part of this communication, but it is unlikely that this function depends only on γ-secretase. Indeed, previous researchers have also postulated the interaction of Aβ (Park et al. 2004) and PS1 (Gray et al. 2000) with HtrA2/Omi, a protein released from the mitochondria to the cytosol in response to apoptosis (Teng and Tang 2005).

Additionally, a variety of proteins serve as scaffolds between the ER and the mitochondria, making of this association one of a kind because it does not depend on cytoskeleton proteins (Paillusson et al. 2016). It makes sense that PS1 is part of a larger scaffolding complex since it interacts with Ca^{2+} signaling proteins, such as IP3R, in charge of the direct transmission of this important element to mitochondria, ending up in the activation of the tricarboxylic acid cycle (TCA) (Kania et al. 2017). IP3R, Grp75, and VDAC are part of the protein complex that helps to stabilize ER and mitochondria connections (Szabadkai et al. 2006).

In the present study, mitochondrial morphological and functional abnormalities were found, but only for the E280A mutation. It is very interesting that abnormal mitochondrial morphology was observed both in primary hippocampal neurons as well as in the hippocampus of adult animals. In the case of primary neurons, a significant number of fragmented mitochondria were found, but also a consistent population of mitochondria remained associated or elongated (Supplemental Figure 2). The mitochondrial morphology in neurons is complex, and, although most studies have shown that alterations in morphology in AD are related to mitochondrial fission (Baek et al. 2017), there is a hypothesis that states that fission in disease states can also be arrested, as an alternative mechanism to react against a challenging condition (Zhang et al. 2016).

Defects in morphology are correlated with a low capacity of the neurons to consume oxygen under different conditions, as well as less ATP turnover, measured with the addition of Oligomycin to inhibit the ATP synthase (complex V) (Kalbacova et al. 2003). Basal respiration was affected from the beginning in hPS1 mutant primary neurons compared to controls. Therefore, it was not unexpected to find that the maximum respiratory capacity, tested with the addition of FCCP, was also impaired

compared to controls. These results clearly show mitochondrial damage without the contribution of Aβ plaques, suggesting that, at least in these mutants, the mitochondrial malfunction lies upstream. These results agree with previous ones in which the respiration capacity is decreased (Yao et al. 2009), but do not reinforce other hypotheses that state that mitochondria are hyperactive and exhibit an enhanced performance of the OXPHOS, a study performed by Sarasija et al. in *C. elegans* and fibroblasts from patients with FAD mutations (Sarasija et al. 2018).

Mitochondrial alterations have been found in other mouse models, like the human APP K670/M671L, human PS1M146L, double transgenic obtained by crossing the ones mentioned before, triple transgenic 3xTgAD and human tau (P301S). Changes include reduced mitochondrial potential, reduced ATP and altered brain energetics (Zhang et al. 2016), which is not surprising for the mice with the more aggressive phenotypes, but points to that in the case of single transgenic, early mitochondrial abnormalities are found and indicate that Aβ pathology is not a necessary driver of such defects. More importantly, it is remarkable that mitochondria were observed to be much more affected on a specific mutation, which emphasizes the various consequences that each mutation exerts in the biology of PS, affecting particular signaling cascades.

MAMs-related changes with PS1 mutations have been published (Schon and Area-Gomez 2010; Area-Gomez et al. 2012; Hedskog et al. 2013; Volgyi et al. 2018), but it is not clear whether they are an epiphenomena of a direct mitochondrial damage and, to test that, the preparation of an enriched-mitochondria fraction from brain mice tissue at different time points helped to characterize the protein profile and to determine if mitochondrial proteome changes are a result of a chronic process and if a putative initiator could be identified.

A proteomic study from Fu et al. (Fu et al. 2009), done in knock-in PS1 mice with the mutation M146V reported that the levels of components of the OXPHOS pathway, mPTP, and energy metabolism increased with age, which could be attributed to a compensatory mechanism. In the present research, 159 mitochondrial proteins were found to be dysregulated in hPS1 mutants. Their biological roles involve mainly mitochondrial respiration and RNA-related processes. None of the members of the γ-

secretase complex were identified contrary to previous researches in which PS1 and PS2 have been reported to be found in mitochondria or MAMs (Area-Gomez et al. 2009; Del Prete et al. 2017; Hayashi et al. 2012).

The results obtained here also indicate that mutations in PS1 influence the mitochondrial proteome, especially the respiratory chain and the synthesis of some of its components, as seen by the differences in expression also detected in mitochondrial ribosomal proteins. Indeed, proteins like the Mrpls and Mrps have been found as potential early markers of AD in blood. In those screenings, 50 genes were identified to be different from individuals with the disease and normal aging controls and eight of those genes belong to mitochondrial functions (Lunnon et al. 2013), while, in another study, components of the OXPHOS were also found to be downregulated in the blood of people with mild cognitive impairment (Lunnon et al. 2012). An extended study from the same group also provided evidence of the vulnerability of mitochondrial ribosomal proteins, affecting the expression of components of the complexes I, IV and V of the OXPHOS in human blood (Lunnon et al. 2017).

Interestingly, the protein Sco-2 was found upregulated in all ages examined in the hPS1E280A mutation. Sco-2 is necessary for the synthesis of COX (Cytochrome c oxidase) or complex IV of the respiratory chain, and they also participate in redox homeostasis (Ekim Kocabey et al. 2019). Although, there is no evidence of a direct modulation of this protein by PS1, these results agree with the findings in brain mitochondria presented here and substantiate the hypothesis that mitochondrial dysfunction is an early event in the pathology and emphasize the importance of intervention at this stage to halt the numerous consequences that the dysfunction of these organelles generate.

5.3 The influence of mutations in PS1 in mitochondrial function

Today, it is well-established that PS1 plays an important role in the regulation of Ca^{2+} signaling. In this study, two different methodologies were employed to show that mutations in PS1 affect directly Ca^{2+} storage and compartment-specific probes were used to evaluate mitochondria and ER Ca^{2+} buffering. Overexpression of hPS1WT

and mutated led to an increase in mitochondrial and cytosolic Ca^{2+} concentrations. ER Ca^{2+} refilling is smaller in PS1 E280A mutant N2a cells, which indicates that normal, functional PS1 is necessary for appropriated Ca^{2+} regulation.

The measurements of total Ca^{2+} and ER Ca^{2+} for hPS1E280A cells went along with similar findings with other PS1 point mutations (Zhang et al. 2010) and confirmed the results for PS1Δ9 (Cedazo-Minguez et al. 2002). Regarding mitochondrial Ca^{2+} concentration, PS1 overexpression, in general, showed an opposite effect to that reported for PS2 overexpression, which decreases mitochondrial Ca^{2+} concentration in SHSY5Y cells (Zampese et al. 2011).

Mutations in PS1 showed to have a high impact in the opening of the mitochondrial transition pore and the mitochondrial membrane potential, eliciting significant differences between mock-transfected cells and the two different mutations used in the experimental model. Mitochondrial function was assessed on N2a cells by the measurement of the mitochondrial membrane potential, which provides information about mitochondrial health and functionality.

With this method, it was found that PS1 overexpression per se was affecting the mitochondria. The mPTP opening was estimated using the Co^{2+}-calcein assay in live cell imaging, as Bonora et al. described (Bonora et al. 2016), (Figure 28 A-B), and, additionally, TMRM was used for an independent assessment of mPTP opening (Figure 28 C). Both assays showed that mPTP opening is significantly faster in PS1 E280A mutant cells, hinting at a mutant PS1-mediated pathway for mitochondrial damage and to a constitutive role for mutant PS1 in mPTP formation.

A very high $\Delta\Psi_m$ was found in hPS1Δ9 cells, statistically different to all experimental groups (Figure 28DE), together with slower mPTP aperture. Correlating this with increased mitochondrial potential could indicate mitochondrial function different to that detected in hPS1E280A. This finding is very interesting since mitochondrial hyperpolarization (increased $\Delta\Psi_m$) moves the mitochondrial transition pore away from the apoptotic threshold (Harvey and Chan 2017).

It should be noted that increased Ca^{2+} levels in hPS1 overexpressing cells could be a result of elevated $\Delta\Psi_m$. Furthermore, PS1 mutant cells responded abnormally to Ca^{2+} overload with PS1E280A accelerating and PS1Δ9 decelerating mPTP opening. The increase of the permeability of the inner mitochondrial membrane is not essential for the flux of mitochondrial Ca^{2+} (De Marchi et al. 2014) as it was observed when 2-APB was used to block the receptor of IP3 (Figure 29).

Assembly and activation of mPTP is part of mitochondrial stress responses and can potentially lead to apoptosis signaling. It has been suggested that Aβ toxicity can affect mPTP, whether indirectly via oxidative stress or directly, increasing Cyclophilin D translocation to the internal mitochondrial membrane and favoring mPTP opening (Du and Yan 2010). Also, a mathematical model has been proposed linking abnormal Ca^{2+} signaling, Aβ deposition and mPTP related apoptosis (Ranjan, Chong, and Zheng 2018). Remarkably, Aβ pathology is absent in the model used in this study and yet, cells overexpressing mutant hPS1 present with abnormal mPTP activity.

More to the point, γ-secretase inhibitors such as DAPT and Compound W effectively inhibit mPTP opening in mock, hPS1WT and hPS1E280A cells pointing to a role for γ-secretase in mPTP modulation through PS1 mutations. Decreased mPTP in hPS1Δ9 cells can be associated with significantly higher $\Delta\Psi_m$. However, γ-secretase dysfunction in hPS1Δ9 cells could also explain mPTP inhibition. Additionally, 2-APB affected mPTP opening only in PS1 mutants, again with contrasting effects between the two PS1 mutations. In those cells, 2-APB effectively compensated abnormal basal mPTP profiles while decreasing mitochondrial and cytoplasmic Ca^{2+} levels. Therefore, Ca^{2+} retention in the ER relieves mitochondrial Ca^{2+} overload in PS1 mutants which avoids abnormal mPTP opening.

This effect can be achieved via mitochondria-ER interaction, given Ca^{2+} exchange between these two organelles, as previously suggested by Toglia et al. in their model (Toglia and Ullah 2016) and the known effect of 2-APB in mitochondrial Ca^{2+} (Peppiatt et al. 2003) (Figure 29). Previous studies suggest increased ER-mitochondrial apposition leading to augmented Ca^{2+} trafficking between the two organelles as one possible explanation for mitochondrial dysfunction in AD (Area-Gomez et al. 2012), which could lead to mitochondrial stress and cell death. This

model of mitochondrial dysfunction in AD also portrays Aβ accumulation and toxicity as a causative factor (Butterfield, Swomley, and Sultana 2013; Umeda et al. 2011).

Independently of its extensive use, hPS1 overexpression in otherwise unmodified murine cells can always bring unexpected effects given the specific functional profiles of human vs. murine PSs (Stanga et al. 2018). The N2a hPS1 overexpression model used here has this limitation, and the results should be interpreted within this context. Nevertheless, we observed specific γ-secretase dependent and independent dysfunction in overexpressing hPS1 mutants.

Previously, an elegant study by Guo et al. in a murine knock-in model determined that PS1 mutations confer increased neuronal vulnerability to excitotoxicity via apoptosis in hippocampal cells. They also showed that impaired mitochondrial function increased susceptibility to Aβ-induced stress (Guo et al. 1999). The same group determined in PS1 transfected PC12 cells increased sensitivity to mitochondrial stress with associated elevated Ca^{2+} in PS1 mutants. Interestingly, CsA was used successfully to prevent apoptosis caused by oxidative stress in their model, and mPTP activation was suggested as a possible mechanism of increased mitochondrial stress in PS1 mutants (Keller et al. 1998). Toglia et al. recently suggested a theoretical model for the involvement of mPTP in PS1 mutants as a result of IP3R altered activity and increased mitochondrial Ca^{2+} uptake (Toglia and Ullah 2016; Toglia et al. 2016). In the current study, both hypotheses were confirmed, the previous findings and the theoretical model, plus a novel finding of γ-secretase as a direct modulator of mPTP independent of mitochondrial Ca^{2+} homeostasis was demonstrated.

In this work, an alternative mechanism for mitochondrial damage in PS1 FAD with altered mPTP is presented. PS1 mutation-dependent alterations in mitochondria detected in the model employed here occur under basal conditions or as a result of acute non-lethal cellular stress. With the previous findings of mitochondrial abnormalities in the cerebella from patients with the E280A mutation (Sepulveda-Falla et al. 2014), it is possible to suggest that in PS1 FAD patients basal cellular stress could be taking place throughout life, increasing vulnerability to damage in

susceptible cells and presenting eventually with cumulative effects leading to the complex endpoint pathology found in AD.

In summary, a PS1E280A-specific phenotype was found characterized by Ca^{2+}-related mitochondrial dysfunction (Figure 30). These results highlight the importance of mitochondrial function and homeostasis in FAD pathology and indicate alternative roles for PS1 in neurodegeneration.

6. Conclusions and Future Directions

The amyloid hypothesis should not be rejected but, at least, re-examined. The lack of effectiveness of all the medications designed to target Aβ tested to date poses new challenges in which new therapeutic approaches must be designed. Many alternative hypotheses have been proposed, from a mere cell cycle pathology, a vascular-derived disease and a systemic inflammation failure to a microtubule disturbance, among others. Additionally, another assumption, like the atypical phosphorylation of tau being mostly negative and contributive for the disease, was recently challenged with the demonstration that not all tau phosphorylation is toxic and that, site-specific phosphorylation helps to inhibit Aβ and neurotoxicity (Ittner et al. 2016).

Recent findings regarding a new mitochondrial degrading system (Hughes et al. 2016) together with the discovery of their new role in cellular quality control and aging provide enough evidence to consider that these organelles are central players in neurodegeneration performing such complicated duties. When AD is viewed as a neurometabolic disease, the role of mitochondria is more than obvious. The correct delivery of oxygen and glucose in the brain is primarily controlled, and a large amount of evidence shows the relationship between the metabolic syndrome and the risk to develop AD (Campos-Pena et al. 2017; Rios et al. 2014; Razay, Vreugdenhil, and Wilcock 2007; Rojas-Gutierrez et al. 2017).

The present results confirm that specific PS1 mutations render the cell more susceptible to mitochondrial dysfunction. Even one single mutation triggers mitochondrial changes, involving γ-secretase dependent and independent mechanisms simultaneously that can be identified without the participation of Aβ toxicity. Although further studies in cellular and animal models need to be done, the possibility is that earlier disease onset, more severe brain atrophy and underlying neurodegeneration in FAD are a result not only of earlier Aβ pathology but of underlying cellular vulnerability to stress due to other PS1 functions.

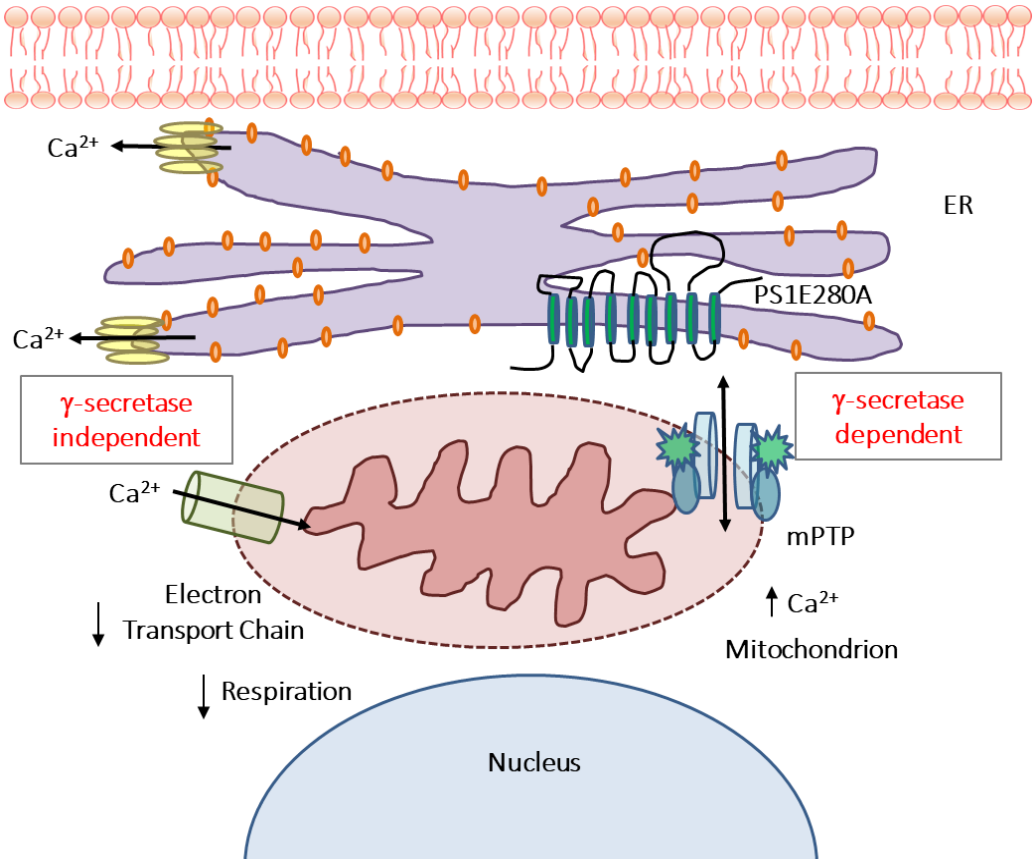

Figure 30. PS1E280A specific mitochondrial dysfunction. Mutation E280A induces a leaking of Ca^{2+} from the ER, which also increases Ca^{2+} concentrations in the cytosol and the mitochondria. High Ca^{2+} levels in the mitochondria affect diverse mitochondrial functions, such as the ETC capacity and respiration; mPTP opening is also a characteristic of the mitochondrial dysfunction in these mutants; mPTP is a large complex whose components are not entirely unveiled. The modulation of the opening of mPTP was depending on γ-secretase, but the mitochondrial and cytosolic accumulation of Ca^{2+} is not. The Δ9 mutation present an opposite behavior, characterized by $\Delta\Psi_m$ hyperpolarization which closes the mPTP.

7. Summary

Presenilins 1 and 2 (PS1 and PS2) are constitutive parts of the γ-secretase catalytic core, and their mutations lead to familial forms of Alzheimer's disease (FAD). Alzheimer's disease is one of the pathologies in which mitochondria are known to be affected, and PS1 has been found in mitochondrial-associated membranes, but its role there is still unclear. In this study, the role of PS1 in mitochondrial morphology and function was evaluated in transgenic mice overexpressing the human mutations G384A and E280A, as well as in primary neurons and N2a cells. Mitochondrial morphology was assessed with electron microscopy and immunofluorescence in hippocampal neurons. Whole brains were dissected from male mice at different ages to isolate enriched mitochondrial fractions for proteomic analysis. Mitochondrial health and functionality assays were also performed in the cells. The mitochondrial morphology of mice carrying the hPS1 E280A mutation, in both primary neurons and adult brains, was significantly different from that of controls. Mitochondrial proteomic analysis indicated variation in the expression of proteins especially related to respiration and mitochondrial ribosomal function. Mitochondrial oxygen consumption showed functional impairment in primary neurons from hPS1 E280A mutants but not in those from the G384A mutation. Stably transfected N2a cells expressing PS1WT, PS1-E280A, and PS1Δexon9 showed an increase in mitochondrial and cytosolic Ca^{2+} concentrations.

Additionally, PS1-E280A cells displayed a prompt opening of the mitochondrial transition pore compared to mock controls, while PS1Δexon9 cells showed the opposite, an effect dependent on γ-secretase activity. Although it is not known if mitochondrial dysfunction is a cause or a consequence of Alzheimer's neurodegeneration, increasing evidence has shown its relevance in cellular processes directly related to neurodegeneration. The present results demonstrate that the expression of PS1 specific mutations modulates mitochondrial morphology, oxygen consumption, and the abundance of ribosomal and respiratory mitochondrial proteins. It is remarkable that the mitochondrial phenotype differed between mutations, being more drastic in the hPS1 E280A mutants, which suggests a mutation-specific mitochondrial pathology in FAD.

8. Zusammenfassung

Presenilin 1 und 2 (PS1 und PS2) sind Bestandteile des katalytischen γ-Sekretase-Komplexes, deren Mutationen zu familiären Alzheimer-Erkrankung (FAD) führen. Morbus Alzheimer stellt eine Pathologie dar, bei welcher bekannt ist, dass Mitochondrien betroffen sind, wobei hier PS1 in Mitochondrien-assoziierten Membranen gefunden wurde. Jedoch ist die Rolle von PS1 in Mitochondrien-assoziierten Membranen bisher unklar. In der vorliegenden Studie wurde die Rolle von PS1 in der mitochondrialen Morphologie und Funktion in transgenen Mäusen, die die humanen PS1-Mutationen G384A und E280A überexprimieren, sowie in primären Neuronen und N2a-Zellen bewertet. Die mitochondriale Morphologie wurde mit Elektronenmikroskopie und Immunfluoreszenz in hippocampalen Neuronen untersucht. Proben von Gehirnen männlicher Mäusen in verschiedenen Altersstufen wurden disseziert, um angereicherte Mitochondrienfraktionen für die Proteomanalyse zu isolieren. Weiterhin wurden mitochondriale Vitalitäts- und Funktionstests auch in Zellenkultursystemen *in vitro* durchgeführt. Signifikante Unterschiede fanden sich in der Mitochondrienmorphologie sowohl in primären Neuronen als auch in erwachsenen Gehirnen von Mäusen, die die hPS1E280A-Mutation trugen, im Gegensatz zu Mitochondrien von Mäusen der Kontrollgruppe. Die mitochondriale Proteomanalyse zeigte zudem eine Variation in der Expression von Proteinen, insbesondere im Zusammenhang mit der Zellatmung und der mitochondrialen ribosomalen Funktion. Der mitochondriale Sauerstoffverbrauch zeigte funktionelle Beeinträchtigungen in primären Neuronen von hPS1E280A-Mutanten, nicht jedoch in den hPS1G384A-Mutanten. N2a Zellen, welche PS1WT, PS1E280A und PS1∆9 stabil exprimieren, zeigten einen Anstieg der mitochondrialen und zytosolischen Calciumkonzentrationen. Darüber hinaus zeigten PS1 E280A-Zellen im Vergleich Kontroll-Zellen eine sehr schnelle Öffnung der mitochondrialen Übergangspore, wohingegen im Fall der PS1 ∆9 eine gegenteilige Wirkung evident war, welche von der γ-Sekretase-Aktivität abhängt. Obwohl nicht bekannt ist, ob eine mitochondriale Dysfunktion eine Ursache oder aber eine Folge bei der Alzheimer-Neurodegeneration ist, mehren sich Hinweise, dass mitochondriale, zelluläre Prozesse direkt mit der Neurodegeneration zusammenhängen. Die Ergebnisse der vorliegenden Arbeit unterstützt diese These, indem die PS1-Expression spezifischer Mutationen die unterstützen Mitochondrienmorphologie, den Sauerstoffverbrauch

und die Sauerstoffmodulation beeinflusst und die Expression von ribosomalen und respiratorischen Mitochondrienproteinen moduliert. Hierbei ist bemerkenswert, dass sich der mitochondriale Phänotyp zwischen den bestimmten PS1 unterscheidet. Dies lässt auf eine mutationsspezifische mitochondriale Pathologie bei der familiären Alzheimer-Krankheit schließen.

9. Appendix

9.1 Supplemental Figures

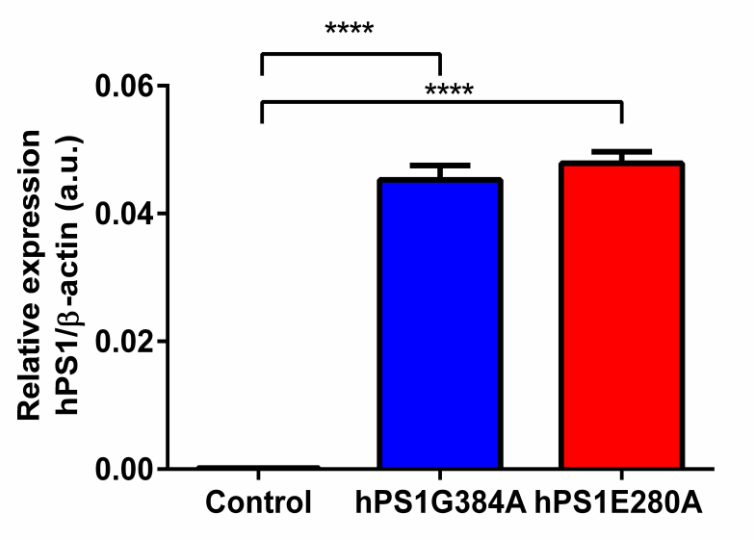

Supplemental Figure 1. **Human PS1 expression in primary neurons tested by qPCR.** RNA was prepared from primary neurons, converted to cDNA and tested with qPCR with specific primers for hPS1 and actin. Three independent experiments were performed, N=9. **P < 0.01, ***P < 0.001. Data are mean ± SEM, One-Way ANOVA.

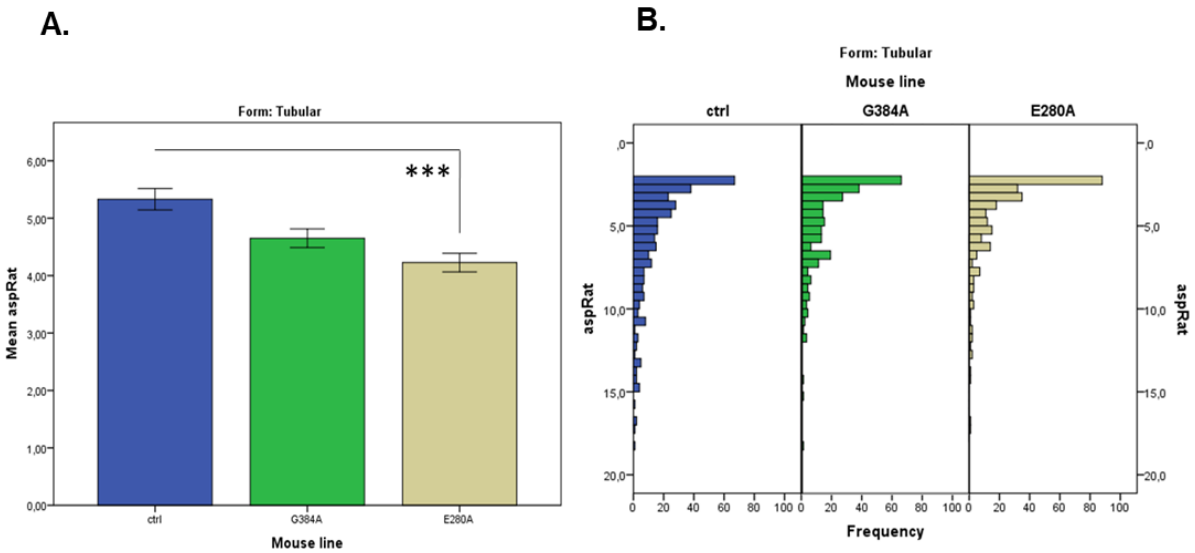

Supplemental Figure 2. **Primary hippocampal neurons from hPS1E280A mice have fewer tubular mitochondria. A.** Mitochondrial morphology was divided into fragmented and tubular. **B.** Frequency bars of the distribution of the different morphologies in the mice lines compared here. Data

are represented as mean ± SEM, *p<0.05. A total number of 30 neurons per experimental group were considered in the study. One-way ANOVA. Scale Bar=30 μm.

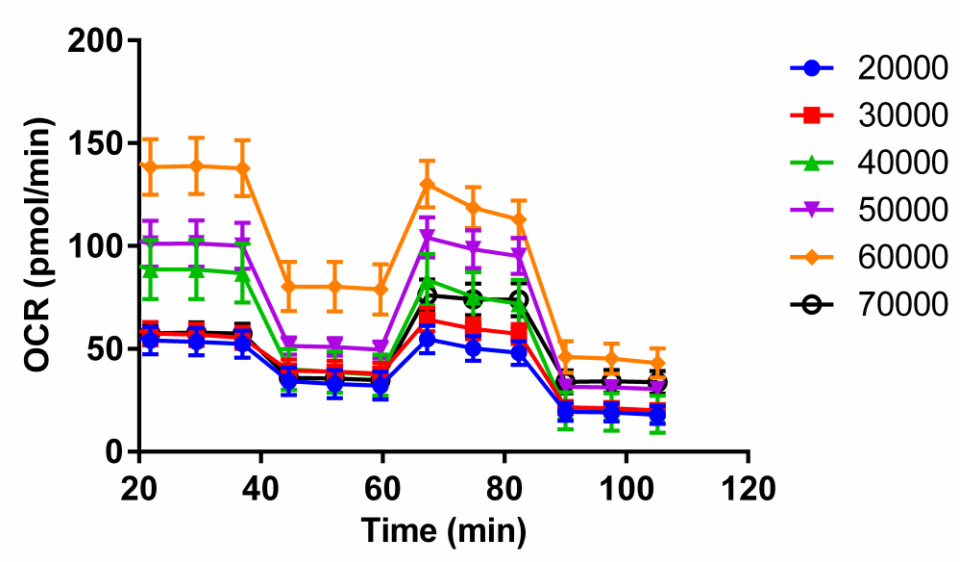

Supplemental Figure 3. **Standardization of the number of primary hippocampal neurons needed for Seahorse assay.** A different number of cells (starting with 20000) were seeded in 96 well/plates and subjected to Seahorse assay. Fifty thousand cells per well were chosen for the subsequent experiments.

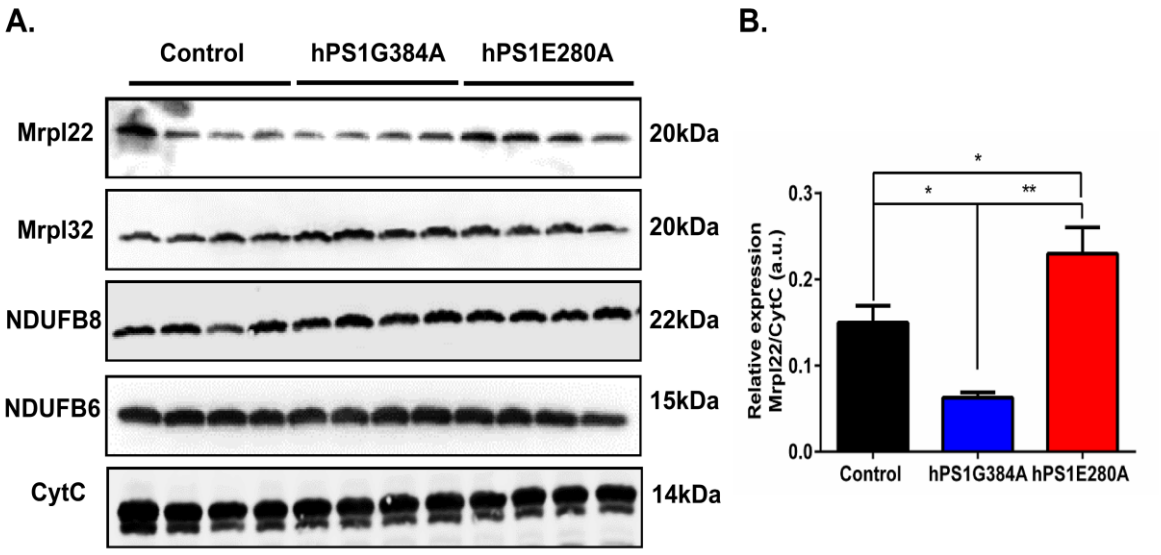

Supplemental Figure 4. **Validation of the dysregulation of Mrlp22**. **A.** Western blots of some proteins in mitochondrial-enriched fractions from brains of 6 months old mice. Mitochondrial enriched fractions lysates were run in polyacrylamide gels and tested for the proteins shown; 10 μg of total protein were loaded and the expression of CytC was used as loading control. **B.** Bar graphs showing the densitometry of the blot for Mrpl22 relative to the expression of CytC. Data are mean ± SEM, Independent T-tests, *P<0.05, **P<0.01, N=4.

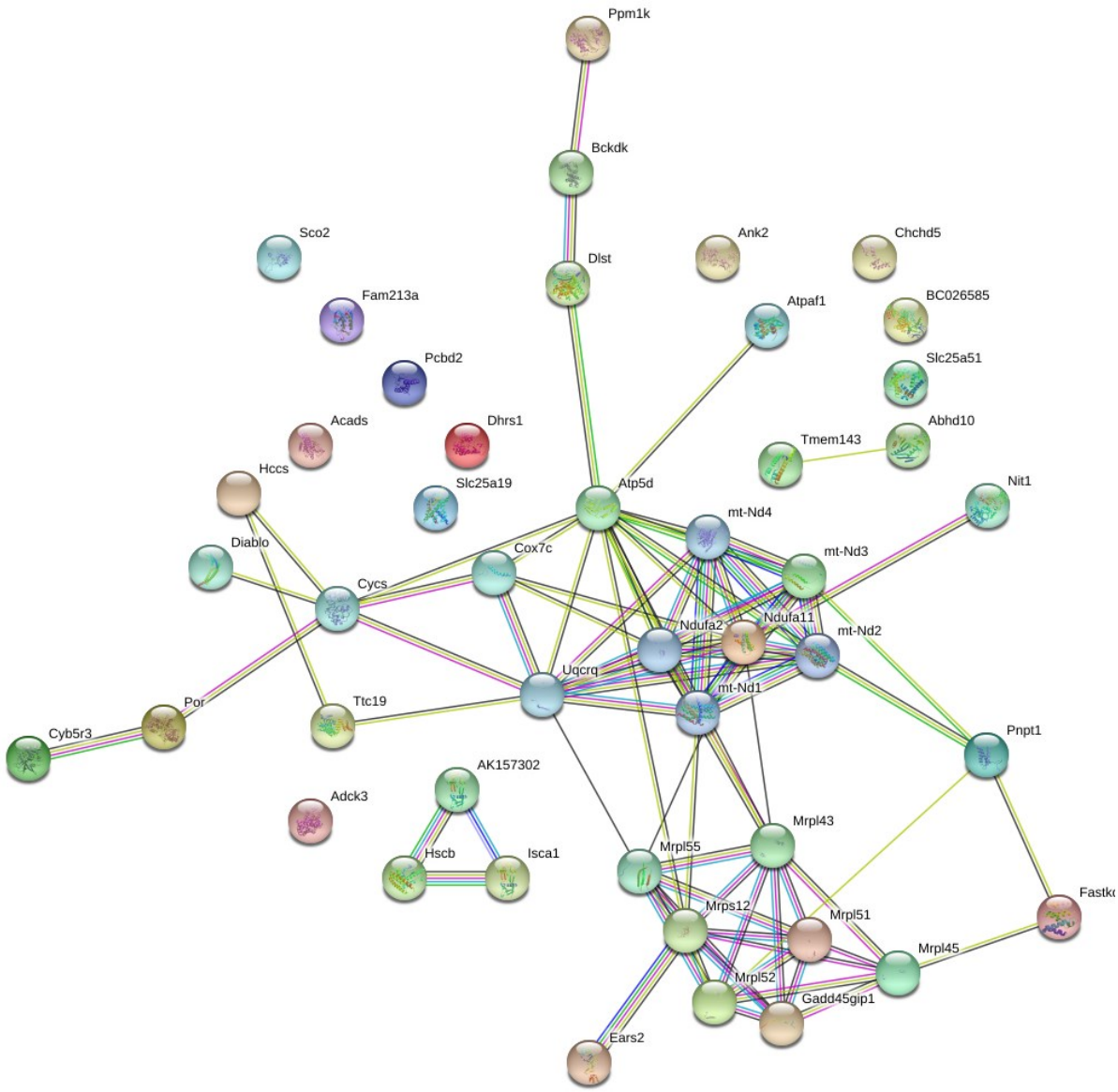

Supplemental Figure 5. Interaction network of the proteins dysregulated in the mitochondrial fractions of mutant hPS1 brains at one month of age. Two clusters of proteins are identified, the one related to mitochondria respiration proteins (Ndufa) and the one related to mitochondrial ribosomal proteins (Mrpl).

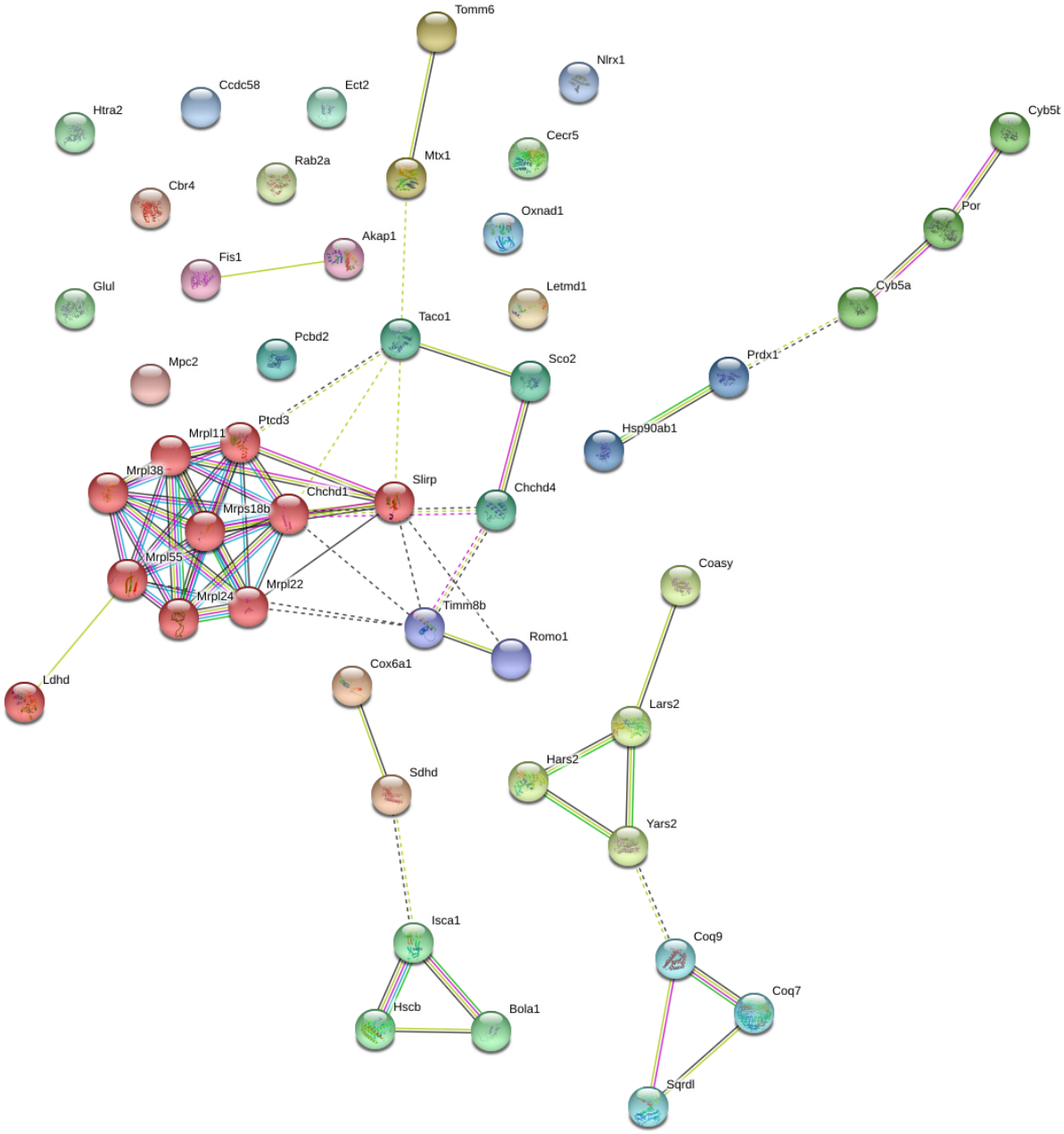

Supplemental Figure 6. Interaction network of the proteins dysregulated in the mitochondrial fractions of mutant hPS1 brains at six months of age. Red balls grouping mitochondrial ribosomal proteins.

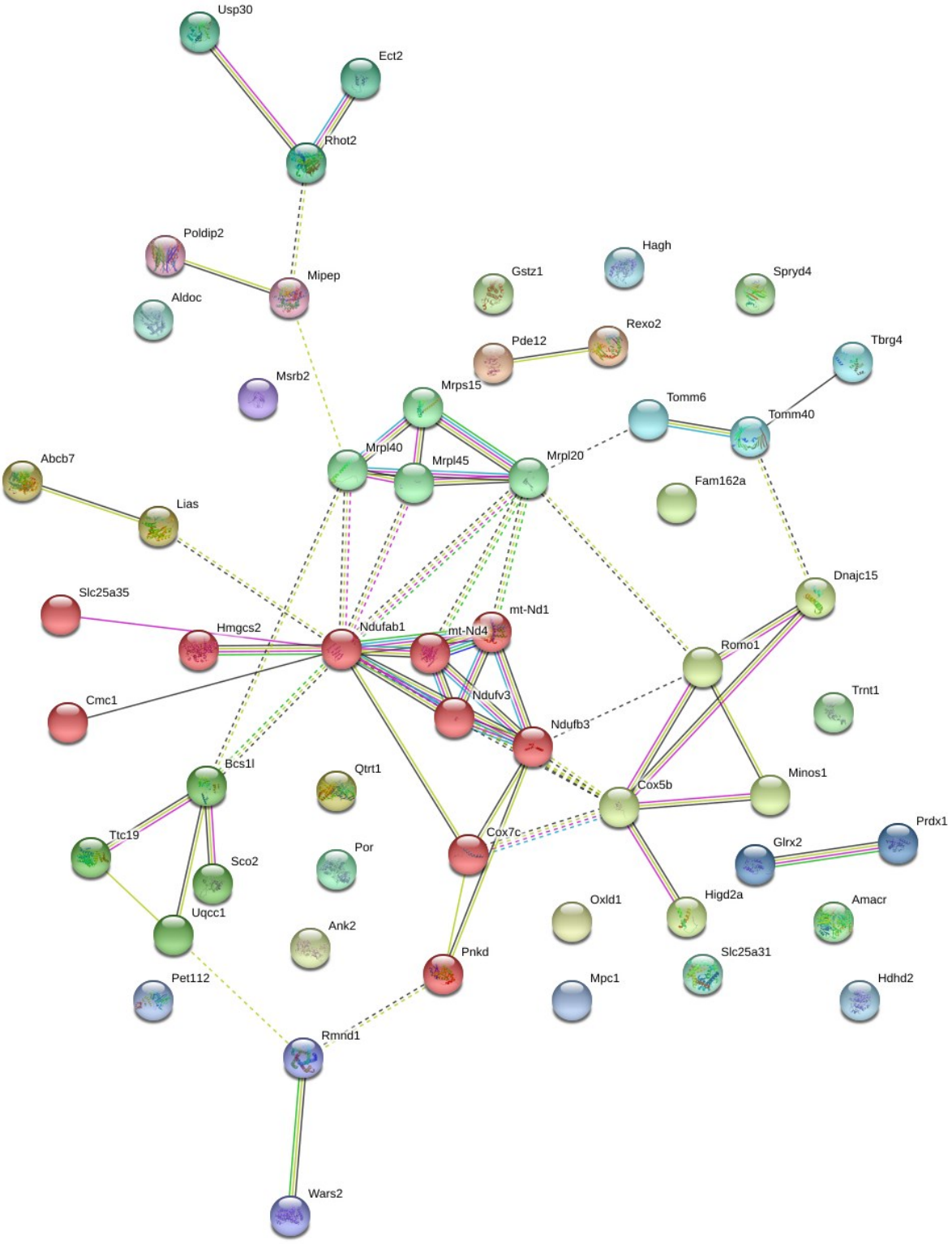

Supplemental Figure 7. Interaction network of the proteins dysregulated in the mitochondrial fractions of mutant hPS1 brains at 12 months of age. Two clusters of proteins are identified, the one related to mitochondria respiration proteins (Ndufa) and the one related to mitochondrial ribosomal proteins (Mrpls).

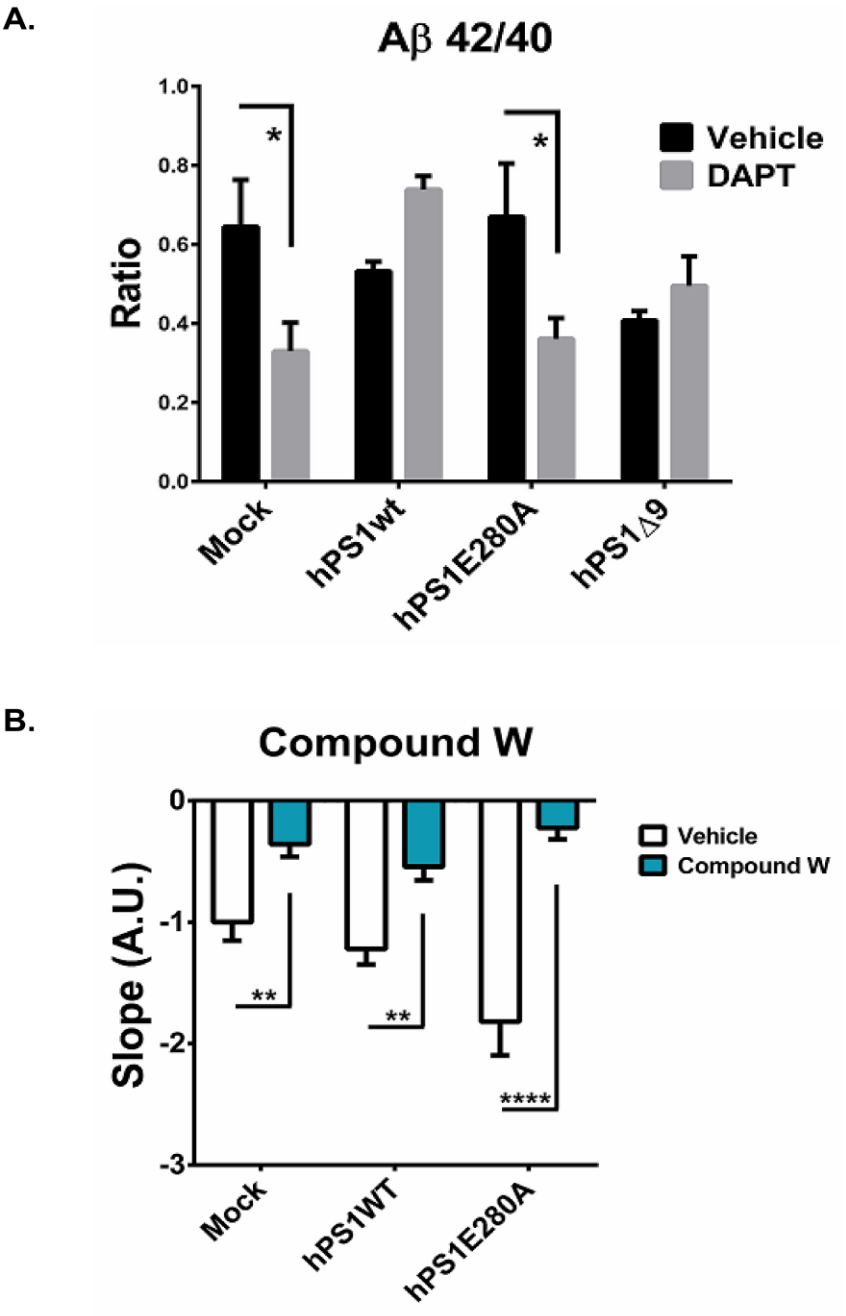

Supplemental Figure 8. Aβ42/Aβ40 production in N2a cells and effect of Compound W in mPTP opening. A. Aβ42/Aβ40 ratio in N2a stably transfected cells treated and non-treated with DAPT 1μM assessed with ELISA after 16h of treatment. DAPT treatment significantly decreased ratios in mock and hPS1E280A cells. **B.** mPTP activity assessed in N2a stably transfected cells treated and non-treated with an alternative γ-secretase inhibitor, Compound W (10mM). Cells were treated for 48h. Compound W significantly decreased MPTP activity in all cell lines. Data are mean ± SEM, *P < 0.05, **P < 0.01, ****P < 0.0001, Two-Way ANOVA.

9.2 Supplemental Tables

Supplemental Table 4. Proteins identified showing increasing and decreasing abundances in hPS1G384A mice vs controls at one month of age.

Fasta Header	Gene	Protein Name	P-Value	FC
RM55_MOUSE	Mrpl55	39S ribosomal protein L55, mitochondrial	3.325E-03	2.254
Q9D6E8_MOUSE	Sco2	Protein SCO2 homolog, mitochondrial	6.824E-03	1.843
DHRS1_MOUSE	Dhrs1	Dehydrogenase/reductase SDR family member 1	3.307E-02	1.631
ABHDA_MOUSE	Abhd10	Mycophenolic acid acyl-glucuronide esterase, mitochondrial	3.351E-02	1.607
COQ8A_MOUSE	Adck3	Atypical kinase ADCK3, mitochondrial	1.547E-02	1.484
G45IP_MOUSE	Gadd45gip1	Growth arrest and DNA damage-inducible protein-interacting protein 1	1.479E-02	-1.191
CCHL_MOUSE	Hccs	Cytochrome c-type heme lyase	2.571E-02	-1.422
Q80XJ6_MOUSE	Slc25a19	Mitochondrial thiamine pyrophosphate carrier	2.780E-02	-1.457
A2AKW0_MOUSE	Slc25a51	Solute carrier family 25 member 51	4.740E-02	-1.492
RM45_MOUSE	Mrpl45	39S ribosomal protein L45, mitochondrial	6.756E-03	-1.684
Q52KC5_MOUSE	Chchd5	Coiled-coil-helix-coiled-coil-helix domain-containing protein 5	7.316E-05	-1.819
RM52_MOUSE	Mrpl52	39S ribosomal protein L52, mitochondrial	1.071E-02	-1.826
I3ITR1_MOUSE	AK157302	Iron-sulfur cluster assembly 1 homolog, mitochondrial	2.151E-03	-1.864
A0A1B0GT63_MOUSE	Tmem143	Transmembrane protein 143	5.093E-03	-2.049
H3BLL2_MOUSE	Atpaf1	ATP synthase mitochondrial F1 complex assembly factor 1	1.083E-02	-2.745

Supplemental Table 5. Proteins identified showing increasing and decreasing abundances in hPS1E280A mice vs controls at one month of age.

Fasta Header	Gene	Protein Name	P-Value	FC
S4R2F3_MOUSE	Ank2	Ankyrin-2	1.262E-02	4.614
Q4FK74_MOUSE	Atp5d	ATP synthase subunit delta, mitochondrial	2.815E-02	2.615
A0A0R4J1R7_MOUSE	Pcbd2	Pterin-4-alpha-carbinolamine dehydratase 2	3.801E-02	2.464
Q9D6E8_MOUSE	Sco2	Protein SCO2 homolog, mitochondrial	4.258E-04	2.212

COX7C_MOUSE	Cox7c	Cytochrome c oxidase subunit 7C, mitochondrial	1.440E-02	1.356
NCPR_MOUSE	Por	NADPH--cytochrome P450 reductase	9.377E-03	1.310
ACADS_MOUSE	Acads	Short-chain specific acyl-CoA dehydrogenase, mitochondrial	3.706E-02	-1.195
TTC19_MOUSE	Ttc19	Tetratricopeptide repeat protein 19, mitochondrial	3.455E-02	-1.242
Q3UCB5_MOUSE	Bckdk	3-methyl-2-oxobutanoate dehydrogenase [lipoamide] kinase, mitochondrial	1.030E-02	-1.262
NIT1_MOUSE	Nit1	Nitrilase homolog 1	2.881E-02	-1.296
Q3U125_MOUSE	Fam213a	Redox-regulatory protein FAM213A	2.216E-03	-1.337
E9PUY1_MOUSE	Mrps12	28S ribosomal protein S12, mitochondrial	1.463E-03	-1.360
Q6ZQ14_MOUSE	Fastkd2	FAST kinase domain-containing protein 2	1.131E-02	-1.370
Q56A15_MOUSE	Cycs	Cytochrome c, somatic	2.322E-02	-1.394
CCHL_MOUSE	Hccs	Cytochrome c-type heme lyase	6.187E-03	-1.404
I3ITR1_MOUSE	Isca1	Iron-sulfur cluster assembly 1 homolog, mitochondrial	2.672E-02	-1.433
B9EHW0_MOUSE	Ppm1k	Protein phosphatase 1K, mitochondrial	1.851E-03	-1.494
PNPT1_MOUSE	Pnpt1	Polyribonucleotide nucleotidyltransferase 1, mitochondrial	2.319E-03	-1.506
SYEM_MOUSE	Ears2	Probable glutamate--tRNA ligase, mitochondrial	2.536E-02	-1.533
DBLOH_MOUSE	Diablo	Diablo homolog, mitochondrial	1.163E-05	-1.917
Q810B1_MOUSE	Mrpl43	39S ribosomal protein L43, mitochondrial	6.724E-03	-1.962
A0A0R4J0T0_MOUSE	Hscb	Iron-sulfur cluster co-chaperone protein HscB, mitochondrial	9.127E-03	-1.973
A0A1B0GT63_MOUSE	Tmem143	Transmembrane protein 143	3.784E-03	-2.022
Q80XJ6_MOUSE	Slc25a19	Mitochondrial thiamine pyrophosphate carrier	2.380E-03	-2.147
H3BLL2_MOUSE	Atpaf1	ATP synthase mitochondrial F1 complex assembly factor 1	1.917E-02	-2.445
Q7GIP5_MOUSE	mt-Nd3	NADH-ubiquinone oxidoreductase chain 3	2.120E-02	-2.475
RM51_MOUSE	Mrpl51	39S ribosomal protein L51, mitochondrial	1.949E-02	-2.669

Supplemental Table 6. Proteins identified showing increasing and decreasing abundances in hPS1E280A mice vs hPS1G384A at one month of age.

Fasta Header	Gene	Protein Name	P-Value	FC
S4R2F3_MOUSE	Ank2	Ankyrin-2	1.702E-02	4.396
Q52KC5_MOUSE	Chchd5	Coiled-coil-helix-coiled-coil-helix domain-containing protein 5	1.576E-05	1.892
S2540_MOUSE	Slc25a40	Solute carrier family 25 member 40	7.182E-03	-1.278
SYWM_MOUSE	Wars2	Tryptophan--tRNA ligase, mitochondrial	3.620E-04	-1.308
QORL2_MOUSE	BC026585	Quinone oxidoreductase-like protein 2	1.991E-02	-1.329
Q6GT24_MOUSE	Prdx6	Peroxiredoxin-6	3.335E-02	-1.486
KAT3_MOUSE	Ccbl2	Kynurenine--oxoglutarate transaminase 3	1.865E-02	-1.502
DBLOH_MOUSE	Diablo	Diablo homolog, mitochondrial	6.369E-03	-1.584
COQ6_MOUSE	Coq6	Ubiquinone biosynthesis monooxygenase COQ6, mitocondrial	4.859E-02	-1.723
ABHDA_MOUSE	Abhd10	Mycophenolic acid acyl-glucuronide esterase, mitocondrial	1.181E-02	-2.013
Q3TQD9_MOUSE	Sardh	Sarcosine dehydrogenase, mitochondrial	1.799E-03	-2.080
DHRS1_MOUSE	Dhrs1	Dehydrogenase/reductase SDR family member 1	4.151E-03	-2.364

Supplemental Table 7. Proteins identified showing increasing and decreasing abundances in hPS1G384A vs controls at six months of age.

Fasta Header	Gene	Protein Name	P-Value	FC
COQ7_MOUSE	Coq7	5-demethoxyubiquinone hydroxylase, mitochondrial	8.282E-04	1.574
Q9DCW5_MOUSE	Cox6a1	Cytochrome c oxidase subunit 6A	2.437E-02	1.410
F6SFF5_MOUSE	Coq9	Ubiquinone biosynthesis protein COQ9, mitochondrial	3.057E-02	1.274
HDHD5_MOUSE	Cecr5	Cat eye syndrome critical region protein 5 homolog	1.115E-02	1.227
TIM8B_MOUSE	Timm8b	Mitochondrial import inner membrane translocase subunit Tim8 B	1.701E-03	1.207
A0A0R4J0T0_MOUSE	Hscb	Iron-sulfur cluster co-chaperone protein HscB, mitochondrial	3.658E-03	1.203
Q14DS6_MOUSE	Lars2	Probable leucine--tRNA ligase, mitochondrial	5.993E-03	-1.227
SYHM_MOUSE	Hars2	Probable histidine--tRNA ligase, mitochondrial	2.656E-02	-1.237
COASY_MOUSE	Coasy	Bifunctional coenzyme A synthase	1.149E-03	-1.246

AKAP1_MOUSE	Akap1	A-kinase anchor protein 1, mitochondrial	4.002E-02	-1.264
NCPR_MOUSE	Por	NADPH--cytochrome P450 reductase	2.722E-02	-1.271
Q71LX8_MOUSE	Hsp90ab1	Heat shock protein HSP 90-beta	1.726E-02	-1.278
RM22_MOUSE	Mrpl22	39S ribosomal protein L22, mitochondrial	1.049E-02	-1.280
RM38_MOUSE	Mrpl38	39S ribosomal protein L38, mitochondrial	1.231E-02	-1.298
D3YX27_MOUSE	Htra2	Serine protease HTRA2, mitochondrial	3.463E-02	-1.298
Q4VAE6_MOUSE	Rhoa;Rhoc	Transforming protein RhoA;Rho-related GTP-binding protein RhoC	2.415E-02	-1.329
MPC2_MOUSE	Mpc2	Mitochondrial pyruvate carrier 2	4.326E-02	-1.357
CCD58_MOUSE	Ccdc58	Coiled-coil domain-containing protein 58	7.372E-03	-1.393
Q8R5C0_MOUSE	Mtx1	Metaxin-1	2.863E-02	-1.401
PTCD3_MOUSE	Ptcd3	Pentatricopeptide repeat domain-containing protein 3, mitochondrial	1.219E-02	-1.403
Q0PD65_MOUSE	Rab2a	Ras-related protein Rab-2A	2.808E-03	-1.432
SQOR_MOUSE	Sqrdl	Sulfide:quinone oxidoreductase, mitochondrial	1.184E-02	-1.451
Q8CEX1_MOUSE	Chchd1	Coiled-coil-helix-coiled-coil-helix domain-containing protein 1	1.003E-03	-1.641
RM11_MOUSE	Mrpl11	39S ribosomal protein L11, mitochondrial	4.529E-04	-1.652
CYB5B_MOUSE	Cyb5b	Cytochrome b5 type B	3.624E-03	-1.668
GLNA_MOUSE	Glul	Glutamine synthetase	3.744E-02	-1.709
TACO1_MOUSE	Taco1	Translational activator of cytochrome c oxidase 1	1.908E-02	-1.814
A0A0R4J1R7_MOUSE	Pcbd2	Pterin-4-alpha-carbinolamine dehydratase 2	2.171E-04	-1.865
BOLA1_MOUSE	Bola1	BolA-like protein 1	3.369E-03	-2.104
PRDX1_MOUSE	Prdx1	Peroxiredoxin-1	8.862E-03	-2.545
G5E850_MOUSE	Cyb5a	Cytochrome b5	3.079E-03	-2.565
LDHD_MOUSE	Ldhd	D-lactate dehydrogenase, mitochondrial	4.915E-04	-2.759

Supplemental Table 8. Proteins identified showing increasing and decreasing abundances in hPS1E280A vs controls at six months of age.

Fasta Header	Gene	Protein Name	P-Value	FC
SYYM_MOUSE	Yars2	Tyrosine--tRNA ligase, mitochondrial;Tyrosine--tRNA ligase	4.689E-07	3.207
RM24_MOUSE	Mrpl22	39S ribosomal protein L22, mitochondrial	2.824E-02	2.120
OXND1_MOUSE	Oxnad1	Oxidoreductase NAD-binding domain-containing protein 1	8.002E-03	1.807
LTMD1_MOUSE	Letmd1	LETM1 domain-containing protein 1	1.865E-02	1.552
F6VE93_MOUSE	Nlgn2;Nlgn4l	Neuroligin-2;Neuroligin 4-like	1.430E-02	1.548
CBR4_MOUSE	Cbr4	Carbonyl reductase family member 4	2.164E-02	1.492
Q3TKB7_MOUSE	Mrps18b	28S ribosomal protein S18b, mitochondrial	2.462E-03	1.346
MIA40_MOUSE	Chchd4	Mitochondrial intermembrane space import and assembly protein 40	5.229E-03	1.256
NLRX1_MOUSE	Nlrx1	NLR family member X1	2.888E-02	1.254
RM55_MOUSE	Mrpl55	39S ribosomal protein L55, mitochondrial	1.159E-02	1.245
ISCA1_MOUSE	Isca1	Iron-sulfur cluster assembly 1 homolog, mitochondrial	1.669E-02	1.228
Q9D6E8_MOUSE	Sco2	Protein SCO2 homolog, mitochondrial	4.260E-03	1.227
CCD58_MOUSE	Ccdc58	Coiled-coil domain-containing protein 58	2.007E-02	-1.225
Q14AR0_MOUSE	Slirp	SRA stem-loop-interacting RNA-binding protein, mitochondrial	3.163E-04	-1.287
BOLA1_MOUSE	Bola1	BolA-like protein 1	4.679E-02	-1.307
TACO1_MOUSE	Taco1	Translational activator of cytochrome c oxidase 1	3.936E-02	-1.388
DHSD_MOUSE	Sdhd	Succinate dehydrogenase [ubiquinone] cytochrome b small subunit	6.836E-04	-1.546
ROMO1_MOUSE	Romo1	Reactive oxygen species modulator 1	1.210E-04	-1.692
FIS1_MOUSE	Fis1	Mitochondrial fission 1 protein	1.275E-02	-2.117
TOM6_MOUSE	Tomm6	Mitochondrial import receptor subunit TOM6 homolog	2.036E-04	-2.405
G5E850_MOUSE	Cyb5a	Cytochrome b5	1.072E-03	-2.793

Supplemental Table 9. Proteins identified showing increasing and decreasing abundances in hPS1G384A vs hPS1E280A at six months of age.

Fasta Header	Gene	Protein Name	P-Value	FC
LDHD_MOUSE	Ldhd	Probable D-lactate dehydrogenase, mitochondrial	1.951E-04	2.942
SYYM_MOUSE	Yars2	Tyrosine--tRNA ligase, mitochondrial;Tyrosine--tRNA ligase	4.357E-04	2.608
RM38_MOUSE	Mrpl38	39S ribosomal protein L38, mitochondrial	2.554E-03	2.494
A0A0R4J1R7_MOUSE	Pcbd2	Pterin-4-alpha-carbinolamine dehydratase 2	4.602E-03	2.464
1433Z_MOUSE	Ywhaz	14-3-3 protein zeta/delta	1.034E-03	2.427
Q5PR72_MOUSE	Pde2a	cGMP-dependent 3,5-cyclic phosphodiesterase	1.932E-03	2.334
COX7C_MOUSE	Cox7c	Cytochrome c oxidase subunit 7C, mitochondrial	1.308E-02	2.273
F6VE93_MOUSE	Nlgn2;Nlgn4l	Neuroligin-2;Neuroligin 4-like	7.289E-05	2.190
Q8CEX1_MOUSE	Chchd1	Coiled-coil-helix-coiled-coil-helix domain-containing protein 1	2.811E-04	2.146
RM22_MOUSE	Mrpl22	39S ribosomal protein L22, mitochondrial	4.748E-03	2.110
Q0PD65_MOUSE	Rab2a	Ras-related protein Rab-2A	3.513E-04	2.107
Q8K133_MOUSE	Rab24	Ras-related protein Rab-24	1.139E-04	2.077
GLNA_MOUSE	Glul	Glutamine synthetase	7.782E-03	2.040
B9EHN0_MOUSE	Uba1	Ubiquitin-like modifier-activating enzyme 1	1.344E-02	2.032
LTMD1_MOUSE	Letmd1	LETM1 domain-containing protein 1	5.665E-03	1.968
Q14DS6_MOUSE	Lars2	Probable leucine--tRNA ligase, mitochondrial	3.427E-03	1.966
Q5SS40_MOUSE	Ywhae	14-3-3 protein epsilon	9.117E-03	1.932
Q6ZWM8_MOUSE	Ppp1cc	Serine/threonine-protein phosphatase PP1-gamma catalytic subunit	3.243E-04	1.841
Q3U9R7_MOUSE	Gsr	Glutathione reductase, mitochondrial	4.536E-05	1.768
PRDX1_MOUSE	Prdx1	Peroxiredoxin-1	1.023E-03	1.744
ISCA1_MOUSE	Isca1	Iron-sulfur cluster assembly 1 homolog, mitochondrial	2.613E-03	1.724
Q3TQD9_MOUSE	Sardh	Sarcosine dehydrogenase, mitochondrial	4.182E-03	1.718
G5E814_MOUSE	Ndufa11	NADH dehydrogenase [ubiquinone] 1 alpha subcomplex subunit 11	6.375E-03	1.713

CBR4_MOUSE	Cbr4	Carbonyl reductase family member 4	1.503E-02	1.673
MCUR1_MOUSE	Mcur1	Mitochondrial calcium uniporter regulator 1	2.955E-02	1.665
Q78ZJ8_MOUSE	Rab11b;Rab11a	Ras-related protein Rab-11B;Ras-related protein Rab-11A	9.274E-03	1.658
PDE12_MOUSE	Pde12	2,5-phosphodiesterase 12	2.385E-03	1.654
MIA40_MOUSE	Chchd4	Mitochondrial intermembrane space import and assembly protein 40	4.851E-04	1.642
Q810B1_MOUSE	Mrpl43	39S ribosomal protein L43, mitochondrial	3.268E-02	1.621
Q7GIP5_MOUSE	Mtnd3	NADH-ubiquinone oxidoreductase chain 3	9.236E-04	1.601
KAT3_MOUSE	Ccbl2	Kynurenine--oxoglutarate transaminase 3	1.317E-03	1.524
SCMC3_MOUSE	Slc25a23	Calcium-binding mitochondrial carrier protein SCaMC-3	4.531E-02	1.507
RT17_MOUSE	Mrps17	28S ribosomal protein S17, mitochondrial	2.183E-04	1.496
PDPR_MOUSE	Pdpr	Pyruvate dehydrogenase phosphatase regulatory subunit	3.382E-02	1.445
UCP5_MOUSE	Slc25a14	Brain mitochondrial carrier protein 1	1.059E-04	1.435
OXND1_MOUSE	Oxnad1	Oxidoreductase NAD-binding domain-containing protein 1	3.963E-04	1.424
USMG5_MOUSE	Usmg5	Up-regulated during skeletal muscle growth protein 5	3.364E-02	1.405
TXTP_MOUSE	Slc25a1	Tricarboxylate transport protein, mitochondrial	3.647E-04	1.389
A0A1B0GT63_MOUSE	Tmem143	Transmembrane protein 143	2.843E-03	1.384
Q8R2U8_MOUSE	Pdk1	[Pyruvate dehydrogenase (acetyl-transferring)] kinase isozyme 1	3.589E-03	1.371
MICU3_MOUSE	Micu3	Calcium uptake protein 3, mitochondrial	8.929E-04	1.362
RM04_MOUSE	Mrpl4	39S ribosomal protein L4, mitochondrial	3.217E-02	1.343
GUF1_MOUSE	Guf1	Translation factor Guf1, mitochondrial	4.148E-04	1.332
Q3TRJ1_MOUSE	Vps35	Vacuolar protein sorting-associated protein 35	7.270E-03	1.315
XPP3_MOUSE	Xpnpep3	Probable Xaa-Pro aminopeptidase 3	4.981E-03	1.296
Q5NCJ9_MOUSE	Uqcr10	Cytochrome b-c1 complex subunit 9	5.549E-03	1.283
A0A0K1W397_MOUSE	Mt-Cyb	Cytochrome b	1.662E-02	1.276
S4R1E5_MOUSE	Gpx4;PHGPx	Glutathione peroxidase	1.434E-02	1.256
Q71LX8_MOUSE	Hsp90ab1	Heat shock protein HSP 90-beta	9.101E-03	1.253

PTCD3_MOUSE	Ptcd3	Pentatricopeptide repeat domain-containing protein 3, mitochondrial	8.265E-03	1.248
H3BLL2_MOUSE	Atpaf1	ATP synthase mitochondrial F1 complex assembly factor 1	1.114E-03	1.234
NCPR_MOUSE	Por	NADPH--cytochrome P450 reductase	2.332E-02	1.211
CN159_MOUSE	Dglucy	UPF0317 protein C14orf159 homolog, mitochondrial	4.332E-02	1.203
A0A1S6GWG5_MOUSE	Mrps9	28S ribosomal protein S9, mitochondrial	1.301E-02	1.202
RM19_MOUSE	Mrpl19	39S ribosomal protein L19, mitochondrial	2.483E-04	1.201
Q9CXU4_MOUSE	Timm23	Mitochondrial import inner membrane translocase subunit Tim23	3.960E-03	1.196
RT05_MOUSE	Mrps5	28S ribosomal protein S5, mitochondrial	4.640E-03	-1.274
Q3TML7_MOUSE	Mtco1	Cytochrome c oxidase subunit 1	3.649E-03	-1.275
TOM6_MOUSE	Tomm6	Mitochondrial import receptor subunit TOM6 homolog	2.112E-03	-1.277
A2AP31_MOUSE	Ndufb6	NADH dehydrogenase [ubiquinone] 1 beta subcomplex subunit 6	2.401E-04	-1.287
TOM40_MOUSE	Tomm40	Mitochondrial import receptor subunit TOM40 homolog	2.224E-02	-1.310
MIC13_MOUSE	Qil1	Protein QIL1	2.285E-03	-1.480
Q9MD82_MOUSE	Mtnd5	NADH-ubiquinone oxidoreductase chain 5	9.267E-03	-1.562
NDUA3_MOUSE	Ndufa3	NADH dehydrogenase [ubiquinone] 1 alpha subcomplex subunit 3	2.313E-03	-1.739
F6SFF5_MOUSE	Coq9	Ubiquinone biosynthesis protein COQ9, mitochondrial	4.724E-03	-1.994
Q9DCW5_MOUSE	Cox6a1	Cytochrome c oxidase subunit 6A	2.863E-03	-2.458

Supplemental Table 10. Proteins identified showing increasing and decreasing abundances in hPS1G384A vs controls at 12 months of age.

Fasta Header	Gene	Protein Name	P-Value	FC
NDUV3_MOUSE	Ndufv3	NADH dehydrogenase [ubiquinone] flavoprotein 3,	5.405E-04	3.656
MSRB2_MOUSE	Msrb2	Methionine-R-sulfoxide reductase B2, mitochondrial	3.613E-02	2.551
ROMO1_MOUSE	Romo1	Reactive oxygen species modulator 1	8.042E-03	2.481
Q9D6H6_MOUSE	Ndufb3	NADH dehydrogenase [ubiquinone] 1 beta subcomplex subunit 3	4.420E-02	2.293

UQCC1_MOUSE	Uqcc1	Ubiquinol-cytochrome-c reductase complex assembly factor 1	1.298E-02	1.882
Q8N7N8_MOUSE	Hmgcs2	Hydroxymethylglutaryl-CoA synthase, mitochondrial	2.653E-03	1.842
UBP30_MOUSE	Usp30	Ubiquitin carboxyl-terminal hydrolase 30	2.022E-02	1.797
Q8BLL4_MOUSE	Mipep	Mitochondrial intermediate peptidase	1.733E-02	1.796
A0A0R4J052_MOUSE	Hagh	Hydroxyacylglutathione hydrolase, mitochondrial	3.745E-02	1.717
A3KGA5_MOUSE	Mtcp1;Cmc4	Cx9C motif-containing protein 4	2.370E-02	1.660
Q78KL9_MOUSE	Rexo2	Oligoribonuclease, mitochondrial	7.777E-03	1.641
COX7C_MOUSE	Cox7c	Cytochrome c oxidase subunit 7C, mitochondrial	9.142E-05	1.442
Q9D881_MOUSE	Cox5b	Cytochrome c oxidase subunit 5B, mitochondrial	2.412E-02	1.199
Q9ME04_MOUSE	Mtnd4	NADH-ubiquinone oxidoreductase chain 4	1.417E-04	-1.325
Q4VAE6_MOUSE	Rhoa;Rhoc	Transforming protein RhoA;Rho-related GTP-binding protein RhoC	1.298E-02	-1.384
B7ZWF9_MOUSE	Oxld1	Oxidoreductase-like domain-containing protein 1	4.529E-04	-1.568
F162A_MOUSE	Fam162a	Protein FAM162A	2.397E-04	-1.622
D3Z786_MOUSE	Mpc1	Mitochondrial pyruvate carrier 1	3.809E-03	-1.644
A0A0R4J1J1_MOUSE	Pnkd	Probable Hydrolase	1.886E-02	-1.650
RT15_MOUSE	Mrps15	28S ribosomal protein S15, mitochondrial	1.167E-02	-1.667
ALDOC_MOUSE	Aldoc	Fructose-bisphosphate aldolase C	1.598E-05	-1.782
TGT_MOUSE	Qtrt1	Queuine tRNA-ribosyltransferase	1.716E-02	-1.841
PRDX1_MOUSE	Prdx1	Peroxiredoxin-1	3.555E-02	-1.949
B2RTC8_MOUSE	Slc25a31	ADP/ATP translocase 4	4.801E-03	-2.266
S4R2F3_MOUSE	Ank2	Ankyrin-2	1.821E-05	-3.693

Supplemental Table 11. Proteins identified showing increasing and decreasing abundances in hPS1E280A vs controls at 12 months of age.

Fasta Header	Gene	Protein Name	P-Value	FC
PDE12_MOUSE	Pde12	2,5-phosphodiesterase 12	9.189E-03	3.121
NCPR_MOUSE	Por	NADPH--cytochrome P450 reductase	3.394E-02	2.947
SYWM_MOUSE	Wars2	Tryptophan--tRNA ligase, mitochondrial	5.099E-03	2.640
Q3UQ95_MOUSE	Glrx2	Glutaredoxin-2, mitochondrial	7.137E-03	2.575
Q505E1_MOUSE	Pisd;Gm20671	Phosphatidylserine decarboxylase proenzyme	6.383E-03	2.459
V9GXI7_MOUSE	Mrpl20	39S ribosomal protein L20, mitochondrial	7.289E-03	2.333
Q8N7N8_MOUSE	Hmgcs2	Hydroxymethylglutaryl-CoA synthase, mitochondrial	1.276E-04	2.261
TTC19_MOUSE	Ttc19	Tetratricopeptide repeat protein 19, mitochondrial	5.760E-04	2.251
HDHD2_MOUSE	Hdhd2	Haloacid dehalogenase-like hydrolase domain-containing protein 2	8.560E-04	2.216
TRNT1_MOUSE	Trnt1	CCA tRNA nucleotidyltransferase 1, mitochondrial	9.397E-03	2.009
GATB_MOUSE	Gatb	Glutamyl-tRNA(Gln) amidotransferase subunit B, mitochondrial	8.713E-03	1.919
MIRO2_MOUSE	Rhot2	Mitochondrial Rho GTPase 2	2.310E-04	1.896
COX7C_MOUSE	Cox7c	Cytochrome c oxidase subunit 7C, mitochondrial	3.809E-02	1.857
A0A1Y7VJZ2_MOUSE	Gstz1	Maleylacetoacetate isomerase	3.223E-02	1.825
FAKD4_MOUSE	Tbrg4	Protein TBRG4	2.658E-02	1.664
Q3TNL9_MOUSE	Mtnd1	NADH-ubiquinone oxidoreductase chain 1	3.134E-02	1.608
F6ZFT1_MOUSE	Ndufab1	Acyl carrier protein;Acyl carrier protein, mitochondrial	2.770E-02	1.599
HIG2A_MOUSE	Higd2a	HIG1 domain family member 2A	2.270E-03	1.585
BCS1_MOUSE	Bcs1l	Mitochondrial chaperone BCS1	1.490E-02	1.474
TOM40_MOUSE	Tomm40	Mitochondrial import receptor subunit TOM40 homolog	4.275E-02	1.448
Q9D6E8_MOUSE	Sco2	Protein SCO2 homolog, mitochondrial	7.293E-03	1.446
Q9D6H6_MOUSE	Ndufb3	NADH dehydrogenase [ubiquinone] 1 beta subcomplex subunit 3	3.679E-02	1.420
A0A0M3HEP3_MOUSE	Lias	Lipoyl synthase, mitochondrial	4.130E-02	1.359

ABCB7_MOUSE	Abcb7	ATP-binding cassette sub-family B member 7, mitochondrial	3.830E-03	1.331
F6SQH7_MOUSE	Poldip2	Polymerase delta-interacting protein 2	3.212E-02	1.328
Q9CVE7_MOUSE	Cmc1	COX assembly mitochondrial protein homolog	3.996E-02	1.295
RMND1_MOUSE	Rmnd1	Required for meiotic nuclear division protein 1 homolog	3.160E-03	1.238
RM45_MOUSE	Mrpl45	39S ribosomal protein L45, mitochondrial	1.524E-02	1.213
DJC15_MOUSE	Dnajc15	DnaJ homolog subfamily C member 15	4.201E-02	1.197
MIC10_MOUSE	Minos1	MICOS complex subunit Mic10	3.694E-02	-1.190
D3Z7C0_MOUSE	Mrpl40	39S ribosomal protein L40, mitochondrial	2.103E-02	-1.365
SPRY4_MOUSE	Spryd4	SPRY domain-containing protein 4	1.814E-02	-1.598
Q91YQ8_MOUSE	Amacr	Alpha-methylacyl-CoA racemase	2.836E-02	-1.784
PRDX1_MOUSE	Prdx1	Peroxiredoxin-1	2.256E-04	-1.957
A0A0A0MQ70_MOUSE	Slc25a35	Solute carrier family 25 member 35	2.425E-03	-2.150
TOM6_MOUSE	Tomm6	Mitochondrial import receptor subunit TOM6 homolog	1.329E-02	-2.241

Supplemental Table 12. Proteins identified showing increasing and decreasing abundances in hPS1G384A vs hPS1E280A at 12 months of age.

Fasta Header	Gene	Protein Name	P-Value	FC
A0A0R4J1J1_MOUSE	Pnkd	Probable Hydrolase	1.532E-03	3.895
D3YZN4_MOUSE	Spg7	Paraplegin	4.157E-04	3.797
NCPR_MOUSE	Por	NADPH--cytochrome P450 reductase	1.556E-03	3.712
B2RTC8_MOUSE	Slc25a31	ADP/ATP translocase 4	2.386E-03	2.916
ALDOC_MOUSE	Aldoc	Fructose-bisphosphate aldolase C	2.583E-03	2.411
Q3UQ95_MOUSE	Glrx2	Glutaredoxin-2, mitochondrial	1.188E-02	2.383
Q810B1_MOUSE	Mrpl43	39S ribosomal protein L43, mitochondrial	5.218E-03	2.367
SYWM_MOUSE	Wars2	Tryptophan--tRNA ligase, mitochondrial	1.405E-02	2.201
TGT_MOUSE	Qtrt1	Queuine tRNA-ribosyltransferase	1.842E-02	2.174
AKAP1_MOUSE	Akap1	A-kinase anchor protein 1, mitochondrial	3.014E-02	2.069
F162A_MOUSE	Fam162a	Protein FAM162A	1.148E-02	2.035

PDE12_MOUSE	Pde12	2,5-phosphodiesterase 12	4.113E-02	2.023
NDUF6_MOUSE	Ndufaf6	NADH dehydrogenase (ubiquinone) complex I, assembly factor 6	3.530E-03	1.905
GATB_MOUSE	Gatb	Glutamyl-tRNA(Gln) amidotransferase subunit B, mitochondrial	2.042E-02	1.901
TACO1_MOUSE	Taco1	Translational activator of cytochrome c oxidase 1	3.755E-02	1.818
HDHD2_MOUSE	Hdhd2	Haloacid dehalogenase-like hydrolase domain-containing protein 2	3.202E-02	1.810
RM16_MOUSE	Mrpl16	39S ribosomal protein L16, mitochondrial	3.148E-02	1.787
F7ABX5_MOUSE	Bad	Bcl2-associated agonist of cell death	3.947E-02	1.673
D3Z786_MOUSE	Mpc1	Mitochondrial pyruvate carrier 1	6.061E-03	1.669
RM22_MOUSE	Mrpl22	39S ribosomal protein L22, mitochondrial	4.000E-02	1.662
J3QMN4_MOUSE	Txnrd2	Thioredoxin reductase 2, mitochondrial	2.458E-02	1.661
MIRO2_MOUSE	Rhot2	Mitochondrial Rho GTPase 2	1.389E-02	1.597
A0A1W2P7G5_MOUSE	Coq10a	Coenzyme Q10 a	2.641E-02	1.578
PLD3A_MOUSE	Slmo1	Protein slowmo homolog 1	4.275E-02	1.556
TTC19_MOUSE	Ttc19	Tetratricopeptide repeat protein 19, mitochondrial	7.333E-04	1.544
HIG2A_MOUSE	Higd2a	HIG1 domain family member 2A	2.887E-03	1.515
A0A0M3HEP3_MOUSE	Lias	Lipoyl synthase, mitochondrial	2.259E-02	1.397
CYB5B_MOUSE	Cyb5b	Cytochrome b5 type B	8.993E-03	1.386
RT15_MOUSE	Mrps15	28S ribosomal protein S15, mitochondrial	4.030E-02	1.316
XPP3_MOUSE	Xpnpep3	Probable Xaa-Pro aminopeptidase 3	4.170E-02	1.292
Q5EBQ0_MOUSE	Vdac3	Voltage-dependent anion-selective channel protein 3	2.325E-02	1.275
RT24_MOUSE	Mrps24	28S ribosomal protein S24, mitochondrial	1.802E-02	1.268
HDDC2_MOUSE	Hddc2	HD domain-containing protein 2	8.835E-03	1.260
E9PVS5_MOUSE	Immt	Micos complex subunit Mic60-1	7.821E-03	1.257
SYYM_MOUSE	Yars2	Tyrosine--tRNA ligase, mitochondrial	2.591E-02	1.248
KAT3_MOUSE	Ccbl2	Kynurenine--oxoglutarate transaminase 3	4.005E-02	1.231
Q5SVY0_MOUSE	Ogdh	2-oxoglutarate dehydrogenase, mitochondrial	3.674E-03	1.205
Q78KL9_MOUSE	Rexo2	Oligoribonuclease, mitochondrial	3.252E-02	-1.246

H3BLL2_MOUSE	Atpaf1	ATP synthase mitochondrial F1 complex assembly factor 1	1.166E-02	-1.483
AP4A_MOUSE	Nudt2	Bis(5-nucleosyl)-tetraphosphatase [asymmetrical]	2.861E-02	-1.691
D3Z7C0_MOUSE	Mrpl40	39S ribosomal protein L40, mitochondrial	6.940E-03	-1.796
Q9D881_MOUSE	Cox5b	Cytochrome c oxidase subunit 5B, mitochondrial	1.793E-02	-1.830
TOM6_MOUSE	Tomm6	Mitochondrial import receptor subunit TOM6 homolog	3.748E-02	-1.956
Q5U5I3_MOUSE	Mrps18a	28S ribosomal protein S18a, mitochondrial	2.895E-02	-2.078
SPRY4_MOUSE	Spryd4	SPRY domain-containing protein 4	1.316E-04	-2.726
NDUV3_MOUSE	Ndufv3	NADH dehydrogenase [ubiquinone] flavoprotein 3, mitochondrial	3.371E-06	-4.686

10. List of Figures

11. List of Abbreviations

AD	**Alzheimer Disease**	**P0/P1**	**Post Natal Day 0/ Post Natal Day 1**
Aβ	**Amyloid Beta**	**mg**	**Milligram**
APP	**Amyloid Precursor Protein**	**DM**	**Dissection Medium**
kDa	**Kilo Dalton**	**min**	**Minutes**
PSs	**Presenilins**	**GGM**	**Glial Growth Medium**
APH1	**Anterior Pharynx-Defective 1**	**x g**	**Relative Centrifugal Force**
PEN2	**Presenilin Enhancer 2**	**µm**	**Micrometer**
AICD	**Amino-terminal APP Intracellular Domain**	**NBM**	**Neurobasal Medium**
ErbB4	**Erb-b2 Receptor Tyrosine Kinase 4**	**PLL**	**Poly L Lysine**
TREM	**Triggering Receptor Expressed on Myeloid Cells**	**IF**	**Immunofluorescence**
CNS	**Central Nervous System**	**LTP**	**Long Term Potentiation**
NTF	**N-Terminal Domain**	**mOsm**	**Milliosmole**
CTF	**C-Terminal Domain**	**kg**	**Kilogram**
PS1	**Presenilin 1**	**°**	**Grades**
CSF1R	**Colony stimulating factor 1 receptor**	**ACSF**	**Artificial Cerebrospinal Fluid**
SAD	**Sporadic Alzheimer´s Disease**	**fEPSPs**	**Field Excitatory Postsynaptic Potential**
ApoE 4	**Apolipoprotein E-ε4**	**mV**	**Millivolts**
BIN1	**Bridging Integrator 1**	**µs**	**Microseconds**
PICALM	**Phosphatidylinositol Binding Clathrin Assembly Protein**	**s**	**Seconds**
ABCA7	**ATP Binding Cassette 7**	**Ca^{2+}**	**Calcium**
EPHA1	**Ephrin Type A Receptor 1**	**Hz**	**Hertz**
SORL1	**Sortilin Related Receptor 1**	**TBS**	**Tris Buffered Saline**
CD2AP	**CD2-associated protein**	**SDS-PAGE**	**Sodium Dodecylsulfate – Polyacrylamide Gel Electrophoresis**
TOMM40	**Translocase of Outer Mitochondrial Membrane 40**	**PVDF**	**Polyvinylidene Difluoride**
FAD	**Familial Alzheimer´s Disease**	**TBST**	**Tris Buffered Saline with Tween**
PS2	**Presenilin 2**	**h**	**Hour**
PKA	**Protein Kinase A**	**D.I. V**	**Days *in vitro***
PKC	**Protein Kinase C**	**NeuN**	**Neuronal N**

GS3Kβ	**Glycogen Synthase Kinase 3 Beta**	**WB**	**Western Blot**
JNK	**c-Jun N-Terminal Kinase**	**cDNA**	**Complementary Deoxyribonucleic Acid**
CDK5	**Cyclin Dependent Kinase 2**	**MAP2**	**Microtubule Associated Protein 2**
mRNA	**Messenger Ribonucleic Acid**	**Opa1**	**Mitochondrial Dynamin Like GTPase 1**
ER	**Endoplasmic Reticulum**	**KDEL**	**Lys-Asp-Glu-Leu Receptor**
NMDA	**N-methyl-D-aspartate**	**FACL4**	**Fatty acid-CoA ligase 4**
NICD	**Notch intracellular domain**	**Grp75**	**Glucose regulated protein**
N2a	**Neuroblastoma 2 a**	**ERO1**	**ER oxidoreductin 1**
WT	**Wild Type**	**VDAC**	**Voltage-Dependent Anion Channel**
cDKO	**conditional double knock-out**	**Tom20**	**Translocase of Outer Membrane 20**
MEF	**Mouse Embryonic Fibroblasts**	**GM130**	**Golgin subfamily A member 2**
DKO	**Double Knock-Out**	**Lamp1**	**Lysosomal-associated membrane protein 1**
DNA	**Desoxyribonucleic Acid**	**Mrpl**	**Mitochondrial ribosomal protein L**
ATP	**Adenosine Triphosphate**	**Mrps**	**Mitochondrial ribosomal protein S**
BACE	**Beta-site APP Cleaving Enzyme**	**Ndufb**	**NADH dehydrogenase [ubiquinone] 1**
PINK1	**PTEN induced kinase 1**	**CytC**	**Cytochrome c**
ROS	**Reactive Oxigen Species**	**PFA**	**Paraformaldehyde**
FKBP38	**38 kDa FK506-Binding Protein**	**RT**	**Room Temperature**
Bcl-2	**B-Cell Lymphoma 2**	**DPBS**	**Dulbecco's Phosphate-Buffered Saline**
Bcl-X_L	**B-cell lymphoma-extra large**	**pH**	**Hydrogen Potential**
MAMs	**Mitochondrial Associated Membranes**	**EM**	**Electron microscopy**
IP3R	**Inositol Trisphosphate Receptor**	**MIB**	**Mitochondrial Isolation Buffer**
SERCA	**Sarco-Endoplasmic Reticulum Ca^{2+} ATPase**	**FASP**	**Filter Aided Sample Preparation**
MCU	**Mitochondrial Ca^{2+} Uniporter**	**µL**	**Microliter**
mPTP	**Mitochondrial Permeability Transition Pore**	**M**	**Molar**
3xTgAD	**Triple transgenic Alzheimer´s Disease Mouse**	**DTT**	**Dithiothreitol**

CSF	**Cerebrospinal Fluid**	**IAA**	**Iodacetamide**
NFT	**Neurofibrillary Tangles**	**LC-MS/MS**	**Liquid Chromatography-Mass Spectrometry**
Zeo	**Zeocin**	**FA**	**Formic Acid**
µg	**Microgram**	**NSI**	**Nano-Electrospray Ionization Source**
mL	**Milliliter**	**Å**	**Armstrong**
qPCR	**Quantitative Polymerase Chain Reaction**	**V**	**Volts**
DMEM	**Dulbecco's Modified Eagle Medium**	**m/z**	**Mass/charge**
FBS	**Fetal Bovine Serum**	**AGC**	**Automatic Gain Control**
°C	**Centigrades**	**FWHM**	**Full Width at Half Maximum**
dNTPs	**Desoxynucleotide Triphosphate (s)**	**HCD**	**Higher-Energy-Collisional-Dissociation**
Tg	**Transgenic**	**ms**	**Mass spectrometry**
C57BL/6	**C57 black 6**	**HPLC**	**High Pressured Liquid Chromatography**
Thy-1	**Thymus Cell Antigen 1**	**ppm**	**Partricles per million**
hPS1	**Human Presenilin 1**	**Da**	**Dalton**
PCR	**Polymerase Chain Reaction**	**FDR**	**False Discovery Ratio**
RNA	**Ribonucleic Acid**	**PBS**	**Phosphate-Buffered Saline**
ng	**Nanogram**	**FCCP**	**Carbonyl Cyanide-4-Phenylhydrazone**
ELISA	**Enzyme-Linked Immunosorbent Assay**	**CsA**	**Cyclosporin A**
Atp5h	**ATP Synthase Subunit d, mitochondrial**	**BSA**	**Bovine serum albumin**
CA1	**Cornu Ammonis 1**	**NDS**	**Normal Donkey Serum**
CA3	**Cornu Ammonis 3**	**HeNe**	**Helium Neon**
mA	**Milliamperes**	**UV**	**Ultraviolet**
µA	**Microamperes**	**AR**	**Aspect Ratio**
SEM	**Standard Error of the Mean**	**F/F**	**Form Factor**
A.U.	**Arbitrary units**	**OCR**	**Oxygen Consumption Rate**
Synapto	**Synaptophysin**	**ECAR**	**Extracellular Acidification Rate**
AEQs	**Aequorins**	**ETC**	**Electron Transport Chain**
CytAEQs	**Cytosolic Aequorins**	**ETS**	**Electron Transport System**
mitAEQs	**Mitochondrial Aequorins**	**SOC**	**Store Operated Channel**
ERAEQs	**ER Aequorins**	**SEM**	**Standard Error of the Mean**
KRB	**Krebs-Ringer Modified Buffer**	**pmol**	**Picomoles**

HEPES	**4-(2-hydroxyethyl)-1-piperazineethanesulfonic acid**
DAPT	**(2*S*)-*N*-[(3,5-Difluorophenyl) acetyl]-L-alanyl-2-phenyl] glycine 1,1-dimethylethyl ester**
2-APB	**2-Aminoethoxydiphenylborane**
nM	**Nanomolar**
µM	**Micromolar**
N.A.	**Numerical Aperture**
CPA	**Cyclopiazonic Acid**
$\Delta\Psi_m$	**Mitochondrial Membrane Potential**
TMRM	**Tetramethylrhodamine**
SFC	**Swept Field Confocal**
Fis1	**Mitochondrial fission 1 protein**
ANOVA	**Analysis of Variance**
OXPHOS	**Oxidative phosphorylation**
TCA	**Tricarboxylic Acid Cycle**
COX	**Cytochrome c Oxidase**
HtrA/Omi	**High temperature requirement protein A2**
Mfn2	**Mitofusin 2**
Mfn1	**Mitofusin 1**
Oligo	**Oligomycin**
FC	**Fold Change**

12. List of Tables

13. List of Supplemental Figures

14. List of Supplemental Tables

15. Bibliography

Alagiakrishnan, K., S. S. Gill, and A. Fagarasanu. 2012. 'Genetics and epigenetics of Alzheimer's disease', *Postgrad Med J*, 88: 522-9.

Ankarcrona, M., and K. Hultenby. 2002. 'Presenilin-1 is located in rat mitochondria', *Biochem Biophys Res Commun*, 295: 766-70.

Annunziata, I., A. Patterson, and A. d'Azzo. 2013. 'Mitochondria-associated ER membranes (MAMs) and glycosphingolipid enriched microdomains (GEMs): isolation from mouse brain', *J Vis Exp*: e50215.

Area-Gomez, E. 2014. 'Assessing the function of mitochondria-associated ER membranes', *Methods Enzymol*, 547: 181-97.

Area-Gomez, E., A. de Groof, E. Bonilla, J. Montesinos, K. Tanji, I. Boldogh, L. Pon, and E. A. Schon. 2018. 'A key role for MAM in mediating mitochondrial dysfunction in Alzheimer disease', *Cell Death Dis*, 9: 335.

Area-Gomez, E., A. J. de Groof, I. Boldogh, T. D. Bird, G. E. Gibson, C. M. Koehler, W. H. Yu, K. E. Duff, M. P. Yaffe, L. A. Pon, and E. A. Schon. 2009. 'Presenilins are enriched in endoplasmic reticulum membranes associated with mitochondria', *Am J Pathol*, 175: 1810-6.

Area-Gomez, E., M. Del Carmen Lara Castillo, M. D. Tambini, C. Guardia-Laguarta, A. J. de Groof, M. Madra, J. Ikenouchi, M. Umeda, T. D. Bird, S. L. Sturley, and E. A. Schon. 2012. 'Upregulated function of mitochondria-associated ER membranes in Alzheimer disease', *EMBO J*, 31: 4106-23.

Arriagada, P. V., J. H. Growdon, E. T. Hedley-Whyte, and B. T. Hyman. 1992. 'Neurofibrillary tangles but not senile plaques parallel duration and severity of Alzheimer's disease', *Neurology*, 42: 631-9.

Auffret, A., V. Gautheron, M. P. Mattson, J. Mariani, and C. Rovira. 2010. 'Progressive age-related impairment of the late long-term potentiation in Alzheimer's disease presenilin-1 mutant knock-in mice', *J Alzheimers Dis*, 19: 1021-33.

Baek, S. H., S. J. Park, J. I. Jeong, S. H. Kim, J. Han, J. W. Kyung, S. H. Baik, Y. Choi, B. Y. Choi, J. S. Park, G. Bahn, J. H. Shin, D. S. Jo, J. Y. Lee, C. G. Jang, T. V. Arumugam, J. Kim, J. W. Han, J. Y. Koh, D. H. Cho, and D. G. Jo. 2017. 'Inhibition of Drp1 Ameliorates Synaptic Depression, Abeta Deposition, and Cognitive Impairment in an Alzheimer's Disease Model', *J Neurosci*, 37: 5099-110.

Balducci, C., B. Mehdawy, L. Mare, A. Giuliani, L. Lorenzini, S. Sivilia, L. Giardino, L. Calza, A. Lanzillotta, I. Sarnico, M. Pizzi, A. Usiello, A. R. Viscomi, S. Ottonello, G. Villetti, B. P. Imbimbo, G. Nistico, G. Forloni, and R. Nistico. 2011. 'The gamma-secretase modulator CHF5074 restores memory and hippocampal synaptic plasticity in plaque-free Tg2576 mice', *J Alzheimers Dis*, 24: 799-816.

Banker, G. A., and W. M. Cowan. 1979. 'Further observations on hippocampal neurons in dispersed cell culture', *J Comp Neurol*, 187: 469-93.

Bateman, R. J., C. Xiong, T. L. Benzinger, A. M. Fagan, A. Goate, N. C. Fox, D. S. Marcus, N. J. Cairns, X. Xie, T. M. Blazey, D. M. Holtzman, A. Santacruz, V. Buckles, A. Oliver, K. Moulder, P. S. Aisen, B. Ghetti, W. E. Klunk, E. McDade, R. N. Martins, C. L. Masters, R. Mayeux, J. M. Ringman, M. N. Rossor, P. R. Schofield, R. A. Sperling, S. Salloway, J. C. Morris, and Network Dominantly Inherited Alzheimer. 2012. 'Clinical and biomarker changes in dominantly inherited Alzheimer's disease', *N Engl J Med*, 367: 795-804.

Beel, A. J., and C. R. Sanders. 2008. 'Substrate specificity of gamma-secretase and other intramembrane proteases', *Cell Mol Life Sci*, 65: 1311-34.

Begley, J. G., W. Duan, S. Chan, K. Duff, and M. P. Mattson. 1999. 'Altered calcium homeostasis and mitochondrial dysfunction in cortical synaptic compartments of presenilin-1 mutant mice', *J Neurochem*, 72: 1030-9.

Behbahani, H., I. G. Shabalina, B. Wiehager, H. Concha, K. Hultenby, N. Petrovic, J. Nedergaard, B. Winblad, R. F. Cowburn, and M. Ankarcrona. 2006. 'Differential role of Presenilin-1 and -2 on mitochondrial membrane potential and oxygen consumption in mouse embryonic fibroblasts', *J Neurosci Res*, 84: 891-902.

Ben-Gedalya, T., L. Moll, M. Bejerano-Sagie, S. Frere, W. A. Cabral, D. Friedmann-Morvinski, I. Slutsky, T. Burstyn-Cohen, J. C. Marini, and E. Cohen. 2015. 'Alzheimer's disease-causing proline substitutions lead to presenilin 1 aggregation and malfunction', *EMBO J*, 34: 2820-39.

Bernardi, P., and V. Petronilli. 1996. 'The permeability transition pore as a mitochondrial calcium release channel: a critical appraisal', *J Bioenerg Biomembr*, 28: 131-8.

Berry, K. P., and E. Nedivi. 2017. 'Spine Dynamics: Are They All the Same?', *Neuron*, 96: 43-55.
Bezprozvanny, I. 2013. 'Presenilins and calcium signaling-systems biology to the rescue', *Sci Signal*, 6: pe24.
Bonora, M., C. Giorgi, A. Bononi, S. Marchi, S. Patergnani, A. Rimessi, R. Rizzuto, and P. Pinton. 2013. 'Subcellular calcium measurements in mammalian cells using jellyfish photoprotein aequorin-based probes', *Nat Protoc*, 8: 2105-18.
Bonora, M., C. Morganti, G. Morciano, C. Giorgi, M. R. Wieckowski, and P. Pinton. 2016. 'Comprehensive analysis of mitochondrial permeability transition pore activity in living cells using fluorescence-imaging-based techniques', *Nat Protoc*, 11: 1067-80.
Bowen, D. M., P. White, J. A. Spillane, M. J. Goodhardt, G. Curzon, P. Iwangoff, W. Meier-Ruge, and A. N. Davison. 1979. 'Accelerated ageing or selective neuronal loss as an important cause of dementia?', *Lancet*, 1: 11-4.
Brown, J. T., J. C. Richardson, G. L. Collingridge, A. D. Randall, and C. H. Davies. 2005. 'Synaptic transmission and synchronous activity is disrupted in hippocampal slices taken from aged TAS10 mice', *Hippocampus*, 15: 110-7.
Burke, S. L., T. Cadet, A. Alcide, J. O'Driscoll, and P. Maramaldi. 2017. 'Psychosocial risk factors and Alzheimer's disease: the associative effect of depression, sleep disturbance, and anxiety', *Aging Ment Health*: 1-8.
Burte, F., V. Carelli, P. F. Chinnery, and P. Yu-Wai-Man. 2015. 'Disturbed mitochondrial dynamics and neurodegenerative disorders', *Nat Rev Neurol*, 11: 11-24.
Busciglio, J., H. Hartmann, A. Lorenzo, C. Wong, K. Baumann, B. Sommer, M. Staufenbiel, and B. A. Yankner. 1997. 'Neuronal localization of presenilin-1 and association with amyloid plaques and neurofibrillary tangles in Alzheimer's disease', *J Neurosci*, 17: 5101-7.
Butterfield, D. A., A. M. Swomley, and R. Sultana. 2013. 'Amyloid beta-peptide (1-42)-induced oxidative stress in Alzheimer disease: importance in disease pathogenesis and progression', *Antioxid Redox Signal*, 19: 823-35.
Campos-Pena, V., D. Toral-Rios, F. Becerril-Perez, C. Sanchez-Torres, Y. Delgado-Namorado, E. Torres-Ossorio, D. Franco-Bocanegra, and K. Carvajal. 2017. 'Metabolic Syndrome as a Risk Factor for Alzheimer's Disease: Is Abeta a Crucial Factor in Both Pathologies?', *Antioxid Redox Signal*, 26: 542-60.
Caroni, P. 1997. 'Overexpression of growth-associated proteins in the neurons of adult transgenic mice', *J Neurosci Methods*, 71: 3-9.
Carreiras, M. C., E. Mendes, M. J. Perry, A. P. Francisco, and J. Marco-Contelles. 2013. 'The multifactorial nature of Alzheimer's disease for developing potential therapeutics', *Curr Top Med Chem*, 13: 1745-70.
Caspersen, C., N. Wang, J. Yao, A. Sosunov, X. Chen, J. W. Lustbader, H. W. Xu, D. Stern, G. McKhann, and S. D. Yan. 2005. 'Mitochondrial Abeta: a potential focal point for neuronal metabolic dysfunction in Alzheimer's disease', *FASEB J*, 19: 2040-1.
Cedazo-Minguez, A., B. O. Popescu, M. Ankarcrona, T. Nishimura, and R. F. Cowburn. 2002. 'The presenilin 1 deltaE9 mutation gives enhanced basal phospholipase C activity and a resultant increase in intracellular calcium concentrations', *J Biol Chem*, 277: 36646-55.
Cohen, L. D., and N. E. Ziv. 2017. 'Recent insights on principles of synaptic protein degradation', *F1000Res*, 6: 675.
Cook, D. G., J. C. Sung, T. E. Golde, K. M. Felsenstein, B. S. Wojczyk, R. E. Tanzi, J. Q. Trojanowski, V. M. Lee, and R. W. Doms. 1996. 'Expression and analysis of presenilin 1 in a human neuronal system: localization in cell bodies and dendrites', *Proc Natl Acad Sci U S A*, 93: 9223-8.
Course, M. M., and X. Wang. 2016. 'Transporting mitochondria in neurons', *F1000Res*, 5.
Coussee, E., P. De Smet, E. Bogaert, I. Elens, P. Van Damme, P. Willems, W. Koopman, L. Van Den Bosch, and G. Callewaert. 2011. 'G37R SOD1 mutant alters mitochondrial complex I activity, Ca(2+) uptake and ATP production', *Cell Calcium*, 49: 217-25.
Cox, J., and M. Mann. 2008. 'MaxQuant enables high peptide identification rates, individualized p.p.b.-range mass accuracies and proteome-wide protein quantification', *Nat Biotechnol*, 26: 1367-72.
Cruts, M., H. Backhovens, S. Y. Wang, G. Van Gassen, J. Theuns, C. D. De Jonghe, A. Wehnert, J. De Voecht, G. De Winter, P. Cras, and et al. 1995. 'Molecular genetic analysis of familial early-onset Alzheimer's disease linked to chromosome 14q24.3', *Hum Mol Genet*, 4: 2363-71.
Csordas, G., P. Varnai, T. Golenar, S. Roy, G. Purkins, T. G. Schneider, T. Balla, and G. Hajnoczky. 2010. 'Imaging interorganelle contacts and local calcium dynamics at the ER-mitochondrial interface', *Mol Cell*, 39: 121-32.

Cummings, J., G. Lee, A. Ritter, and K. Zhong. 2018. 'Alzheimer's disease drug development pipeline: 2018', *Alzheimers Dement (N Y)*, 4: 195-214.
Cupers, P., M. Bentahir, K. Craessaerts, I. Orlans, H. Vanderstichele, P. Saftig, B. De Strooper, and W. Annaert. 2001. 'The discrepancy between presenilin subcellular localization and gamma-secretase processing of amyloid precursor protein', *J Cell Biol*, 154: 731-40.
Cha, M. Y., S. H. Han, S. M. Son, H. S. Hong, Y. J. Choi, J. Byun, and I. Mook-Jung. 2012. 'Mitochondria-specific accumulation of amyloid beta induces mitochondrial dysfunction leading to apoptotic cell death', *PLoS One*, 7: e34929.
Chapman, P. F., G. L. White, M. W. Jones, D. Cooper-Blacketer, V. J. Marshall, M. Irizarry, L. Younkin, M. A. Good, T. V. Bliss, B. T. Hyman, S. G. Younkin, and K. K. Hsiao. 1999. 'Impaired synaptic plasticity and learning in aged amyloid precursor protein transgenic mice', *Nat Neurosci*, 2: 271-6.
Chen, H., and D. C. Chan. 2009. 'Mitochondrial dynamics--fusion, fission, movement, and mitophagy--in neurodegenerative diseases', *Hum Mol Genet*, 18: R169-76.
Chen, J. X., and S. S. Yan. 2010. 'Role of mitochondrial amyloid-beta in Alzheimer's disease', *J Alzheimers Dis*, 20 Suppl 2: S569-78.
Cheung, K. H., D. Shineman, M. Muller, C. Cardenas, L. Mei, J. Yang, T. Tomita, T. Iwatsubo, V. M. Lee, and J. K. Foskett. 2008. 'Mechanism of Ca2+ disruption in Alzheimer's disease by presenilin regulation of InsP3 receptor channel gating', *Neuron*, 58: 871-83.
Cho, B., H. M. Cho, Y. Jo, H. D. Kim, M. Song, C. Moon, H. Kim, K. Kim, H. Sesaki, I. J. Rhyu, H. Kim, and W. Sun. 2017. 'Constriction of the mitochondrial inner compartment is a priming event for mitochondrial division', *Nat Commun*, 8: 15754.
Chong, C. M., M. Ke, Y. Tan, Z. Huang, K. Zhang, N. Ai, W. Ge, D. Qin, J. H. Lu, and H. Su. 2018. 'Presenilin 1 deficiency suppresses autophagy in human neural stem cells through reducing gamma-secretase-independent ERK/CREB signaling', *Cell Death Dis*, 9: 879.
Chow, V. W., M. P. Mattson, P. C. Wong, and M. Gleichmann. 2010. 'An overview of APP processing enzymes and products', *Neuromolecular Med*, 12: 1-12.
Chui, D. H., H. Tanahashi, K. Ozawa, S. Ikeda, F. Checler, O. Ueda, H. Suzuki, W. Araki, H. Inoue, K. Shirotani, K. Takahashi, F. Gallyas, and T. Tabira. 1999. 'Transgenic mice with Alzheimer presenilin 1 mutations show accelerated neurodegeneration without amyloid plaque formation', *Nat Med*, 5: 560-4.
Dagda, R. K., S. J. Cherra, 3rd, S. M. Kulich, A. Tandon, D. Park, and C. T. Chu. 2009. 'Loss of PINK1 function promotes mitophagy through effects on oxidative stress and mitochondrial fission', *J Biol Chem*, 284: 13843-55.
Danielson, E., and S. H. Lee. 2014. 'SynPAnal: software for rapid quantification of the density and intensity of protein puncta from fluorescence microscopy images of neurons', *PLoS One*, 9: e115298.
De Marchi, E., M. Bonora, C. Giorgi, and P. Pinton. 2014. 'The mitochondrial permeability transition pore is a dispensable element for mitochondrial calcium efflux', *Cell Calcium*, 56: 1-13.
De Strooper, B., T. Iwatsubo, and M. S. Wolfe. 2012. 'Presenilins and gamma-secretase: structure, function, and role in Alzheimer Disease', *Cold Spring Harb Perspect Med*, 2: a006304.
De Strooper, B., and E. Karran. 2016. 'The Cellular Phase of Alzheimer's Disease', *Cell*, 164: 603-15.
Del Prete, D., J. M. Suski, B. Oules, D. Debayle, A. S. Gay, S. Lacas-Gervais, R. Bussiere, C. Bauer, P. Pinton, P. Paterlini-Brechot, M. R. Wieckowski, F. Checler, and M. Chami. 2017. 'Localization and Processing of the Amyloid-beta Protein Precursor in Mitochondria-Associated Membranes', *J Alzheimers Dis*, 55: 1549-70.
Devi, L., B. M. Prabhu, D. F. Galati, N. G. Avadhani, and H. K. Anandatheerthavarada. 2006. 'Accumulation of amyloid precursor protein in the mitochondrial import channels of human Alzheimer's disease brain is associated with mitochondrial dysfunction', *J Neurosci*, 26: 9057-68.
Doody, R. S., R. Raman, M. Farlow, T. Iwatsubo, B. Vellas, S. Joffe, K. Kieburtz, F. He, X. Sun, R. G. Thomas, P. S. Aisen, Committee Alzheimer's Disease Cooperative Study Steering, E. Siemers, G. Sethuraman, R. Mohs, and Group Semagacestat Study. 2013. 'A phase 3 trial of semagacestat for treatment of Alzheimer's disease', *N Engl J Med*, 369: 341-50.
Dorostkar, M. M., C. Zou, L. Blazquez-Llorca, and J. Herms. 2015. 'Analyzing dendritic spine pathology in Alzheimer's disease: problems and opportunities', *Acta Neuropathol*, 130: 1-19.
Du, H., and S. S. Yan. 2010. 'Mitochondrial permeability transition pore in Alzheimer's disease: cyclophilin D and amyloid beta', *Biochim Biophys Acta*, 1802: 198-204.
Duggan, S. P., and J. V. McCarthy. 2016. 'Beyond gamma-secretase activity: The multifunctional nature of presenilins in cell signalling pathways', *Cell Signal*, 28: 1-11.

Ekim Kocabey, A., L. Kost, M. Gehlhar, G. Rodel, and U. Gey. 2019. 'Mitochondrial Sco proteins are involved in oxidative stress defense', *Redox Biol*, 21: 101079.
Elder, G. A., M. A. Gama Sosa, and R. De Gasperi. 2010. 'Transgenic mouse models of Alzheimer's disease', *Mt Sinai J Med*, 77: 69-81.
Elder, G. A., M. A. Gama Sosa, R. De Gasperi, D. L. Dickstein, and P. R. Hof. 2010. 'Presenilin transgenic mice as models of Alzheimer's disease', *Brain Struct Funct*, 214: 127-43.
Elrod, J. W., R. Wong, S. Mishra, R. J. Vagnozzi, B. Sakthievel, S. A. Goonasekera, J. Karch, S. Gabel, J. Farber, T. Force, J. H. Brown, E. Murphy, and J. D. Molkentin. 2010. 'Cyclophilin D controls mitochondrial pore-dependent Ca(2+) exchange, metabolic flexibility, and propensity for heart failure in mice', *J Clin Invest*, 120: 3680-7.
Eriksson, O., P. Pollesello, and E. Geimonen. 1999. 'Regulation of total mitochondrial Ca2+ in perfused liver is independent of the permeability transition pore', *Am J Physiol*, 276: C1297-302.
Fernandez, M. A., J. A. Klutkowski, T. Freret, and M. S. Wolfe. 2014. 'Alzheimer presenilin-1 mutations dramatically reduce trimming of long amyloid beta-peptides (Abeta) by gamma-secretase to increase 42-to-40-residue Abeta', *J Biol Chem*, 289: 31043-52.
Filadi, R., E. Greotti, G. Turacchio, A. Luini, T. Pozzan, and P. Pizzo. 2016. 'Presenilin 2 Modulates Endoplasmic Reticulum-Mitochondria Coupling by Tuning the Antagonistic Effect of Mitofusin 2', *Cell Rep*, 15: 2226-38.
Fitzjohn, S. M., F. Kuenzi, R. A. Morton, T. W. Rosahl, H. Lewis, D. Smith, G. R. Seabrook, and G. L. Collingridge. 2010. 'A study of long-term potentiation in transgenic mice over-expressing mutant forms of both amyloid precursor protein and presenilin-1', *Mol Brain*, 3: 21.
Fitzjohn, S. M., R. A. Morton, F. Kuenzi, T. W. Rosahl, M. Shearman, H. Lewis, D. Smith, D. S. Reynolds, C. H. Davies, G. L. Collingridge, and G. R. Seabrook. 2001. 'Age-related impairment of synaptic transmission but normal long-term potentiation in transgenic mice that overexpress the human APP695SWE mutant form of amyloid precursor protein', *J Neurosci*, 21: 4691-8.
Friedman, J. R., and J. Nunnari. 2014. 'Mitochondrial form and function', *Nature*, 505: 335-43.
Fu, Y. J., S. Xiong, M. A. Lovell, and B. C. Lynn. 2009. 'Quantitative proteomic analysis of mitochondria in aging PS-1 transgenic mice', *Cell Mol Neurobiol*, 29: 649-64.
Fujimoto, M., and T. Hayashi. 2011. 'New insights into the role of mitochondria-associated endoplasmic reticulum membrane', *Int Rev Cell Mol Biol*, 292: 73-117.
Gandy, S. 2005. 'The role of cerebral amyloid beta accumulation in common forms of Alzheimer disease', *J Clin Invest*, 115: 1121-9.
Garcia-Escudero, V., P. Martin-Maestro, G. Perry, and J. Avila. 2013. 'Deconstructing mitochondrial dysfunction in Alzheimer disease', *Oxid Med Cell Longev*, 2013: 162152.
Giacomello, M., I. Drago, M. Bortolozzi, M. Scorzeto, A. Gianelle, P. Pizzo, and T. Pozzan. 2010. 'Ca2+ hot spots on the mitochondrial surface are generated by Ca2+ mobilization from stores, but not by activation of store-operated Ca2+ channels', *Mol Cell*, 38: 280-90.
Goate, A., M. C. Chartier-Harlin, M. Mullan, J. Brown, F. Crawford, L. Fidani, L. Giuffra, A. Haynes, N. Irving, L. James, and et al. 1991. 'Segregation of a missense mutation in the amyloid precursor protein gene with familial Alzheimer's disease', *Nature*, 349: 704-6.
Gogvadze, V., J. D. Robertson, B. Zhivotovsky, and S. Orrenius. 2001. 'Cytochrome c release occurs via Ca2+-dependent and Ca2+-independent mechanisms that are regulated by Bax', *J Biol Chem*, 276: 19066-71.
Gray, C. W., R. V. Ward, E. Karran, S. Turconi, A. Rowles, D. Viglienghi, C. Southan, A. Barton, K. G. Fantom, A. West, J. Savopoulos, N. J. Hassan, H. Clinkenbeard, C. Hanning, B. Amegadzie, J. B. Davis, C. Dingwall, G. P. Livi, and C. L. Creasy. 2000. 'Characterization of human HtrA2, a novel serine protease involved in the mammalian cellular stress response', *Eur J Biochem*, 267: 5699-710.
Gray, N. E., and J. F. Quinn. 2015. 'Alterations in mitochondrial number and function in Alzheimer's disease fibroblasts', *Metab Brain Dis*, 30: 1275-8.
Greenough, M. A., I. Volitakis, Q. X. Li, K. Laughton, G. Evin, M. Ho, A. H. Dalziel, J. Camakaris, and A. I. Bush. 2011. 'Presenilins promote the cellular uptake of copper and zinc and maintain copper chaperone of SOD1-dependent copper/zinc superoxide dismutase activity', *J Biol Chem*, 286: 9776-86.
Guo, L., J. Tian, and H. Du. 2017. 'Mitochondrial Dysfunction and Synaptic Transmission Failure in Alzheimer's Disease', *J Alzheimers Dis*, 57: 1071-86.
Guo, Q., L. Sebastian, B. L. Sopher, M. W. Miller, C. B. Ware, G. M. Martin, and M. P. Mattson. 1999. 'Increased vulnerability of hippocampal neurons from presenilin-1 mutant knock-in mice to

amyloid beta-peptide toxicity: central roles of superoxide production and caspase activation', *J Neurochem*, 72: 1019-29.
Haapasalo, A., and D. M. Kovacs. 2011. 'The many substrates of presenilin/gamma-secretase', *J Alzheimers Dis*, 25: 3-28.
Hall, A. M., and E. D. Roberson. 2012. 'Mouse models of Alzheimer's disease', *Brain Res Bull*, 88: 3-12.
Han, S. H., and I. Mook-Jung. 2014. 'Diverse molecular targets for therapeutic strategies in Alzheimer's disease', *J Korean Med Sci*, 29: 893-902.
Hanna, A., K. Iremonger, P. Das, D. Dickson, T. Golde, and C. Janus. 2012. 'Age-related increase in amyloid plaque burden is associated with impairment in conditioned fear memory in CRND8 mouse model of amyloidosis', *Alzheimers Res Ther*, 4: 21.
Hansson, C. A., S. Frykman, M. R. Farmery, L. O. Tjernberg, C. Nilsberth, S. E. Pursglove, A. Ito, B. Winblad, R. F. Cowburn, J. Thyberg, and M. Ankarcrona. 2004. 'Nicastrin, presenilin, APH-1, and PEN-2 form active gamma-secretase complexes in mitochondria', *J Biol Chem*, 279: 51654-60.
Hansson Petersen, C. A., N. Alikhani, H. Behbahani, B. Wiehager, P. F. Pavlov, I. Alafuzoff, V. Leinonen, A. Ito, B. Winblad, E. Glaser, and M. Ankarcrona. 2008. 'The amyloid beta-peptide is imported into mitochondria via the TOM import machinery and localized to mitochondrial cristae', *Proc Natl Acad Sci U S A*, 105: 13145-50.
Hardy, J. 2007. 'Putting presenilins centre stage. Introduction to the Talking Point on the role of presenilin mutations in Alzheimer disease', *EMBO Rep*, 8: 134-5.
Hardy, J. A., and G. A. Higgins. 1992. 'Alzheimer's disease: the amyloid cascade hypothesis', *Science*, 256: 184-5.
Harvey, L. D., and S. Y. Chan. 2017. 'Emerging Metabolic Therapies in Pulmonary Arterial Hypertension', *J Clin Med*, 6.
Hayashi, H., H. Nakagami, M. Takeichi, M. Shimamura, N. Koibuchi, E. Oiki, N. Sato, H. Koriyama, M. Mori, R. Gerardo Araujo, A. Maeda, R. Morishita, K. Tamai, and Y. Kaneda. 2012. 'HIG1, a novel regulator of mitochondrial gamma-secretase, maintains normal mitochondrial function', *FASEB J*, 26: 2306-17.
Hayashi, T., R. Rizzuto, G. Hajnoczky, and T. P. Su. 2009. 'MAM: more than just a housekeeper', *Trends Cell Biol*, 19: 81-8.
Hayashi, T., and T. P. Su. 2007. 'Sigma-1 receptor chaperones at the ER-mitochondrion interface regulate Ca(2+) signaling and cell survival', *Cell*, 131: 596-610.
Hedskog, L., C. M. Pinho, R. Filadi, A. Ronnback, L. Hertwig, B. Wiehager, P. Larssen, S. Gellhaar, A. Sandebring, M. Westerlund, C. Graff, B. Winblad, D. Galter, H. Behbahani, P. Pizzo, E. Glaser, and M. Ankarcrona. 2013. 'Modulation of the endoplasmic reticulum-mitochondria interface in Alzheimer's disease and related models', *Proc Natl Acad Sci U S A*, 110: 7916-21.
Heo, S., G. H. Diering, C. H. Na, R. S. Nirujogi, J. L. Bachman, A. Pandey, and R. L. Huganir. 2018. 'Identification of long-lived synaptic proteins by proteomic analysis of synaptosome protein turnover', *Proc Natl Acad Sci U S A*, 115: E3827-E36.
Herms, J., and M. M. Dorostkar. 2016. 'Dendritic Spine Pathology in Neurodegenerative Diseases', *Annu Rev Pathol*, 11: 221-50.
Herrup, K. 2015. 'The case for rejecting the amyloid cascade hypothesis', *Nat Neurosci*, 18: 794-9.
Huang, W. J., X. Zhang, and W. W. Chen. 2016. 'Role of oxidative stress in Alzheimer's disease', *Biomed Rep*, 4: 519-22.
Huang, W., H. Y. Ma, Y. Huang, Y. Li, G. L. Wang, Q. Jiang, F. Wang, and A. S. Xiong. 2017. 'Comparative proteomic analysis provides novel insights into chlorophyll biosynthesis in celery under temperature stress', *Physiol Plant*, 161: 468-85.
Hughes, A. L., C. E. Hughes, K. A. Henderson, N. Yazvenko, and D. E. Gottschling. 2016. 'Selective sorting and destruction of mitochondrial membrane proteins in aged yeast', *Elife*, 5.
Hwang, K. D., M. S. Bak, S. J. Kim, S. Rhee, and Y. S. Lee. 2017. 'Restoring synaptic plasticity and memory in mouse models of Alzheimer's disease by PKR inhibition', *Mol Brain*, 10: 57.
Iqbal, K., and I. Grundke-Iqbal. 2010. 'Alzheimer's disease, a multifactorial disorder seeking multitherapies', *Alzheimers Dement*, 6: 420-4.
Irizarry, M. C., M. McNamara, K. Fedorchak, K. Hsiao, and B. T. Hyman. 1997. 'APPSw transgenic mice develop age-related A beta deposits and neuropil abnormalities, but no neuronal loss in CA1', *J Neuropathol Exp Neurol*, 56: 965-73.
Irizarry, M. C., F. Soriano, M. McNamara, K. J. Page, D. Schenk, D. Games, and B. T. Hyman. 1997. 'Abeta deposition is associated with neuropil changes, but not with overt neuronal loss in the human amyloid precursor protein V717F (PDAPP) transgenic mouse', *J Neurosci*, 17: 7053-9.

Ishihara, N., M. Nomura, A. Jofuku, H. Kato, S. O. Suzuki, K. Masuda, H. Otera, Y. Nakanishi, I. Nonaka, Y. Goto, N. Taguchi, H. Morinaga, M. Maeda, R. Takayanagi, S. Yokota, and K. Mihara. 2009. 'Mitochondrial fission factor Drp1 is essential for embryonic development and synapse formation in mice', *Nat Cell Biol*, 11: 958-66.

Ittner, A., S. W. Chua, J. Bertz, A. Volkerling, J. van der Hoven, A. Gladbach, M. Przybyla, M. Bi, A. van Hummel, C. H. Stevens, S. Ippati, L. S. Suh, A. Macmillan, G. Sutherland, J. J. Kril, A. P. Silva, J. P. Mackay, A. Poljak, F. Delerue, Y. D. Ke, and L. M. Ittner. 2016. 'Site-specific phosphorylation of tau inhibits amyloid-beta toxicity in Alzheimer's mice', *Science*, 354: 904-08.

Izeddin, I., C. G. Specht, M. Lelek, X. Darzacq, A. Triller, C. Zimmer, and M. Dahan. 2011. 'Super-resolution dynamic imaging of dendritic spines using a low-affinity photoconvertible actin probe', *PLoS One*, 6: e15611.

Jacobsen, J. S., C. C. Wu, J. M. Redwine, T. A. Comery, R. Arias, M. Bowlby, R. Martone, J. H. Morrison, M. N. Pangalos, P. H. Reinhart, and F. E. Bloom. 2006. 'Early-onset behavioral and synaptic deficits in a mouse model of Alzheimer's disease', *Proc Natl Acad Sci U S A*, 103: 5161-6.

Jahn, H. 2013. 'Memory loss in Alzheimer's disease', *Dialogues Clin Neurosci*, 15: 445-54.

Jankowsky, J. L., and H. Zheng. 2017. 'Practical considerations for choosing a mouse model of Alzheimer's disease', *Mol Neurodegener*, 12: 89.

Jeyaraju, D. V., G. Cisbani, and L. Pellegrini. 2009. 'Calcium regulation of mitochondria motility and morphology', *Biochim Biophys Acta*, 1787: 1363-73.

Jones, E. V., D. Cook, and K. K. Murai. 2012. 'A neuron-astrocyte co-culture system to investigate astrocyte-secreted factors in mouse neuronal development', *Methods Mol Biol*, 814: 341-52.

Jonsson, T., J. K. Atwal, S. Steinberg, J. Snaedal, P. V. Jonsson, S. Bjornsson, H. Stefansson, P. Sulem, D. Gudbjartsson, J. Maloney, K. Hoyte, A. Gustafson, Y. Liu, Y. Lu, T. Bhangale, R. R. Graham, J. Huttenlocher, G. Bjornsdottir, O. A. Andreassen, E. G. Jonsson, A. Palotie, T. W. Behrens, O. T. Magnusson, A. Kong, U. Thorsteinsdottir, R. J. Watts, and K. Stefansson. 2012. 'A mutation in APP protects against Alzheimer's disease and age-related cognitive decline', *Nature*, 488: 96-9.

Kalbacova, M., M. Vrbacky, Z. Drahota, and Z. Melkova. 2003. 'Comparison of the effect of mitochondrial inhibitors on mitochondrial membrane potential in two different cell lines using flow cytometry and spectrofluorometry', *Cytometry A*, 52: 110-6.

Kang, D. E., S. Soriano, M. P. Frosch, T. Collins, S. Naruse, S. S. Sisodia, G. Leibowitz, F. Levine, and E. H. Koo. 1999. 'Presenilin 1 facilitates the constitutive turnover of beta-catenin: differential activity of Alzheimer's disease-linked PS1 mutants in the beta-catenin-signaling pathway', *J Neurosci*, 19: 4229-37.

Kang, J., H. G. Lemaire, A. Unterbeck, J. M. Salbaum, C. L. Masters, K. H. Grzeschik, G. Multhaup, K. Beyreuther, and B. Muller-Hill. 1987. 'The precursor of Alzheimer's disease amyloid A4 protein resembles a cell-surface receptor', *Nature*, 325: 733-6.

Kania, E., G. Roest, T. Vervliet, J. B. Parys, and G. Bultynck. 2017. 'IP3 Receptor-Mediated Calcium Signaling and Its Role in Autophagy in Cancer', *Front Oncol*, 7: 140.

Karch, C. M., C. Cruchaga, and A. M. Goate. 2014. 'Alzheimer's disease genetics: from the bench to the clinic', *Neuron*, 83: 11-26.

Katzman, R. 1993. 'Education and the prevalence of dementia and Alzheimer's disease', *Neurology*, 43: 13-20.

Kawamata, H., and G. Manfredi. 2017. 'Proteinopathies and OXPHOS dysfunction in neurodegenerative diseases', *J Cell Biol*, 216: 3917-29.

Keller, J. N., Q. Guo, F. W. Holtsberg, A. J. Bruce-Keller, and M. P. Mattson. 1998. 'Increased sensitivity to mitochondrial toxin-induced apoptosis in neural cells expressing mutant presenilin-1 is linked to perturbed calcium homeostasis and enhanced oxyradical production', *J Neurosci*, 18: 4439-50.

Khandelwal, A., D. Chandu, C. M. Roe, R. Kopan, and R. S. Quatrano. 2007. 'Moonlighting activity of presenilin in plants is independent of gamma-secretase and evolutionarily conserved', *Proc Natl Acad Sci U S A*, 104: 13337-42.

Kitazawa, M., R. Medeiros, and F. M. Laferla. 2012. 'Transgenic mouse models of Alzheimer disease: developing a better model as a tool for therapeutic interventions', *Curr Pharm Des*, 18: 1131-47.

Kopan, R., and M. X. Ilagan. 2004. 'Gamma-secretase: proteasome of the membrane?', *Nat Rev Mol Cell Biol*, 5: 499-504.

Krols, M., G. Bultynck, and S. Janssens. 2016. 'ER-Mitochondria contact sites: A new regulator of cellular calcium flux comes into play', *J Cell Biol*, 214: 367-70.

Kubista, M., J. M. Andrade, M. Bengtsson, A. Forootan, J. Jonak, K. Lind, R. Sindelka, R. Sjoback, B. Sjogreen, L. Strombom, A. Stahlberg, and N. Zoric. 2006. 'The real-time polymerase chain reaction', *Mol Aspects Med*, 27: 95-125.

Lanz, T. A., D. B. Carter, and K. M. Merchant. 2003. 'Dendritic spine loss in the hippocampus of young PDAPP and Tg2576 mice and its prevention by the ApoE2 genotype', *Neurobiol Dis*, 13: 246-53.

Larson, J., and E. Munkacsy. 2015. 'Theta-burst LTP', *Brain Res*, 1621: 38-50.

Leal, N. S., G. Dentoni, B. Schreiner, O. P. Kamarainen, N. Partanen, S. K. Herukka, A. M. Koivisto, M. Hiltunen, T. Rauramaa, V. Leinonen, and M. Ankarcrona. 2018. 'Alterations in mitochondria-endoplasmic reticulum connectivity in human brain biopsies from idiopathic normal pressure hydrocephalus patients', *Acta Neuropathol Commun*, 6: 102.

Lee, J. H., W. H. Yu, A. Kumar, S. Lee, P. S. Mohan, C. M. Peterhoff, D. M. Wolfe, M. Martinez-Vicente, A. C. Massey, G. Sovak, Y. Uchiyama, D. Westaway, A. M. Cuervo, and R. A. Nixon. 2010. 'Lysosomal proteolysis and autophagy require presenilin 1 and are disrupted by Alzheimer-related PS1 mutations', *Cell*, 141: 1146-58.

Lee, M. K., H. H. Slunt, L. J. Martin, G. Thinakaran, G. Kim, S. E. Gandy, M. Seeger, E. Koo, D. L. Price, and S. S. Sisodia. 1996. 'Expression of presenilin 1 and 2 (PS1 and PS2) in human and murine tissues', *J Neurosci*, 16: 7513-25.

Lee, S. H., D. Lutz, M. Mossalam, V. Y. Bolshakov, M. Frotscher, and J. Shen. 2017. 'Presenilins regulate synaptic plasticity and mitochondrial calcium homeostasis in the hippocampal mossy fiber pathway', *Mol Neurodegener*, 12: 48.

Lemere, C. A., F. Lopera, K. S. Kosik, C. L. Lendon, J. Ossa, T. C. Saido, H. Yamaguchi, A. Ruiz, A. Martinez, L. Madrigal, L. Hincapie, J. C. Arango, D. C. Anthony, E. H. Koo, A. M. Goate, D. J. Selkoe, and J. C. Arango. 1996. 'The E280A presenilin 1 Alzheimer mutation produces increased A beta 42 deposition and severe cerebellar pathology', *Nat Med*, 2: 1146-50.

Lewis, J. A., and J. R. Tata. 1973. 'A rapidly sedimenting fraction of rat liver endoplasmic reticulum', *J Cell Sci*, 13: 447-59.

Li, N., K. Liu, Y. Qiu, Z. Ren, R. Dai, Y. Deng, and H. Qing. 2016. 'Effect of Presenilin Mutations on APP Cleavage; Insights into the Pathogenesis of FAD', *Front Aging Neurosci*, 8: 51.

Lian, H., E. Roy, and H. Zheng. 2016. 'Protocol for Primary Microglial Culture Preparation', *Bio Protoc*, 6.

Liu, Y. Q., M. Q. Jia, Z. H. Xie, X. F. Liu, Yang Hui, X. L. Zheng, H. Q. Yuan, and J. Z. Bi. 2017. 'Arrestins contribute to amyloid beta-induced cell death via modulation of autophagy and the alpha7nAch receptor in SH-SY5Y cells', *Sci Rep*, 7: 3446.

Livak, K. J., and T. D. Schmittgen. 2001. 'Analysis of relative gene expression data using real-time quantitative PCR and the 2(-Delta Delta C(T)) Method', *Methods*, 25: 402-8.

Lu, P., X. C. Bai, D. Ma, T. Xie, C. Yan, L. Sun, G. Yang, Y. Zhao, R. Zhou, S. H. W. Scheres, and Y. Shi. 2014. 'Three-dimensional structure of human gamma-secretase', *Nature*, 512: 166-70.

Lunnon, K., Z. Ibrahim, P. Proitsi, A. Lourdusamy, S. Newhouse, M. Sattlecker, S. Furney, M. Saleem, H. Soininen, I. Kloszewska, P. Mecocci, M. Tsolaki, B. Vellas, G. Coppola, D. Geschwind, A. Simmons, S. Lovestone, R. Dobson, A. Hodges, and Consortium AddNeuroMed. 2012. 'Mitochondrial dysfunction and immune activation are detectable in early Alzheimer's disease blood', *J Alzheimers Dis*, 30: 685-710.

Lunnon, K., A. Keohane, R. Pidsley, S. Newhouse, J. Riddoch-Contreras, E. B. Thubron, M. Devall, H. Soininen, I. Kloszewska, P. Mecocci, M. Tsolaki, B. Vellas, L. Schalkwyk, R. Dobson, A. N. Malik, J. Powell, S. Lovestone, A. Hodges, and Consortium AddNeuroMed. 2017. 'Mitochondrial genes are altered in blood early in Alzheimer's disease', *Neurobiol Aging*, 53: 36-47.

Lunnon, K., M. Sattlecker, S. J. Furney, G. Coppola, A. Simmons, P. Proitsi, M. K. Lupton, A. Lourdusamy, C. Johnston, H. Soininen, I. Kloszewska, P. Mecocci, M. Tsolaki, B. Vellas, D. Geschwind, S. Lovestone, R. Dobson, A. Hodges, and Consortium dNeuroMed. 2013. 'A blood gene expression marker of early Alzheimer's disease', *J Alzheimers Dis*, 33: 737-53.

Lustbader, J. W., M. Cirilli, C. Lin, H. W. Xu, K. Takuma, N. Wang, C. Caspersen, X. Chen, S. Pollak, M. Chaney, F. Trinchese, S. Liu, F. Gunn-Moore, L. F. Lue, D. G. Walker, P. Kuppusamy, Z. L. Zewier, O. Arancio, D. Stern, S. S. Yan, and H. Wu. 2004. 'ABAD directly links Abeta to mitochondrial toxicity in Alzheimer's disease', *Science*, 304: 448-52.

Maarouf, C. L., I. D. Daugs, T. A. Kokjohn, D. G. Walker, J. M. Hunter, J. C. Kruchowsky, R. Woltjer, J. Kaye, E. M. Castano, M. N. Sabbagh, T. G. Beach, and A. E. Roher. 2011. 'Alzheimer's disease and non-demented high pathology control nonagenarians: comparing and contrasting the biochemistry of cognitively successful aging', *PLoS One*, 6: e27291.

Maillard, I., T. Fang, and W. S. Pear. 2005. 'Regulation of lymphoid development, differentiation, and function by the Notch pathway', *Annu Rev Immunol*, 23: 945-74.
Malthankar-Phatak, G., S. Poplawski, N. Toraskar, and R. Siman. 2012. 'Combination therapy prevents amyloid-dependent and -independent structural changes', *Neurobiol Aging*, 33: 1273-83.
Mamada, N., D. Tanokashira, K. Ishii, A. Tamaoka, and W. Araki. 2017. 'Mitochondria are devoid of amyloid beta-protein (Abeta)-producing secretases: Evidence for unlikely occurrence within mitochondria of Abeta generation from amyloid precursor protein', *Biochem Biophys Res Commun*, 486: 321-28.
Manoharan, S., G. J. Guillemin, R. S. Abiramasundari, M. M. Essa, M. Akbar, and M. D. Akbar. 2016. 'The Role of Reactive Oxygen Species in the Pathogenesis of Alzheimer's Disease, Parkinson's Disease, and Huntington's Disease: A Mini Review', *Oxid Med Cell Longev*, 2016: 8590578.
Manza, L. L., S. L. Stamer, A. J. Ham, S. G. Codreanu, and D. C. Liebler. 2005. 'Sample preparation and digestion for proteomic analyses using spin filters', *Proteomics*, 5: 1742-5.
Marchi, S., M. Bonora, S. Patergnani, C. Giorgi, and P. Pinton. 2017. 'Methods to Assess Mitochondrial Morphology in Mammalian Cells Mounting Autophagic or Mitophagic Responses', *Methods Enzymol*, 588: 171-86.
Martin, J. J., J. Gheuens, M. Bruyland, P. Cras, A. Vandenberghe, C. L. Masters, K. Beyreuther, R. Dom, C. Ceuterick, U. Lubke, and et al. 1991. 'Early-onset Alzheimer's disease in 2 large Belgian families', *Neurology*, 41: 62-8.
McDade, E., G. Wang, B. A. Gordon, J. Hassenstab, T. L. S. Benzinger, V. Buckles, A. M. Fagan, D. M. Holtzman, N. J. Cairns, A. M. Goate, D. S. Marcus, J. C. Morris, K. Paumier, C. Xiong, R. Allegri, S. B. Berman, W. Klunk, J. Noble, J. Ringman, B. Ghetti, M. Farlow, R. A. Sperling, J. Chhatwal, S. Salloway, N. R. Graff-Radford, P. R. Schofield, C. Masters, M. N. Rossor, N. C. Fox, J. Levin, M. Jucker, R. J. Bateman, and Network Dominantly Inherited Alzheimer. 2018. 'Longitudinal cognitive and biomarker changes in dominantly inherited Alzheimer disease', *Neurology*, 91: e1295-e306.
Morishima, Y., Y. Gotoh, J. Zieg, T. Barrett, H. Takano, R. Flavell, R. J. Davis, Y. Shirasaki, and M. E. Greenberg. 2001. 'Beta-amyloid induces neuronal apoptosis via a mechanism that involves the c-Jun N-terminal kinase pathway and the induction of Fas ligand', *J Neurosci*, 21: 7551-60.
Murayama, M., S. Tanaka, J. Palacino, O. Murayama, T. Honda, X. Sun, K. Yasutake, N. Nihonmatsu, B. Wolozin, and A. Takashima. 1998. 'Direct association of presenilin-1 with beta-catenin', *FEBS Lett*, 433: 73-7.
Nakazono, T., T. N. Lam, A. Y. Patel, M. Kitazawa, T. Saito, T. C. Saido, and K. M. Igarashi. 2017. 'Impaired In Vivo Gamma Oscillations in the Medial Entorhinal Cortex of Knock-in Alzheimer Model', *Front Syst Neurosci*, 11: 48.
Nalbantoglu, J., G. Tirado-Santiago, A. Lahsaini, J. Poirier, O. Goncalves, G. Verge, F. Momoli, S. A. Welner, G. Massicotte, J. P. Julien, and M. L. Shapiro. 1997. 'Impaired learning and LTP in mice expressing the carboxy terminus of the Alzheimer amyloid precursor protein', *Nature*, 387: 500-5.
Neely, K. M., K. N. Green, and F. M. LaFerla. 2011. 'Presenilin is necessary for efficient proteolysis through the autophagy-lysosome system in a gamma-secretase-independent manner', *J Neurosci*, 31: 2781-91.
Nelson, O., H. Tu, T. Lei, M. Bentahir, B. de Strooper, and I. Bezprozvanny. 2007. 'Familial Alzheimer disease-linked mutations specifically disrupt Ca2+ leak function of presenilin 1', *J Clin Invest*, 117: 1230-9.
Nelson, P. T., H. Braak, and W. R. Markesbery. 2009. 'Neuropathology and cognitive impairment in Alzheimer disease: a complex but coherent relationship', *J Neuropathol Exp Neurol*, 68: 1-14.
Nimchinsky, E. A., B. L. Sabatini, and K. Svoboda. 2002. 'Structure and function of dendritic spines', *Annu Rev Physiol*, 64: 313-53.
Oakley, H., S. L. Cole, S. Logan, E. Maus, P. Shao, J. Craft, A. Guillozet-Bongaarts, M. Ohno, J. Disterhoft, L. Van Eldik, R. Berry, and R. Vassar. 2006. 'Intraneuronal beta-amyloid aggregates, neurodegeneration, and neuron loss in transgenic mice with five familial Alzheimer's disease mutations: potential factors in amyloid plaque formation', *J Neurosci*, 26: 10129-40.
Oddo, S., A. Caccamo, J. D. Shepherd, M. P. Murphy, T. E. Golde, R. Kayed, R. Metherate, M. P. Mattson, Y. Akbari, and F. M. LaFerla. 2003. 'Triple-transgenic model of Alzheimer's disease with plaques and tangles: intracellular Abeta and synaptic dysfunction', *Neuron*, 39: 409-21.
Olmos-Alonso, A., S. T. Schetters, S. Sri, K. Askew, R. Mancuso, M. Vargas-Caballero, C. Holscher, V. H. Perry, and D. Gomez-Nicola. 2016. 'Pharmacological targeting of CSF1R inhibits

microglial proliferation and prevents the progression of Alzheimer's-like pathology', *Brain*, 139: 891-907.
Padurariu, M., A. Ciobica, I. Mavroudis, D. Fotiou, and S. Baloyannis. 2012. 'Hippocampal neuronal loss in the CA1 and CA3 areas of Alzheimer's disease patients', *Psychiatr Danub*, 24: 152-8.
Paillusson, S., R. Stoica, P. Gomez-Suaga, D. H. W. Lau, S. Mueller, T. Miller, and C. C. J. Miller. 2016. 'There's Something Wrong with my MAM; the ER-Mitochondria Axis and Neurodegenerative Diseases', *Trends Neurosci*, 39: 146-57.
Parent, A., D. J. Linden, S. S. Sisodia, and D. R. Borchelt. 1999. 'Synaptic transmission and hippocampal long-term potentiation in transgenic mice expressing FAD-linked presenilin 1', *Neurobiol Dis*, 6: 56-62.
Park, H. J., Y. M. Seong, J. Y. Choi, S. Kang, and H. Rhim. 2004. 'Alzheimer's disease-associated amyloid beta interacts with the human serine protease HtrA2/Omi', *Neurosci Lett*, 357: 63-7.
Passer, B. J., L. Pellegrini, P. Vito, J. K. Ganjei, and L. D'Adamio. 1999. 'Interaction of Alzheimer's presenilin-1 and presenilin-2 with Bcl-X(L). A potential role in modulating the threshold of cell death', *J Biol Chem*, 274: 24007-13.
Patterson, Christina. 2018. "World Alzheimer Report 2018." In. London: Alzheimer´s Disease International
Peppiatt, C. M., T. J. Collins, L. Mackenzie, S. J. Conway, A. B. Holmes, M. D. Bootman, M. J. Berridge, J. T. Seo, and H. L. Roderick. 2003. '2-Aminoethoxydiphenyl borate (2-APB) antagonises inositol 1,4,5-trisphosphate-induced calcium release, inhibits calcium pumps and has a use-dependent and slowly reversible action on store-operated calcium entry channels', *Cell Calcium*, 34: 97-108.
Pera, M., D. Larrea, C. Guardia-Laguarta, J. Montesinos, K. R. Velasco, R. R. Agrawal, Y. Xu, R. B. Chan, G. Di Paolo, M. F. Mehler, G. S. Perumal, F. P. Macaluso, Z. Z. Freyberg, R. Acin-Perez, J. A. Enriquez, E. A. Schon, and E. Area-Gomez. 2017. 'Increased localization of APP-C99 in mitochondria-associated ER membranes causes mitochondrial dysfunction in Alzheimer disease', *EMBO J*, 36: 3356-71.
Pimplikar, S. W., R. A. Nixon, N. K. Robakis, J. Shen, and L. H. Tsai. 2010. 'Amyloid-independent mechanisms in Alzheimer's disease pathogenesis', *J Neurosci*, 30: 14946-54.
Poirel, O., S. Mella, C. Videau, L. Ramet, M. A. Davoli, E. Herzog, P. Katsel, N. Mechawar, V. Haroutunian, J. Epelbaum, S. Daumas, and S. El Mestikawy. 2018. 'Moderate decline in select synaptic markers in the prefrontal cortex (BA9) of patients with Alzheimer's disease at various cognitive stages', *Sci Rep*, 8: 938.
Poston, C. N., S. C. Krishnan, and C. R. Bazemore-Walker. 2013. 'In-depth proteomic analysis of mammalian mitochondria-associated membranes (MAM)', *J Proteomics*, 79: 219-30.
Ranjan, B., K. H. Chong, and J. Zheng. 2018. 'Composite mathematical modeling of calcium signaling behind neuronal cell death in Alzheimer's disease', *BMC Syst Biol*, 12: 10.
Razay, G., A. Vreugdenhil, and G. Wilcock. 2007. 'The metabolic syndrome and Alzheimer disease', *Arch Neurol*, 64: 93-6.
Reaume, A. G., D. S. Howland, S. P. Trusko, M. J. Savage, D. M. Lang, B. D. Greenberg, R. Siman, and R. W. Scott. 1996. 'Enhanced amyloidogenic processing of the beta-amyloid precursor protein in gene-targeted mice bearing the Swedish familial Alzheimer's disease mutations and a "humanized" Abeta sequence', *J Biol Chem*, 271: 23380-8.
Reifert, J., D. Hartung-Cranston, and S. C. Feinstein. 2011. 'Amyloid beta-mediated cell death of cultured hippocampal neurons reveals extensive Tau fragmentation without increased full-length tau phosphorylation', *J Biol Chem*, 286: 20797-811.
Richardson, J. A., and D. K. Burns. 2002. 'Mouse models of Alzheimer's disease: a quest for plaques and tangles', *ILAR J*, 43: 89-99.
Rios, J. A., P. Cisternas, M. Arrese, S. Barja, and N. C. Inestrosa. 2014. 'Is Alzheimer's disease related to metabolic syndrome? A Wnt signaling conundrum', *Prog Neurobiol*, 121: 125-46.
Rojas-Gutierrez, E., G. Munoz-Arenas, S. Trevino, B. Espinosa, R. Chavez, K. Rojas, G. Flores, A. Diaz, and J. Guevara. 2017. 'Alzheimer's disease and metabolic syndrome: A link from oxidative stress and inflammation to neurodegeneration', *Synapse*.
Rowland, A. A., and G. K. Voeltz. 2012. 'Endoplasmic reticulum-mitochondria contacts: function of the junction', *Nat Rev Mol Cell Biol*, 13: 607-25.
Ruan, L., C. Zhou, E. Jin, A. Kucharavy, Y. Zhang, Z. Wen, L. Florens, and R. Li. 2017. 'Cytosolic proteostasis through importing of misfolded proteins into mitochondria', *Nature*, 543: 443-46.
Saito, T., Y. Matsuba, N. Mihira, J. Takano, P. Nilsson, S. Itohara, N. Iwata, and T. C. Saido. 2014. 'Single App knock-in mouse models of Alzheimer's disease', *Nat Neurosci*, 17: 661-3.

Saito, T., Y. Matsuba, N. Yamazaki, S. Hashimoto, and T. C. Saido. 2016. 'Calpain Activation in Alzheimer's Model Mice Is an Artifact of APP and Presenilin Overexpression', *J Neurosci*, 36: 9933-6.

Sala Frigerio, C., and B. De Strooper. 2016. 'Alzheimer's Disease Mechanisms and Emerging Roads to Novel Therapeutics', *Annu Rev Neurosci*, 39: 57-79.

Sannerud, R., C. Esselens, P. Ejsmont, R. Mattera, L. Rochin, A. K. Tharkeshwar, G. De Baets, V. De Wever, R. Habets, V. Baert, W. Vermeire, C. Michiels, A. J. Groot, R. Wouters, K. Dillen, K. Vints, P. Baatsen, S. Munck, R. Derua, E. Waelkens, G. S. Basi, M. Mercken, M. Vooijs, M. Bollen, J. Schymkowitz, F. Rousseau, J. S. Bonifacino, G. Van Niel, B. De Strooper, and W. Annaert. 2016. 'Restricted Location of PSEN2/gamma-Secretase Determines Substrate Specificity and Generates an Intracellular Abeta Pool', *Cell*, 166: 193-208.

Sarasija, S., J. T. Laboy, Z. Ashkavand, J. Bonner, Y. Tang, and K. R. Norman. 2018. 'Presenilin mutations deregulate mitochondrial Ca(2+) homeostasis and metabolic activity causing neurodegeneration in Caenorhabditis elegans', *Elife*, 7.

Sasaguri, H., P. Nilsson, S. Hashimoto, K. Nagata, T. Saito, B. De Strooper, J. Hardy, R. Vassar, B. Winblad, and T. C. Saido. 2017. 'APP mouse models for Alzheimer's disease preclinical studies', *EMBO J*, 36: 2473-87.

Saura, C. A., S. Y. Choi, V. Beglopoulos, S. Malkani, D. Zhang, B. S. Shankaranarayana Rao, S. Chattarji, R. J. Kelleher, 3rd, E. R. Kandel, K. Duff, A. Kirkwood, and J. Shen. 2004. 'Loss of presenilin function causes impairments of memory and synaptic plasticity followed by age-dependent neurodegeneration', *Neuron*, 42: 23-36.

Scheff, S. W., J. H. Neltner, and P. T. Nelson. 2014. 'Is synaptic loss a unique hallmark of Alzheimer's disease?', *Biochem Pharmacol*, 88: 517-28.

Schon, E. A., and E. Area-Gomez. 2010. 'Is Alzheimer's disease a disorder of mitochondria-associated membranes?', *J Alzheimers Dis*, 20 Suppl 2: S281-92.

Schrader, M., L. F. Godinho, J. L. Costello, and M. Islinger. 2015. 'The different facets of organelle interplay-an overview of organelle interactions', *Front Cell Dev Biol*, 3: 56.

Schreiner, B., L. Hedskog, B. Wiehager, and M. Ankarcrona. 2015. 'Amyloid-beta peptides are generated in mitochondria-associated endoplasmic reticulum membranes', *J Alzheimers Dis*, 43: 369-74.

Sepulveda-Falla, D., A. Barrera-Ocampo, C. Hagel, A. Korwitz, M. F. Vinueza-Veloz, K. Zhou, M. Schonewille, H. Zhou, L. Velazquez-Perez, R. Rodriguez-Labrada, A. Villegas, I. Ferrer, F. Lopera, T. Langer, C. I. De Zeeuw, and M. Glatzel. 2014. 'Familial Alzheimer's disease-associated presenilin-1 alters cerebellar activity and calcium homeostasis', *J Clin Invest*, 124: 1552-67.

Shaked, G. M., M. P. Kummer, D. C. Lu, V. Galvan, D. E. Bredesen, and E. H. Koo. 2006. 'Abeta induces cell death by direct interaction with its cognate extracellular domain on APP (APP 597-624)', *FASEB J*, 20: 1254-6.

Sheikh, S., Safia, E. Haque, and S. S. Mir. 2013. 'Neurodegenerative Diseases: Multifactorial Conformational Diseases and Their Therapeutic Interventions', *J Neurodegener Dis*, 2013: 563481.

Sherrington, R., E. I. Rogaev, Y. Liang, E. A. Rogaeva, G. Levesque, M. Ikeda, H. Chi, C. Lin, G. Li, K. Holman, T. Tsuda, L. Mar, J. F. Foncin, A. C. Bruni, M. P. Montesi, S. Sorbi, I. Rainero, L. Pinessi, L. Nee, I. Chumakov, D. Pollen, A. Brookes, P. Sanseau, R. J. Polinsky, W. Wasco, H. A. Da Silva, J. L. Haines, M. A. Perkicak-Vance, R. E. Tanzi, A. D. Roses, P. E. Fraser, J. M. Rommens, and P. H. St George-Hyslop. 1995. 'Cloning of a gene bearing missense mutations in early-onset familial Alzheimer's disease', *Nature*, 375: 754-60.

Shilling, D., D. O. Mak, D. E. Kang, and J. K. Foskett. 2012. 'Lack of evidence for presenilins as endoplasmic reticulum Ca2+ leak channels', *J Biol Chem*, 287: 10933-44.

Sobhanifar, S., B. Schneider, F. Lohr, D. Gottstein, T. Ikeya, K. Mlynarczyk, W. Pulawski, U. Ghoshdastider, M. Kolinski, S. Filipek, P. Guntert, F. Bernhard, and V. Dotsch. 2010. 'Structural investigation of the C-terminal catalytic fragment of presenilin 1', *Proc Natl Acad Sci U S A*, 107: 9644-9.

Sorrentino, V., M. Romani, L. Mouchiroud, J. S. Beck, H. Zhang, D. D'Amico, N. Moullan, F. Potenza, A. W. Schmid, S. Rietsch, S. E. Counts, and J. Auwerx. 2017. 'Enhancing mitochondrial proteostasis reduces amyloid-beta proteotoxicity', *Nature*, 552: 187-93.

Stanga, S., C. Vrancx, B. Tasiaux, C. Marinangeli, H. Karlstrom, and P. Kienlen-Campard. 2018. 'Specificity of presenilin-1- and presenilin-2-dependent gamma-secretases towards substrate processing', *J Cell Mol Med*, 22: 823-33.

Sun, L., R. Zhou, G. Yang, and Y. Shi. 2017. 'Analysis of 138 pathogenic mutations in presenilin-1 on the in vitro production of Abeta42 and Abeta40 peptides by gamma-secretase', *Proc Natl Acad Sci U S A*, 114: E476-E85.

Szabadkai, G., K. Bianchi, P. Varnai, D. De Stefani, M. R. Wieckowski, D. Cavagna, A. I. Nagy, T. Balla, and R. Rizzuto. 2006. 'Chaperone-mediated coupling of endoplasmic reticulum and mitochondrial Ca2+ channels', *J Cell Biol*, 175: 901-11.

Tagami, S., K. Yanagida, T. S. Kodama, M. Takami, N. Mizuta, H. Oyama, K. Nishitomi, Y. W. Chiu, T. Okamoto, T. Ikeuchi, G. Sakaguchi, T. Kudo, Y. Matsuura, A. Fukumori, M. Takeda, Y. Ihara, and M. Okochi. 2017. 'Semagacestat Is a Pseudo-Inhibitor of gamma-Secretase', *Cell Rep*, 21: 259-73.

Tanahashi, H., S. Kawakatsu, M. Kaneko, H. Yamanaka, K. Takahashi, and T. Tabira. 1996. 'Sequence analysis of presenilin-1 gene mutation in Japanese Alzheimer's disease patients', *Neurosci Lett*, 218: 139-41.

Tanemura, K., D. H. Chui, T. Fukuda, M. Murayama, J. M. Park, T. Akagi, Y. Tatebayashi, T. Miyasaka, T. Kimura, T. Hashikawa, Y. Nakano, T. Kudo, M. Takeda, and A. Takashima. 2006. 'Formation of tau inclusions in knock-in mice with familial Alzheimer disease (FAD) mutation of presenilin 1 (PS1)', *J Biol Chem*, 281: 5037-41.

Tanzi, R. E. 2012. 'The genetics of Alzheimer disease', *Cold Spring Harb Perspect Med*, 2.

Teng, F. Y., and B. L. Tang. 2005. 'Widespread gamma-secretase activity in the cell, but do we need it at the mitochondria?', *Biochem Biophys Res Commun*, 328: 1-5.

Toglia, P., K. H. Cheung, D. D. Mak, and G. Ullah. 2016. 'Impaired mitochondrial function due to familial Alzheimer's disease-causing presenilins mutants via Ca disruptions', *Cell Calcium*.

Toglia, P., and G. Ullah. 2016. 'The gain-of-function enhancement of IP3-receptor channel gating by familial Alzheimer's disease-linked presenilin mutants increases the open probability of mitochondrial permeability transition pore', *Cell Calcium*, 60: 13-24.

Tong, B. C., C. S. Lee, W. H. Cheng, K. O. Lai, J. K. Foskett, and K. H. Cheung. 2016. 'Familial Alzheimer's disease-associated presenilin 1 mutants promote gamma-secretase cleavage of STIM1 to impair store-operated Ca2+ entry', *Sci Signal*, 9: ra89.

Tu, H., O. Nelson, A. Bezprozvanny, Z. Wang, S. F. Lee, Y. H. Hao, L. Serneels, B. De Strooper, G. Yu, and I. Bezprozvanny. 2006. 'Presenilins form ER Ca2+ leak channels, a function disrupted by familial Alzheimer's disease-linked mutations', *Cell*, 126: 981-93.

Tucker, S., C. Moller, K. Tegerstedt, A. Lord, H. Laudon, J. Sjodahl, L. Soderberg, E. Spens, C. Sahlin, E. R. Waara, A. Satlin, P. Gellerfors, G. Osswald, and L. Lannfelt. 2015. 'The murine version of BAN2401 (mAb158) selectively reduces amyloid-beta protofibrils in brain and cerebrospinal fluid of tg-ArcSwe mice', *J Alzheimers Dis*, 43: 575-88.

Umeda, T., T. Tomiyama, N. Sakama, S. Tanaka, M. P. Lambert, W. L. Klein, and H. Mori. 2011. 'Intraneuronal amyloid beta oligomers cause cell death via endoplasmic reticulum stress, endosomal/lysosomal leakage, and mitochondrial dysfunction in vivo', *J Neurosci Res*, 89: 1031-42.

Urano, Y., I. Hayashi, N. Isoo, P. C. Reid, Y. Shibasaki, N. Noguchi, T. Tomita, T. Iwatsubo, T. Hamakubo, and T. Kodama. 2005. 'Association of active gamma-secretase complex with lipid rafts', *J Lipid Res*, 46: 904-12.

V. N. Mukhin, K. I. Pavlov, and V. M. Klimenko. 2017. 'Mechanisms of Neuron Loss in Alzheimer's Disease.' in Springer Science+Business Media New York (ed.), *Neuroscience and Behavioral Physiology*.

Van Cauwenberghe, C., C. Van Broeckhoven, and K. Sleegers. 2016. 'The genetic landscape of Alzheimer disease: clinical implications and perspectives', *Genet Med*, 18: 421-30.

Van Dam, D., and P. P. De Deyn. 2011. 'Animal models in the drug discovery pipeline for Alzheimer's disease', *Br J Pharmacol*, 164: 1285-300.

Vance, J. E. 1990. 'Phospholipid synthesis in a membrane fraction associated with mitochondria', *J Biol Chem*, 265: 7248-56.

———. 2014. 'MAM (mitochondria-associated membranes) in mammalian cells: lipids and beyond', *Biochim Biophys Acta*, 1841: 595-609.

Vetrivel, K. S., H. Cheng, W. Lin, T. Sakurai, T. Li, N. Nukina, P. C. Wong, H. Xu, and G. Thinakaran. 2004. 'Association of gamma-secretase with lipid rafts in post-Golgi and endosome membranes', *J Biol Chem*, 279: 44945-54.

Volgyi, K., K. Badics, F. J. Sialana, P. Gulyassy, E. B. Udvari, V. Kis, L. Drahos, G. Lubec, K. A. Kekesi, and G. Juhasz. 2018. 'Early Presymptomatic Changes in the Proteome of Mitochondria-Associated Membrane in the APP/PS1 Mouse Model of Alzheimer's Disease', *Mol Neurobiol*, 55: 7839-57.

Volianskis, A., R. Kostner, M. Molgaard, S. Hass, and M. S. Jensen. 2010. 'Episodic memory deficits are not related to altered glutamatergic synaptic transmission and plasticity in the CA1 hippocampus of the APPswe/PS1deltaE9-deleted transgenic mice model of ss-amyloidosis', *Neurobiol Aging*, 31: 1173-87.

Walter, J. 2015. 'Twenty Years of Presenilins--Important Proteins in Health and Disease', *Mol Med*, 21 Suppl 1: S41-8.

Walls, K. C., P. Coskun, J. L. Gallegos-Perez, N. Zadourian, K. Freude, S. Rasool, M. Blurton-Jones, K. N. Green, and F. M. LaFerla. 2012. 'Swedish Alzheimer mutation induces mitochondrial dysfunction mediated by HSP60 mislocalization of amyloid precursor protein (APP) and beta-amyloid', *J Biol Chem*, 287: 30317-27.

Wang, H. Q., Y. Nakaya, Z. Du, T. Yamane, M. Shirane, T. Kudo, M. Takeda, K. Takebayashi, Y. Noda, K. I. Nakayama, and M. Nishimura. 2005. 'Interaction of presenilins with FKBP38 promotes apoptosis by reducing mitochondrial Bcl-2', *Hum Mol Genet*, 14: 1889-902.

Wang, J., H. Tanila, J. Puolivali, I. Kadish, and T. van Groen. 2003. 'Gender differences in the amount and deposition of amyloidbeta in APPswe and PS1 double transgenic mice', *Neurobiol Dis*, 14: 318-27.

Wei, A. C., T. Liu, S. Cortassa, R. L. Winslow, and B. O'Rourke. 2011. 'Mitochondrial Ca2+ influx and efflux rates in guinea pig cardiac mitochondria: low and high affinity effects of cyclosporine A', *Biochim Biophys Acta*, 1813: 1373-81.

Wei, W., X. Wang, and J. W. Kusiak. 2002. 'Signaling events in amyloid beta-peptide-induced neuronal death and insulin-like growth factor I protection', *J Biol Chem*, 277: 17649-56.

Wei, Z., G. G. Gabriel, L. Rui, X. Cao, P. R. Pennington, J. Chlan-Fourney, A. J. Nazarali, G. B. Baker, and D. D. Mousseau. 2012. 'Monoamine oxidase-A physically interacts with presenilin-1(M146V) in the mouse cortex', *J Alzheimers Dis*, 28: 403-22.

Wieckowski, M. R., C. Giorgi, M. Lebiedzinska, J. Duszynski, and P. Pinton. 2009. 'Isolation of mitochondria-associated membranes and mitochondria from animal tissues and cells', *Nat Protoc*, 4: 1582-90.

Wieczorek, S., F. Combes, C. Lazar, Q. Giai Gianetto, L. Gatto, A. Dorffer, A. M. Hesse, Y. Coute, M. Ferro, C. Bruley, and T. Burger. 2017. 'DAPAR & ProStaR: software to perform statistical analyses in quantitative discovery proteomics', *Bioinformatics*, 33: 135-36.

Wu, B., H. Yamaguchi, F. A. Lai, and J. Shen. 2013. 'Presenilins regulate calcium homeostasis and presynaptic function via ryanodine receptors in hippocampal neurons', *Proc Natl Acad Sci U S A*, 110: 15091-6.

Xia, D., H. Watanabe, B. Wu, S. H. Lee, Y. Li, E. Tsvetkov, V. Y. Bolshakov, J. Shen, and R. J. Kelleher, 3rd. 2015. 'Presenilin-1 knockin mice reveal loss-of-function mechanism for familial Alzheimer's disease', *Neuron*, 85: 967-81.

Xie, T., C. Yan, R. Zhou, Y. Zhao, L. Sun, G. Yang, P. Lu, D. Ma, and Y. Shi. 2014. 'Crystal structure of the gamma-secretase component nicastrin', *Proc Natl Acad Sci U S A*, 111: 13349-54.

Xu, T. H., Y. Yan, Y. Kang, Y. Jiang, K. Melcher, and H. E. Xu. 2016. 'Alzheimer's disease-associated mutations increase amyloid precursor protein resistance to gamma-secretase cleavage and the Abeta42/Abeta40 ratio', *Cell Discov*, 2: 16026.

Yao, J., R. W. Irwin, L. Zhao, J. Nilsen, R. T. Hamilton, and R. D. Brinton. 2009. 'Mitochondrial bioenergetic deficit precedes Alzheimer's pathology in female mouse model of Alzheimer's disease', *Proc Natl Acad Sci U S A*, 106: 14670-5.

Youle, R. J., and M. Karbowski. 2005. 'Mitochondrial fission in apoptosis', *Nat Rev Mol Cell Biol*, 6: 657-63.

Zahs, K. R., and K. H. Ashe. 2010. "Too much good news' - are Alzheimer mouse models trying to tell us how to prevent, not cure, Alzheimer's disease?', *Trends Neurosci*, 33: 381-9.

Zampese, E., C. Fasolato, M. J. Kipanyula, M. Bortolozzi, T. Pozzan, and P. Pizzo. 2011. 'Presenilin 2 modulates endoplasmic reticulum (ER)-mitochondria interactions and Ca2+ cross-talk', *Proc Natl Acad Sci U S A*, 108: 2777-82.

Zhang, A., C. D. Williamson, D. S. Wong, M. D. Bullough, K. J. Brown, Y. Hathout, and A. M. Colberg-Poley. 2011. 'Quantitative proteomic analyses of human cytomegalovirus-induced restructuring of endoplasmic reticulum-mitochondrial contacts at late times of infection', *Mol Cell Proteomics*, 10: M111 009936.

Zhang, C., E. McNeil, L. Dressler, and R. Siman. 2007. 'Long-lasting impairment in hippocampal neurogenesis associated with amyloid deposition in a knock-in mouse model of familial Alzheimer's disease', *Exp Neurol*, 204: 77-87.

Zhang, H., S. Sun, A. Herreman, B. De Strooper, and I. Bezprozvanny. 2010. 'Role of presenilins in neuronal calcium homeostasis', *J Neurosci*, 30: 8566-80.

Zhang, L., S. Trushin, T. A. Christensen, B. V. Bachmeier, B. Gateno, A. Schroeder, J. Yao, K. Itoh, H. Sesaki, W. W. Poon, K. H. Gylys, E. R. Patterson, J. E. Parisi, R. Diaz Brinton, J. L. Salisbury, and E. Trushina. 2016. 'Altered brain energetics induces mitochondrial fission arrest in Alzheimer's Disease', *Sci Rep*, 6: 18725.

Zhang, M. Y., R. Katzman, D. Salmon, H. Jin, G. J. Cai, Z. Y. Wang, G. Y. Qu, I. Grant, E. Yu, P. Levy, and et al. 1990. 'The prevalence of dementia and Alzheimer's disease in Shanghai, China: impact of age, gender, and education', *Ann Neurol*, 27: 428-37.

Zhang, S., M. Zhang, F. Cai, and W. Song. 2013. 'Biological function of Presenilin and its role in AD pathogenesis', *Transl Neurodegener*, 2: 15.

Zhang, X., Y. Li, H. Xu, and Y. W. Zhang. 2014. 'The gamma-secretase complex: from structure to function', *Front Cell Neurosci*, 8: 427.

Zolochevska, O., N. Bjorklund, R. Woltjer, J. E. Wiktorowicz, and G. Taglialatela. 2018. 'Postsynaptic Proteome of Non-Demented Individuals with Alzheimer's Disease Neuropathology', *J Alzheimers Dis*, 65: 659-82.

16. Acknowledgements

I want to express my sincere gratitude to all the people that have contributed in different ways to this work. In the first place to Prof. Markus Glatzel and Dr. Diego Sepulveda-Falla, for letting me work at the Institute and for the support during these years. To all the members of the Institute of Neuropathology and, especially, to David Wasilewski, for his great help with experiments, but most of all for his friendship. Thanks for trying to teach me German, it was always funny to teach you Spanish, I am sure that you are going to be a great scientist.

Special thanks to Beata Szalay and Giovanna Galliciotti, for their help with protocols, training and scientific advice. My gratitude also to Prof. Christian Hagel, for his kind disposition to help me with electron microscopy and for his feedback as supervisor of my project. I am especially appreciative to Prof. Christian Lohr for teaching me calcium imaging techniques and for giving me the opportunity to work in his laboratory and Dr. Virgilio Failla for his help during microscopy experiments.

I also thank the members of the Animal Facility, especially Gesa Roessler and Ema Almasi for taking care of the animals and being so helpful with the “Terminierte Verpaarung” experiments. My deepest gratitude to the collaborators of this project: Dr. Laura Heikaus, Dr. Gee and Sabine Graf, for their outstanding work with the proteomics and LTP experiments, respectively.

An essential part of this project was developed thanks to Prof. Paolo Pinton, Dr. Claudia Morganti, Claudio Baldini and Dr. Giampaolo Morciano from the University of Ferrara. Many thanks for a great time in beautiful Italy, it was an unforgettable experience to share our common interests in the fascinating area of mitochondrial biology.

I had the privilege to be part of the GRK1459 Research Training Group, and I would like to thank Dr. Dorthe Labonté and Prof. Braulke for letting me be part of this great group, for all the seminars, retreats and courses that contributed significantly to my professional development.

I am also truly grateful to the DAAD and especially to my “Antsprechpartnerin” Silke Hamacher. They do a fantastic work helping students like me to do research. It is an honor to be a *DAADian.* Finally, I would like to thank my parents, my sisters, my beautiful niece, my husband, and my friends, for all the love and patience; despite the distance, you were always there, and this work is entirely dedicated to you.

17. Curriculum Vitae

Lebenslauf entfällt aus datenschutzrechtlichen Gründen.

18. Statutory Declaration

Eidesstattliche Versicherung

Ich versichere ausdrücklich, dass ich die Arbeit selbständig und ohne fremde Hilfe verfasst, andere als die von mir angegebenen Quellen und Hilfsmittel nicht benutzt und die aus den benutzten Werken wörtlich oder inhaltlich entnommenen Stellen einzeln nach Ausgabe (Auflage und Jahr des Erscheinens), Band und Seite des benutzten Werkes kenntlich gemacht habe.
Ferner versichere ich, dass ich die Dissertation bisher nicht einem Fachvertreter an einer anderen Hochschule zur Überprüfung vorgelegt oder mich anderweitig um Zulassung zur Promotion beworben habe.
Ich erkläre mich einverstanden, dass meine Dissertation vom Dekanat der Medizinischen Fakultät mit einer gängigen Software zur Erkennung von Plagiaten überprüft werden kann.